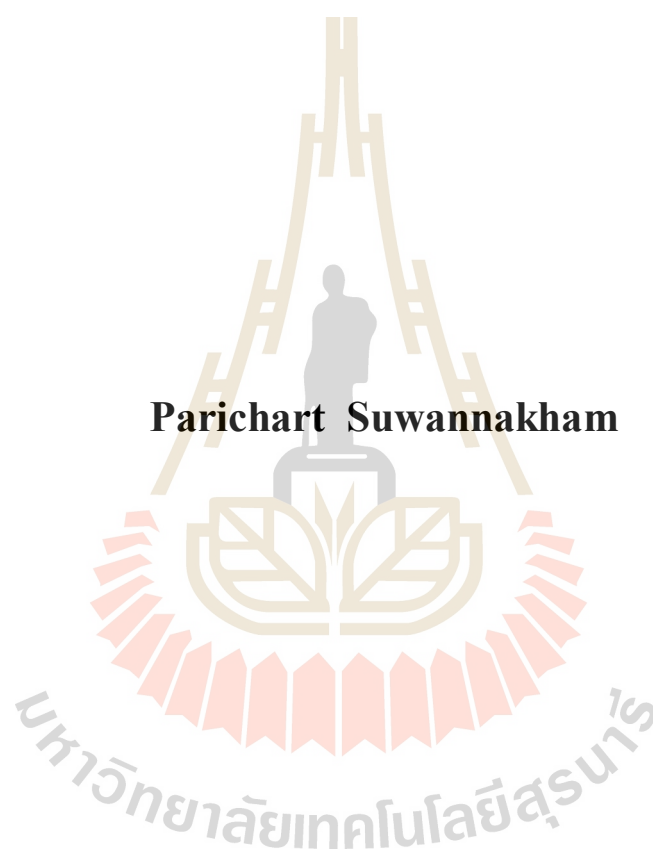


**STRUCTURAL DIFFUSION OF PROTON IN
PHOSPHORIC ACID-HYDRONIUM ION-
WATER COMPLEXES**



Parichart Suwannakham

**A Thesis Submitted in Partial Fulfillment of the Requirements for the
Degree of Doctor of Philosophy in Chemistry**

Suranaree University of Technology

Academic Year 2015

การแพร่เชิงโครงสร้างของโปรตอนในสารเชิงซ้อน
กรดฟอสฟอริก-ไอออนไฮดรอกไซด์



นางสาวปาริชาติ สุวรรณคำ

วิทยานิพนธ์นี้เป็นส่วนหนึ่งของการศึกษาตามหลักสูตรปริญญาวิทยาศาสตรดุษฎีบัณฑิต
สาขาวิชาเคมี
มหาวิทยาลัยเทคโนโลยีสุรนารี
ปีการศึกษา 2558

**STRUCTURAL DIFFUSION OF PROTON IN
PHOSPHORIC ACID-HYDRONIUM ION-
WATER COMPLEXES**

Suranaree University of Technology has approved this thesis submitted in partial fulfillment of the requirements for the Degree of Doctor of Philosophy.

Thesis Examining Committee

(Assoc. Prof. Dr. Jatuporn Wittayakun)

Chairperson

(Prof. Dr. Kritsana Sagarik)

Member (Thesis Advisor)

(Assoc. Prof. Dr. Viwat Vchirawongkwin)

Member

(Assoc. Prof. Dr. Anan Tongraar)

Member

(Assoc. Prof. Dr. Visit Vao-Soongnern)

Member

(Prof. Dr. Sukit Limpijumnong)

Vice Rector for Academic Affairs
and Innovation

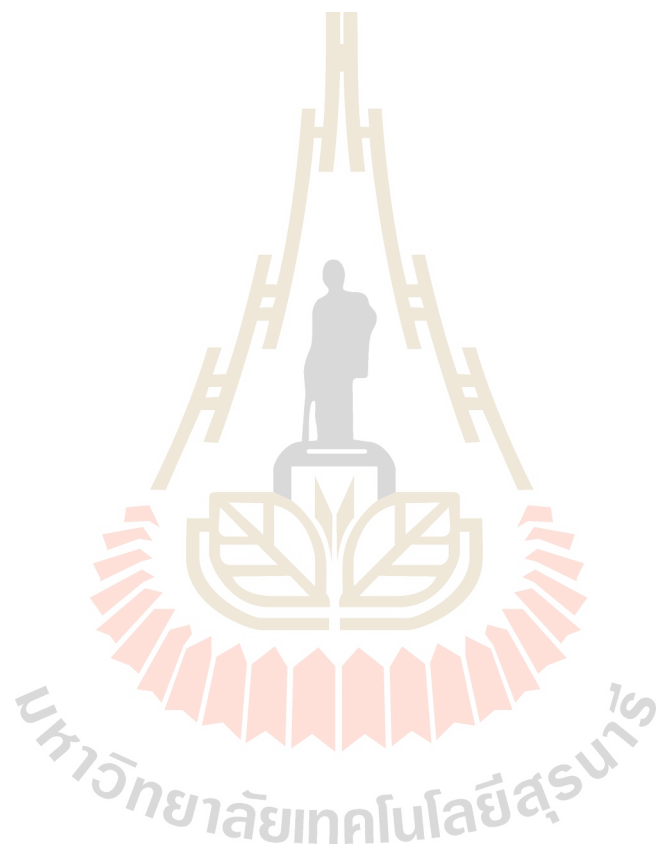
(Prof. Dr. Santi Maensiri)

Dean of Institute of Science

ปาริชาติ สุวรรณคำ : การแพร่เชิงโครงสร้างของโปรตอนในสารเชิงซ้อนกรดฟอสฟอริก-ไอออนไฮโดรเนียม-น้ำ (STRUCTURAL DIFFUSION OF PROTON IN PHOSPHORIC ACID-HYDRONIUM ION-WATER COMPLEXES) อาจารย์ที่ปรึกษา : ศาสตราจารย์ ดร.กฤษณะ ศาคริก, 122 หน้า.

วิทยานิพนธ์เรื่องนี้ศึกษาพลวัต (dynamics) และกลไกการแตกตัว (dissociation) และการถ่ายโอน (transfer) โปรตอนในสารเชิงซ้อนกรดฟอสฟอริก (H_3PO_4)-ไอออนไฮโดรเนียม (H_3O^+)-น้ำ (H_2O) โดยใช้แบบจำลองการละลายล่วงหน้า (presolvation model) และใช้สารเชิงซ้อน $\text{H}_3\text{PO}_4\text{-H}_3\text{O}^+ - n\text{H}_2\text{O}$ เมื่อ $n = 1-3$ เป็นแบบจำลองระบบ และการคำนวณแอบ อินิซิโอ (*ab initio* calculations) และวิธีการจำลองพลวัตเชิงโมเลกุลบอร์น-ออปเพนไฮเมอร์ (Born-Oppenheimer molecular dynamic, BOMD) ที่ระดับ RIMP2/TZVP เป็นแบบจำลองการคำนวณผลการคำนวณเชิงสถิต (static results) แสดงว่าสารเชิงซ้อนระหว่างกลาง (intermediate complex) ที่เสถียรและเล็กที่สุดในการแตกตัวของโปรตอน ($n = 1$) เกิดขึ้นในสถานะแวดล้อมค่าคงที่ไดอิเล็กทริกเฉพาะที่ต่ำ (low local-dielectric constant environment, $\epsilon = 1$) ในทางตรงข้ามการถ่ายโอนโปรตอนจากระดับชั้นไฮเดรชันที่หนึ่ง (first hydration shell) ไปสู่ระดับชั้นไฮเดรชันที่สอง (second hydration shell) ขับเคลื่อนโดยการกระเพื่อม (fluctuation) ของจำนวนโมเลกุลน้ำในสถานะแวดล้อมค่าคงที่ไดอิเล็กทริกเฉพาะที่สูง (high local-dielectric constant environment, $\epsilon = 78$) ผ่านสารเชิงซ้อนซุนเดล (Zundel complex) ในโซ่พันธะไฮโดรเจนแบบเส้นตรง ($n = 3$) ผลการคำนวณผิวพลังงานศักย์สองมิติ (two-dimensional potential energy surface, 2D-PES) ของสารเชิงซ้อนระหว่างกลาง ($n = 1$) แสดงความถี่ที่เป็นลักษณะเฉพาะของการสั่น (vibrational frequencies) และความถี่ที่เป็นลักษณะเฉพาะของ ^1H NMR สำหรับโปรตอนที่เคลื่อนที่บนวิถี oscillatory shuttling และ structural diffusion สามรูปแบบ ซึ่งสามารถนำไปใช้ในการติดตามพลวัตของการแตกตัวของโปรตอนในกลุ่มโมเลกุลที่มีพันธะไฮโดรเจนได้ การจำลองพลวัต BOMD ในช่วงอุณหภูมิ 298–430 K ยืนยันกลไกปฏิกิริยาการแตกตัวและการถ่ายโอนโปรตอนที่เสนอ โดยแสดงความสอดคล้องระหว่างผลการคำนวณทางทฤษฎีและข้อมูลทางการทดลอง เมื่อนำกระบวนการขึ้นกำหนดอัตรา (rate-determining process) ที่เสนอโดยทฤษฎีมาพิจารณา ผลการคำนวณทางทฤษฎียังเสนอบทบาทของตัวทำละลายที่มีขั้ว (polar solvent) และยืนยันว่าพลวัตและกลไกปฏิกิริยาการถ่ายโอนโปรตอนในกลุ่มโมเลกุลที่มีพันธะไฮโดรเจนที่มีประจุบวกสามารถศึกษาจากสารเชิงซ้อนระหว่างกลาง โดยมีข้อแม้ว่าแบบจำลองการละลายล่วงหน้า

ที่เลือกมามีความเหมาะสมและต้องนำกระบวนการขั้นกำหนดอัตราที่สำคัญทุกกระบวนการ
มาพิจารณาในการคำนวณด้วย



สาขาวิชาเคมี
ปีการศึกษา 2558

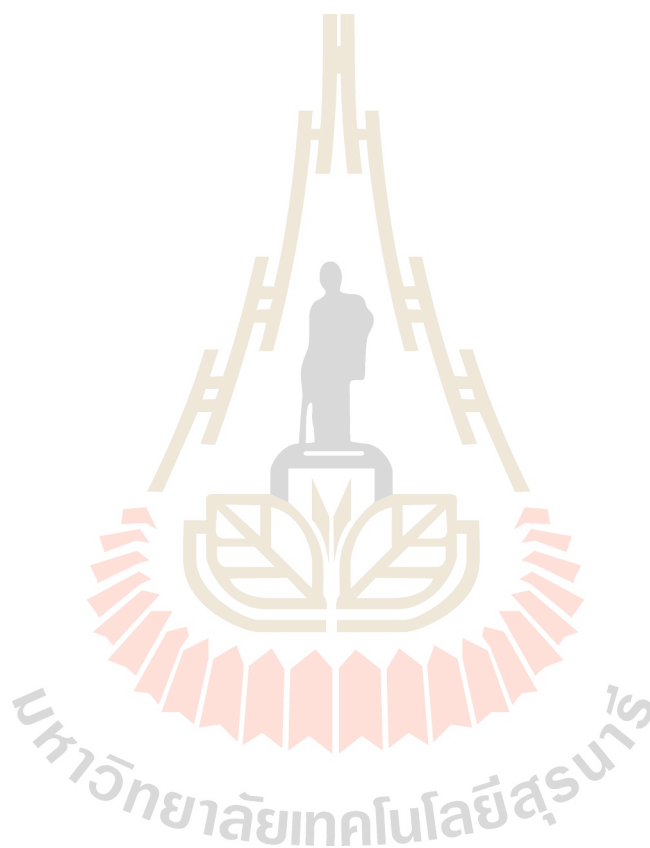
ลายมือชื่อนักศึกษา _____
ลายมือชื่ออาจารย์ที่ปรึกษา _____

PARICHART SUWANNAKHAM : STRUCTURAL DIFFUSION OF
PROTON IN PHOSPHORIC ACID-HYDRONIUM ION-WATER
COMPLEXES. THESIS ADVISOR : PROF. KRITSANA SAGARIK, Ph.D.
122 PP.

H-BOND/PROTON DISSOCIATION/PROTON TRANSFER/PHOSPHORIC ACID/
BOMD SIMULATIONS/VIBRATIONAL SPECTRA/¹H NMR SPECTRA

This thesis studied the dynamics and mechanisms of proton dissociation and transfer in phosphoric acid-hydronium ion-water complexes based on the concept of presolvation using the $\text{H}_3\text{PO}_4\text{-H}_3\text{O}^+\text{-}n\text{H}_2\text{O}$ complexes ($n = 1\text{-}3$) as the model systems and *ab initio* calculations and Born–Oppenheimer molecular dynamics (BOMD) simulations at the RIMP2/TZVP level as model calculations. The static results showed that the smallest, most stable intermediate complex for proton dissociation ($n = 1$) is formed in a low local-dielectric constant environment (*e.g.*, $\epsilon = 1$), whereas proton transfer from the first to the second hydration shell is driven by fluctuations in the number of water molecules in a high local-dielectric constant environment (*e.g.*, $\epsilon = 78$) through the Zundel complex in a linear H-bond chain ($n = 3$). The two-dimensional potential energy surfaces (2D-PES) of the intermediate complex ($n = 1$) suggested three characteristic vibrational and ¹H NMR frequencies associated with a proton moving on the oscillatory shuttling and structural diffusion paths, which can be used to monitor the dynamics of proton dissociation in the H-bond clusters. The BOMD simulations over the temperature range of 298–430 K validated the proposed proton dissociation and transfer mechanisms by showing that good

agreement between the theoretical and experimental data can be achieved with the proposed rate-determining processes. The theoretical results suggest the roles played by the polar solvent and iterate that insights into the dynamics and mechanisms of proton transfer in the protonated H-bond clusters can be obtained from intermediate complexes provided that an appropriate presolvation model is selected and that all of the important rate-determining processes are included in the model calculations.



School of Chemistry

Academic Year 2015

Student's Signature _____

Advisor's Signature _____

ACKNOWLEDGEMENTS

I would like to gratefully and sincerely thank Prof. Dr. Kritsana Sagarik my thesis advisor for his academic guidance, advice, encouragement and support during my graduate studies at Suranaree University of Technology (SUT). Besides my advisor, I would also like to thank thesis committees for their time and comments. My sincere thanks also go to all lecturers at the School of Chemistry, SUT for their help and support. In addition, I would like to express my sincere thanks to Assoc. Prof. Dr. Thomas S. Hofer and Univ.-Prof. Dr. DDDDr.h.c. Bernd Michael Rode for their hospitality and research opportunities at the University of Innsbruck, Austria.

This research work was supported by the Royal Golden Jubilee (RGJ) Ph.D. Program of Thailand Research Fund (TRF) and SUT (Grant No. PHD/0085/2552). Furthermore, I would also like to acknowledge the School of Chemistry and the School of Mathematics, Institute of Science, SUT, as well as the National Electronics and Computer Technology Center and the National Nanotechnology Center for providing computer facilities. The reproduction of the Wiley Materials in this thesis is licensed by John Wiley and Sons, Inc. (license number: 3802230758506).

Finally, I would like to express my deepest gratitude to my parents, sister and brothers for their supports, love and continual encouragement during my education.

Parichart Suwannakham

CONTENTS

	Page
ABSTRACT IN THAI.....	I
ABSTRACT IN ENGLISH.....	III
ACKNOWLEDGEMENTS.....	V
CONTENTS.....	VI
LIST OF TABLES.....	VIII
LIST OF FIGURES.....	IX
LIST OF ABBREVIATIONS.....	XIV
CHAPTER	
I INTRODUCTION.....	1
1.1 Literature reviews.....	1
1.2 References.....	9
II COMPUTATIONAL METHODOLOGY.....	11
2.1 Presolvation model.....	11
2.2 Quantum chemical methods.....	14
2.3 Static calculations.....	16
2.3.1 Structures and energies.....	16
2.3.2 Vibrational and NMR spectra.....	17
2.4 Dynamic calculations.....	20
2.4.1 BOMD simulations.....	20

CONTENTS (Continued)

	Page
2.4.2 Vibrational and NMR spectra.....	22
2.5 References.....	26
III RESULTS AND DISCUSSION.....	32
3.1 Static results.....	32
3.1.1 B3LYP and RIMP2 calculations.....	32
3.1.2 Structures and solvent effects.....	64
3.1.3 Two-dimensional potential energy surfaces.....	70
3.1.4 Characteristic NMR spectra on 2D-PES.....	74
3.2 Dynamic results.....	77
3.2.1 Structures and energies.....	77
3.2.2 Activation energies of proton dissociation and transfer.....	80
3.2.3 Vibrational and NMR spectra.....	83
3.3 References.....	95
IV CONCLUSION.....	97
APPENDICES.....	101
APPENDIX A LIST OF PUBLICATION.....	102
APPENDIX B LIST OF PRESENTATIONS.....	120
CURRICULUM VITAE.....	122

LIST OF TABLES

Table		Page
3.1	Static results of the $\text{H}_3\text{PO}_4\text{-H}_3\text{O}^+ \text{-}n\text{H}_2\text{O}$ complexes, $n = 1\text{--}3$, obtained from B3LYP/TZVP calculations, both in the gas phase and continuum aqueous solution	33
3.2	Static results of the $\text{H}_3\text{PO}_4\text{-H}_3\text{O}^+ \text{-}n\text{H}_2\text{O}$ complexes, $n = 1\text{--}3$, obtained from RIMP2/TZVP calculations, both in the gas phase and continuum aqueous solution	43

LIST OF FIGURES

Figure	Page
1.1 Two-dimensional potential energy surface (2D-PES) as a function of H-bond distances (R_{O-O}) and Asymmetric stretching coordinates (Δd_{DA}) of the Zundel complex, obtained from RIMP2/TZVP calculations.....	7
2.1 Definitions of the velocity vectors used in the calculations of the symmetric and asymmetric O-H stretching frequencies, as well as the O-O vibrational frequencies.....	23
3.1 Linear H-bond structures of the $H_3PO_4-H_3O^+-nH_2O$ complexes ($n = 1-3$) potentially involved in proton dissociation and transfer, obtained from the RIMP2/TZVP calculations in the gas phase and continuum aqueous solvent.....	53
3.2 Correlations between the results obtained from the RIMP2/TZVP and B3LYP/TZVP calculations. ΔE and ΔE^{sol} are interaction and solvation energies, respectively.....	55
3.3 Correlations between the results obtained from the RIMP2/TZVP and B3LYP/TZVP calculations. R_{O-O} = H-bond distances.....	56
3.4 Correlations between the results obtained from the RIMP2/TZVP and B3LYP/TZVP calculations. Δd_{DA} = asymmetric stretching coordinates.....	57

LIST OF FIGURES (Continued)

Figure	Page
3.5	Correlations between the results obtained from the RIMP2/TZVP and B3LYP/TZVP calculations. ν^{OH} = asymmetric O-H stretching frequencies..... 58
3.6	Correlations between the results obtained from the RIMP2/TZVP and B3LYP/TZVP calculations. $\sigma_{\text{H}^+}^{\text{corr}}$ = ^1H NMR shielding constants..... 59
3.7	Plots of the asymmetric O-H stretching frequency (ν^{OH}) as a function of the asymmetric stretching coordinate (Δd_{DA}) in the gas phase and continuum aqueous solvent 61
3.8	Plot of ^1H NMR shielding constant ($\sigma_{\text{H}^+}^{\text{corr}}$) and asymmetric stretching coordinate (Δd_{DA}) in the gas phase 62
3.9	Correlation between the asymmetric O-H stretching frequency (ν^{OH}) and the ^1H NMR shielding constant ($\sigma_{\text{H}^+}^{\text{corr}}$) in the gas phase 63
3.10	Effects of extension of the linear H-bond chains in the gas phase 65
3.11	Effects of extension of the linear H-bond chains in continuum aqueous solvent 67
3.12	Examples of the elementary steps of proton dissociation (I and II) and transfer (III) in $\text{H}_3\text{PO}_4\text{-H}_3\text{O}^+-n\text{H}_2\text{O}$ complexes ($n = 1-3$)..... 69
3.13	Two-dimensional potential energy surface (2D-PES) of a proton in H-bond (1) of structure G2-[1] as a function of H-bond distances ($R_{\text{O-O}}$) and asymmetric stretching coordinate (Δd_{DA}) 72

LIST OF FIGURES (Continued)

Figure	Page
3.14 Two-dimensional potential energy surface (2D-PES) of a proton in H-bond (1) of structure C2-[1] as a function of H-bond distances (R_{O-O}) and asymmetric stretching coordinate (Δd_{DA})	73
3.15 Plots of the ^1H NMR shielding constant ($\sigma_{\text{H}^+}^{\text{corr}}$) and R_{O-H} of a proton on the low-interaction energy path (structural diffusion path, AC) and on the path with the highest $\Delta E^{\ddagger, \text{RIMP2/TZVP}}$ (transition state path, DE), obtained from the RIMP2/TZVP calculations in the gas phase	75
3.16 Plots of the ^1H NMR shielding constant ($\sigma_{\text{H}^+}^{\text{corr}}$) and R_{O-H} of a proton on the low-interaction energy path (structural diffusion path, AC) and on the path with the highest $\Delta E^{\ddagger, \text{RIMP2/TZVP}}$ (transition state path, DE), obtained from the RIMP2/TZVP calculations in continuum aqueous solvent.....	76
3.17 Variations in the H-bond distances (R_{O-O}) and O-H distances (R_{O-H}) in H-bonds determined through BOMD simulations at 298 K. (a) and (b) Structures G2-[1] and C2-[1] , respectively. Panels (I) and (II) are the R_{O-O} and R_{O-H} of H-bond (1) . Panels (III) and (IV) are the R_{O-O} and R_{O-H} of H-bond (2)	79

LIST OF FIGURES (Continued)

Figure	Page
3.18 Variations in the H-bond distances (R_{O-O}) and O-H distances (R_{O-H}) in H-bonds determined through BOMD simulations at 298 K. (a) and (b) Structures G4-[1] and C4-[1] , respectively. Panels (I) and (II) are the R_{O-O} and R_{O-H} of H-bond (1) . Panels (V) and (VI) are the R_{O-O} and R_{O-H} of H-bond (3)	79
3.19 Arrhenius plots obtained from the BOMD simulations over the temperature range of 298–430 K for proton dissociation in H-bond (1) of structure G2-[1]	81
3.20 Arrhenius plots obtained from the BOMD simulations over the temperature range of 298–430 K for proton transfer in H-bond (3) of structure C4-[1]	82
3.21 Vibrational spectra of a proton in H-bond (1) of structure G2-[1] obtained from BOMD simulations at (a) 298 K, (b) 315 K, and (c) 350 K.....	84
3.22 Trends in the characteristic oscillatory shuttling (peak A) and structural diffusion (peaks B and C) frequencies of proton dissociation in H-bond (1) of structure G2-[1] obtained from BOMD simulations over the temperature range of 298–430 K.....	88

LIST OF FIGURES (Continued)

Figure	Page
3.23	Vibrational spectra of proton transfer in H-bond (3) of structure C4-[1] obtained from BOMD simulations at 298 K 89
3.24	Examples of the ^1H NMR chemical shift spectra of proton dissociation in H-bond (1) of structure G2-[1] obtained from BOMD simulations at (a) 350 K, (b) 380 K, and (c) 400 K, respectively 92
3.25	Plots of the natural log of the effective transverse relaxation time (T_2^*) as a function of $1000/T$ for peaks A and B 94

LIST OF ABBREVIATIONS

fs	=	Femtosecond
kJ/mol	=	Kilo Joule per mole
ps	=	Picosecond
wt. %	=	Percentage by weight
A–H···B	=	Hydrogen-bond between the proton donor A and proton acceptor B
d_{A-H}	=	A–H distance
$d_{B···H}$	=	B···H distance
$O··H^+···O$	=	Shared-proton structure
$O-H^+···O$	=	Close-contact structure
CF_3SO_3H	=	Trifluoromethanesulfonic (triflic) acid
H_3PO_3	=	Phosphonic acid
H_3PO_4	=	Phosphoric acid
$H_2PO_4^-$	=	Dihydrogen phosphate anion
$H_3P_2O_7^-$	=	Trihydrogen phosphate anion
$H_4PO_4^+$	=	Protonated phosphoric acid
H^+	=	Proton
H_3O^+	=	Oxonium ion
$H_5O_2^+$	=	Zundel complex
Mg^{2+}	=	Magnesium (II) ion

LIST OF ABBREVIATIONS (Continued)

NO_x	=	Nitrogen oxide
SO_x	=	Sulfur oxide
$-\text{SO}_3\text{H}$	=	Sulfonic acid group
$-\text{SO}_3^-$	=	Sulfonate group
μ	=	Dipole moment
k	=	First-order rate constant
η	=	Viscosity
λ	=	Number of water molecules per phosphonic or phosphoric acid molecule
τ_{res}	=	Relaxation of the hydrogen-bond network
ε	=	Relative permittivity or dielectric constant
T_2^*	=	Effective transverse relaxation times
Δd_{DA}	=	Asymmetric stretching coordinate
Δd_{DA}^*	=	Threshold asymmetric stretching coordinate
$R_{\text{O-O}}$	=	Hydrogen-bond distance
$R_{\text{O-O}}^*$	=	Threshold hydrogen-bond distance
$R_{\text{O-H}}$	=	O-H distance
$\sigma_{\text{H}^+}^{\text{HF}}$	=	Isotropic shielding constants obtained at the Hartree–Fock level
$\sigma_{\text{H}^+}^{\text{RIMP2}}$	=	Isotropic shielding constants obtained at the RIMP2 level

LIST OF ABBREVIATIONS (Continued)

σ_{H^+}	=	Isotropic shielding constant at the B3LYP/TZVP level
$\sigma_{\text{H}^+}^{\text{corr}}$	=	Isotropic shielding constant at the RIMP2/TZVP level
$\sigma_{\text{H}^+}^{\text{corr,MD}}$	=	^1H NMR shielding constant obtained from BOMD simulations at the RIMP2/TZVP level
δ_{H^+}	=	^1H NMR chemical shifts at the B3LYP/TZVP level
$\delta_{\text{H}^+}^{\text{corr}}$	=	^1H NMR chemical shifts at the RIMP2/TZVP level
$\Delta\delta_{\text{H}^+}^{\text{corr,MD}}$	=	The change in the ^1H NMR line width
ν^{OH}	=	Asymmetric O-H stretching frequency
$\nu^{\text{OH}*}$	=	Threshold asymmetric O-H stretching frequency
$\nu^{\text{OH,MD}}$	=	Characteristic asymmetric O-H stretching frequency from MD simulations
$\nu_{\text{A}}^{\text{OH,MD}}$	=	Characteristic asymmetric O-H stretching frequency associated with the oscillatory shuttling motion
$\nu_{\text{B}}^{\text{OH,MD}}$	=	Characteristic asymmetric O-H stretching frequencies associated with the structural diffusion motion (H_3PO_4)
$\nu_{\text{C}}^{\text{OH,MD}}$	=	Characteristic asymmetric O-H stretching frequencies associated with the structural diffusion motion (H_2O)
$\Delta\nu_{\text{BA}}^{\text{OH,MD}}$	=	Vibrational energy for the interconversion between the protonated H_4PO_4^+ (peak B) and shared-proton (peak A)

LIST OF ABBREVIATIONS (Continued)

$\Delta v_{CA}^{\text{OH,MD}}$	=	Vibrational energy for the interconversion between the protonated (H_3O^+ , peak C) and shared-proton (peak A)
ΔE	=	Interaction energy
ΔE^{sol}	=	Solvation energy
$\Delta E^{\ddagger, \text{Arr}}$	=	Activation energies obtained from the Arrhenius equation
$\Delta E^{\ddagger, \text{NMR}}$	=	The activation energies for the exchange between the shared-proton and close-contact structures obtained from the ^1H NMR chemical shift spectra
$\Delta E_{BA}^{\ddagger, \text{vib}}$	=	The activation energies for the interconversion between the protonated H_4PO_4^+ (peak B) and shared-proton (peak A)
$\Delta E_{CA}^{\ddagger, \text{vib}}$	=	The activation energies for the interconversion between the protonated H_3O^+ (peak C) and shared-proton (peak A)
2D-PES	=	Two-dimensional potential energy surface
B3LYP	=	Becke three-parameters hybrid functional combined with Lee-Yang-Parr correlation function
BOMD	=	Born-Oppenheimer molecular dynamics
COSMO	=	Conductor-like screening model
CPMD	=	Car-Parrinello molecular dynamics

LIST OF ABBREVIATIONS (Continued)

D	=	Diffusion coefficient
DFT	=	Density functional theory
FTIR	=	Fourier transform infrared spectroscopy
FWHM	=	Full width at half-maxima
GIAO	=	Gauge including atomic orbital
H-bond	=	Hydrogen bond
HF	=	Hartree-Fock
^1H PFG NMR	=	Proton pulse magnetic field gradient nuclear magnetic resonance
^1H PGSE	=	Proton pulsed gradient Hahn spin-echo technique
^{31}P PGSE	=	Phosphorus pulsed gradient Hahn spin-echo technique
IR	=	Infrared
MD	=	Molecular dynamics
MP2	=	Second order Møller-Plesset perturbation theory
MSD	=	Mean-square displacement
NMR	=	Nuclear magnetic resonance
NVT	=	Canonical ensemble
PBI	=	Polybenzimidazole
PEM	=	Polymer electrolyte membrane
PEMFC	=	Polymer electrolyte membrane fuel cells
PAFC	=	Phosphoric acid fuel cells
QMCF	=	Quantum mechanical charge field

LIST OF ABBREVIATIONS (Continued)

R^2	=	Correlation coefficient
RI	=	Resolution of Identity
RIMP2	=	Resolution of Identity Second-order Møller-Plesset perturbation theory
T-model	=	Test-particle model
TZVP	=	Triple zeta valence plus polarization function
VACF	=	Velocity autocorrelation function

CHAPTER I

INTRODUCTION

1.1 Literature reviews

Fuel cell is a promising energy technology that generates electricity at high efficiency without emission of both greenhouse gas CO₂ and environmental pollutants such as NO_x and SO_x (Ahmed and Föger, 2010). The efficiency of fuel cell depends on transportation of protons (H⁺) generated at the anode across liquid electrolyte or solid proton exchange membrane (PEM) to the cathode (Larminie, Dicks, Larminie, and Dicks, 2013). The majority of commercially available proton exchange membrane fuel cells (PEMFC) use Nafion[®], a polymer electrolyte membrane introduced by DuPont in 1967 (Vincent and Scrosati, 1997). However, PEMFC is too expensive to be competitive or economically-feasible and when operated at high temperature (*e.g.* above 353 K), the porous polymer membrane dehydrates, leading to a significant drop in the performance (Jayashree, Mitchell, Natarajan, Markoski, and Kenis, 2007). For these reasons, the development of alternative proton conducting materials for high temperature fuel cells has been of interest in the past decades (Sundmacher, 2010; Sharaf and Orhan, 2014).

As an acid with proton solvating ability and self-ionization property, concentrated phosphoric acid (H_3PO_4) has been employed effectively in fuel cells (Schuster and Meyer, 2003; Sundmacher, 2010). Through the three hydrogen atoms, H_3PO_4 can form extensive hydrogen-bond (H-bond) network in the liquid state, leading to high efficiency of phosphoric acid fuel cells (PAFC). The self-ionization property and high intrinsic-proton concentration allow the proton transfer process in liquid H_3PO_4 to be nearly exclusively through the structural diffusion mechanism, which is regarded as the protonic-chain conduction mechanism (Greenwood and Thompson, 1959). However, the introduction of an ionizing solute other than water into liquid H_3PO_4 breaks the protonated H-bond chains, resulting in a decrease in its proton conductivity in the liquid state (Munson and Lazarus, 1967). Although theoretical and experimental results on proton transfer reactions have been accumulated, the structural diffusion mechanisms in concentrated and hydrated H_3PO_4 are not completely understood. Since the basic chemistry of H_3PO_4 has been discussed in details in many review articles, only some important theoretical and experimental results relevant to the present study will be briefly summarized.

Dry H_3PO_4 and phosphonic acid (H_3PO_3) were studied in the temperature range of 343–433 K, using ^1H PFG NMR (proton pulse magnetic field gradient nuclear magnetic resonance) and impedance spectroscopy (Schuster, Kreuer, Steininger, and Maier, 2008). The high intrinsic proton conductivity was reported to be due to the fast structural diffusion of proton defects which exist at high concentration and with high self-diffusion coefficient (D). The proton transfer reactions in H_3PO_3 are similar to H_3PO_4 , with a slightly higher number of water molecules per phosphonic acid molecule ($\lambda \approx 2.5$ compared to ≈ 1.5). The lower rate

of structural diffusion compared to vehicle diffusion (about 90% for H_3PO_3 compared to about 98% for H_3PO_4) was concluded to be a consequence of weaker H-bond network formed from H_3PO_3 compared to H_3PO_4 . It was proposed that, H_3PO_3 could be immobilized to organic structure by forming stable P-C covalent bonds, leading to a new type of effective polymeric proton conducting materials applicable in PEMFC.

Structures and energetic of proton transfer in H_3PO_4 clusters were studied using quantum chemical calculations at the B3LYP/6-311G** level and two to six H_3PO_4 molecules as model systems (Vilčiauskas, Paddison, and Kreuer, 2009). The interaction energies of the H_3PO_4 clusters were found to correlate with the number and type of H-bonds in the clusters, with the stabilities increasing up to and including $(\text{H}_3\text{PO}_4)_6$. B3LYP/6-311G** calculations revealed how H_3PO_4 molecules in the clusters facilitate proton transfer, whereas the calculations of the partial atomic charges both before and after proton transfers indicated a higher degree of charge delocalization in larger clusters.

Microscopic mechanism of proton transfer in neat liquid H_3PO_4 was discussed based on the results of Car-Parrinello molecular dynamics (CPMD) simulations on 54 H_3PO_4 molecules (Vilčiauskas, Tuckerman, Bester, Paddison, and Kreuer, 2012), in which the fast proton transfer was suggested to involve a structural diffusion which is driven by specific H-bond rearrangements in the surrounding environment. It was concluded that, in neat liquid H_3PO_4 , strong, polarizable H-bonds produce coupled-proton motion, and a pronounced protic dielectric response of the medium, which lead to the formation of extended, polarized H-bond chain, whereas in aqueous media, proton can only be displaced over short distances, and the transportation of excess charge defects is driven by “local H-bond rearrangement” (Vilčiauskas, Tuckerman,

Bester, Paddison, and Kreuer, 2012). The extent of the H-bond network of water affected in the presence of proton was studied (Tielrooij, Timmer, Bakker, and Bonn, 2009), in which structure dynamics of the proton in liquid water were investigated using terahertz time-domain spectroscopy and polarization-resolved femtosecond mid infrared pump-probe spectroscopy, and the number of affected water molecules around protons were reported. In contrast to the conclusion in Vilčiauskas *et al.*, it was found that “addition of protons results in a very strong decrease of the dielectric response of liquid water that corresponds to 1962 water molecules per dissolved proton. The depolarization results from water molecules (about 4) that are irrotationally bound to the proton and from the motion of water (corresponding to the response of about 15 water molecules) involved in the transfer of the proton charge.” Small and multivalent cations have stronger hydration, and larger depolarization effects, for example, only about 10 water molecules are affected by addition of larger cations such as Mg^{2+} .

In aqueous solution, self-diffusion coefficients of mobile species in 85 wt% (14.6 M) of H_3PO_4 in the temperature range of 293–353 K were studied using 1H and ^{31}P pulsed gradient Hahn spin-echo (PGSE) techniques (Chung, Bajue, and Greenbaum, 2000). The values of the self-diffusion coefficients (D) showed that proton diffuses much faster than the phosphorus carrying species. Most importantly, the dynamic information obtained from both nuclear species revealed a linear relationship of the Arrhenius plot, with the activation energies of 25 and 36 kJ/mol for 1H and ^{31}P species, respectively. Based on the temperature dependence of $D \times \eta$, water-mediated proton transfer between phosphate groups was proposed. Chung *et al.* (2000) suggested that two approaches were applied in the calculations of

the activation energies namely, from the slope of the linewidth-temperature dependence (the full width at half-maxima or FWHM), and from a simple Arrhenius-type equation. It was reported that the activation energies obtained from the conventional ^1H NMR (FWHM) and ^1H PGSE NMR techniques (Arrhenius-type equation) are not the same due to different time and length scales probed by each technique; the conventional ^1H NMR probes microscopic dynamics, whereas the ^1H NMR PGSE is sensitive to macroscopic motions (Chung, Bajue, and Greenbaum, 2000). Analyses of the results obtained from these two ^1H NMR techniques yielded the activation energies of 11 and 25 kJ/mol, respectively. Because the conventional ^1H NMR peaks showed motional narrowing at elevated temperatures, this thesis anticipated that the smaller activation energy (11 kJ/mol) is associated with the local motions such as rotations.

At Computational Chemistry Research Laboratory, School of Chemistry, Suranaree University of Technology, the characteristic vibrational and ^1H NMR spectra of the transferring protons in protonated water clusters were studied through theoretical methods using the $\text{H}^+(\text{H}_2\text{O})_n$ complexes ($n = 2-5$) as model systems and *ab initio* calculations at the RIMP2/TZVP level and Born–Oppenheimer molecular dynamics (BOMD) simulations as the model calculations (Lao-ngam, Phonyiem, Chaiwongwattana, Kawazoe, and Sagarik, 2013). The theoretical investigations were based on the concept of presolvation (Vilčiauskas, Tuckerman, Bester, Paddison, and Kreuer, 2012), and a presolvation model was selected and used in the static and dynamic calculations. The two-dimensional potential energy surface (2D-PES) of the proton (Figure 1.1) in the smallest, most stable intermediate complex (the Zundel complex, H_5O_2^+) was constructed as a function of the H-bond distance ($R_{\text{O}\cdots\text{O}}$) and the

asymmetric stretching coordinate (Δd_{DA}), and this information was used to identify and characterize the low-interaction energy path (structural diffusion path) and the path with $\Delta d_{DA} = 0$ Å (oscillatory shuttling path). For these strong, protonated H-bonds, the *ab initio* gauge including atomic orbital (GIAO) method showed that the ^1H NMR shielding constant ($\sigma_{\text{H}^+}^{\text{corr}}$) of the proton moving on the oscillatory shuttling path varies over a narrow range and is sensitive only to the H-bond distances ($R_{\text{O-O}}$ and $R_{\text{O-H}}$) and not to the water coordination number and the local chemical environment. In contrast, the $\sigma_{\text{H}^+}^{\text{corr}}$ of a proton moving on the structural diffusion path varies exponentially with $R_{\text{O-H}}$. The BOMD simulations over the temperature range 350–430 K revealed that the activation energies for proton exchange in the smallest, most stable intermediate complex, which were obtained from the first-order rate constants (k), vibrational spectra, and a simple ^1H NMR line-shape analysis, are consistent and in good agreement with the experimental results. The theoretical results suggested guidelines and possibilities, as well as a complementary method, for the study of the structural diffusion processes in strong, protonated H-bonds using vibrational and ^1H NMR spectra.

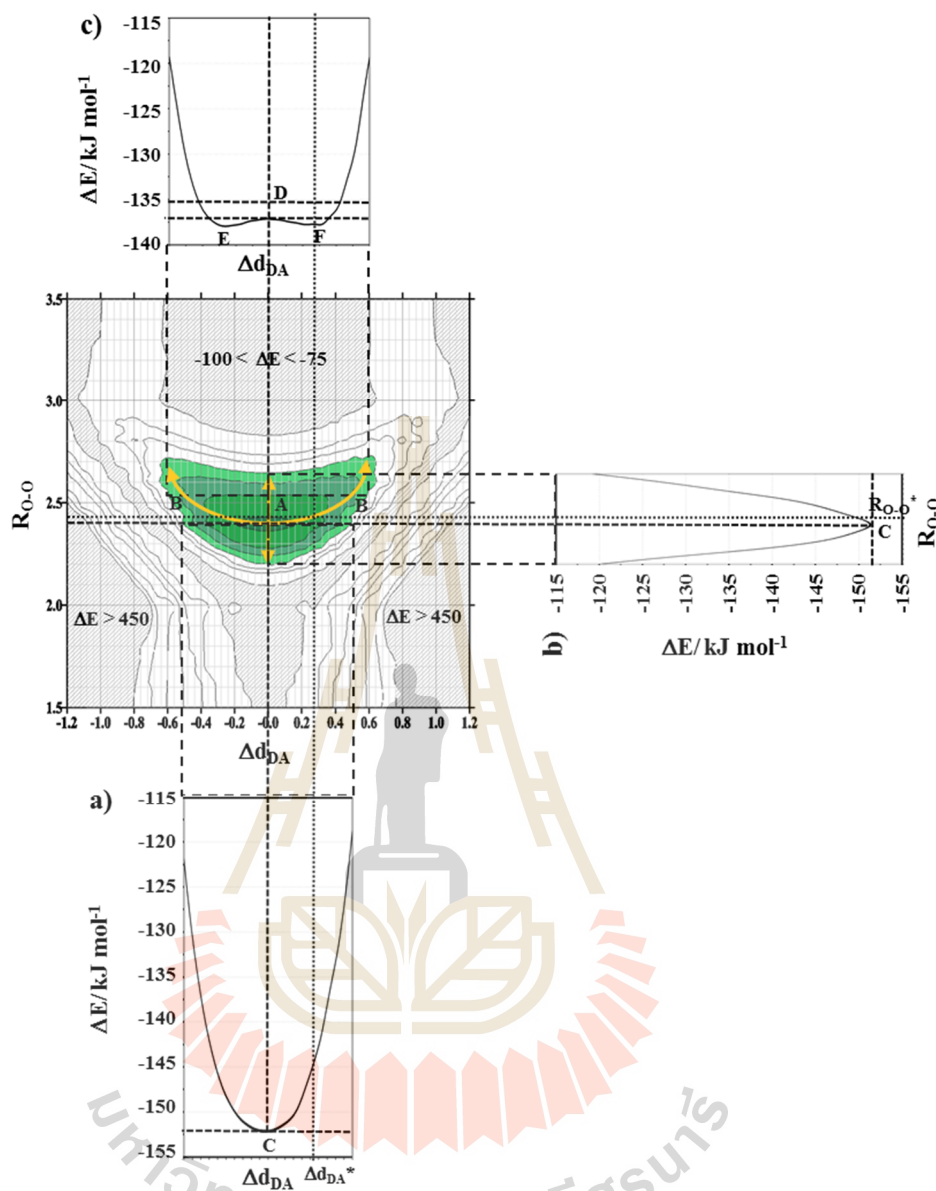
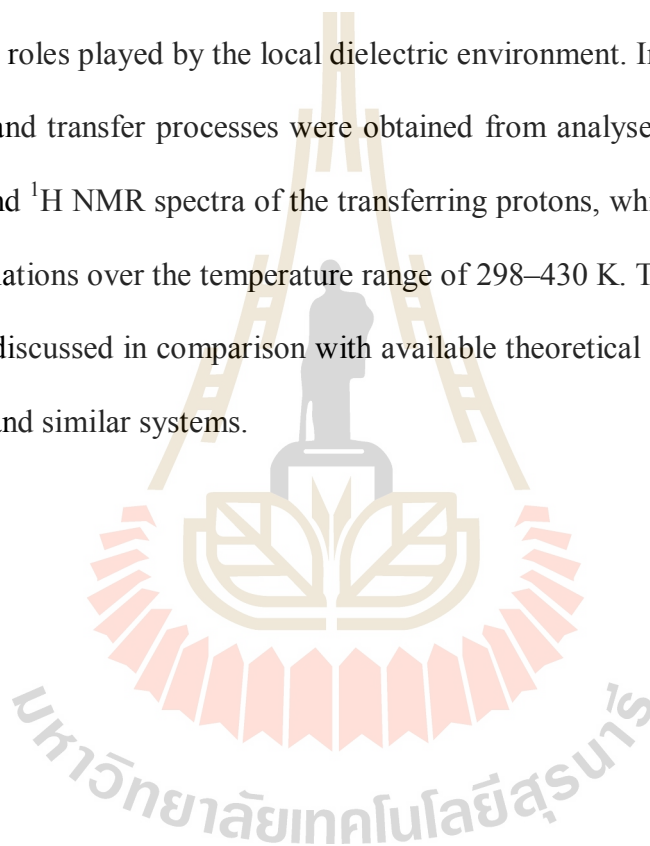


Figure 1.1 Two-dimensional potential energy surface as a function of R_{O-O} and Δd_{DA} of the Zundel complex, obtained from RIMP2/TZVP calculations. a) and b) Single-well potential at C. c) Double-well potential at E and F. R_{O-O} = H-bond distance; R_{O-O}^* = threshold H-bond distance; Δd_{DA} = asymmetric stretching coordinate; Δd_{DA}^* = threshold asymmetric stretching coordinate. both positive and negative values of Δd_{DA} were used in the plot (Lao-ngam, Phonyiem, Chaiwongwattana, Kawazoe, and Sagarik, 2013).

To acquire fundamental information on proton conduction in PAFC, the dynamics and mechanisms of proton dissociation and transfer in hydrated H_3PO_4 clusters under excess proton conditions were studied in this work. The theoretical study emphasized the dynamics and H-bond arrangements in a short-time scale which could promote intermediate complex formation, and showed how H_3O^+ and H_5O_2^+ facilitate and mediate proton dissociation and transfer in the hydrated H_3PO_4 clusters, as well as the roles played by the local dielectric environment. Insights into the proton dissociation and transfer processes were obtained from analyses of the characteristic vibrational and ^1H NMR spectra of the transferring protons, which were derived from BOMD simulations over the temperature range of 298–430 K. The static and dynamic results were discussed in comparison with available theoretical and experimental data on the same and similar systems.



1.2 References

- Ahmed, K., and Föger, K. (2010). Fuel Processing for High-Temperature High-Efficiency Fuel Cells. **Industrial & Engineering Chemistry Research**. 49: 7239-7256.
- Chung, S. H., Bajue, S., and Greenbaum, S. G. (2000). Mass transport of phosphoric acid in water: A ^1H and ^{31}P pulsed gradient spin-echo nuclear magnetic resonance study. **The Journal of Chemical Physics**. 112: 8515-8521.
- Greenwood, N. N., and Thompson, A. (1959). 701. The mechanism of electrical conduction in fused phosphoric and trideuterophosphoric acids. **Journal of the Chemical Society (Resumed)**: 3485-3492.
- Jayashree, R. S., Mitchell, M., Natarajan, D., Markoski, L. J., and Kenis, P. J. A. (2007). Microfluidic Hydrogen Fuel Cell with a Liquid Electrolyte. **Langmuir**. 23: 6871-6874.
- Lao-ngam, C., Phonyiem, M., Chaiwongwattana, S., Kawazoe, Y., and Sagarik, K. (2013). Characteristic NMR spectra of proton transfer in protonated water clusters. **Chemical Physics**. 420: 50-61.
- Larminie, J., Dicks, A., Larminie, J., and Dicks, A. (2013). Introduction *Fuel Cell Systems Explained* (pp. 1-24): John Wiley & Sons, Ltd.,
- Munson, R. A., and Lazarus, M. E. (1967). Influence of ionic solutes upon the conductivity of molten phosphoric acid. **The Journal of Physical Chemistry**. 71: 3245-3248.
- Schuster, M., Kreuer, K.-D., Steininger, H., and Maier, J. (2008). Proton conductivity and diffusion study of molten phosphonic acid H_3PO_3 . **Solid State Ionics**. 179: 523-528.

- Schuster, M. F. H., and Meyer, W. H. (2003). Anhydrous proton-conducting polymers. **Annual Review of Materials Research**. 33: 233-261.
- Sharaf, O. Z., and Orhan, M. F. (2014). An overview of fuel cell technology: Fundamentals and applications. **Renewable and Sustainable Energy Reviews**. 32: 810-853.
- Sundmacher, K. (2010). Fuel Cell Engineering: Toward the Design of Efficient Electrochemical Power Plants. **Industrial & Engineering Chemistry Research**. 49: 10159-10182.
- Tielrooij, K. J., Timmer, R. L. A., Bakker, H. J., and Bonn, M. (2009). Structure Dynamics of the Proton in Liquid Water Probed with Terahertz Time-Domain Spectroscopy. **Physical Review Letters**. 102: 198303.
- Vilčiauskas, L., Paddison, S. J., and Kreuer, K.-D. (2009). *Ab Initio* Modeling of Proton Transfer in Phosphoric Acid Clusters. **The Journal of Physical Chemistry A**. 113: 9193-9201.
- Vilčiauskas, L., Tuckerman, M. E., Bester, G., Paddison, S. J., and Kreuer, K.-D. (2012). The mechanism of proton conduction in phosphoric acid. **Nature Chemistry**. 4: 461-466.
- Vincent, C. A., and Scrosati, B. (1997). 1 - Introduction. In C. A. V. Scrosati (Ed.), *Modern Batteries (Second Edition)* (pp. 1-17). Oxford: Butterworth-Heinemann.

CHAPTER II

COMPUTATIONAL METHODOLOGY

2.1 Presolvation model

Because proton transfers in H-bonds are complicated, care must be exercised in selecting the model systems. In this work, the concept of presolvation (Greenwood and Thompson, 1959) was applied in the study of proton dissociation and transfer in hydrated H_3PO_4 clusters; “the local energy fluctuations and dynamics in aqueous solution lead to the weakening or breaking of some H-bonds in the first and second hydration shells, resulting in a reduction in the water coordination number such that the proton accepting species possesses a hydration structure corresponding to the species into which it will be transformed to complete the structural diffusion process” (Chaiwongwattana, Lao-ngam, Phonyiem, Vchirawongkwin, and Sagarik, submitted). Because some H-bonds in the first and second hydration shells are instantaneously disrupted, the presolvation state can be resolved, and the dynamics of the structural diffusion process can be studied using an appropriate presolvation model. The formation of the presolvation state generally requires removal of some solvent environment, and takes place through the protonic-chain conduction mechanism (Greenwood and Thompson, 1959; Glezakou, Dupuis, and Mundy, 2007; Sagarik, Phonyiem, Lao-ngam, and Chaiwongwattana, 2008; Phonyiem, Chaiwongwattana, Lao-ngam, and Sagarik, 2011; Lao-ngam, Phonyiem, Chaiwongwattana, Kawazoe, and Sagarik, 2013). The concept of presolvation is supported by the observation that,

due to the local geometrical requirements, H-bonds in aqueous solution can be considered as “forming” or “breaking”; experiments based on thermochemistry and vibrational spectroscopy have shown that 10–70% of H-bonds in water can be considered as broken within the temperature range of 273–299 K (Watts and McGee, 1976). Although the proton dissociation and transfer processes in hydrated H_3PO_4 clusters are the main interest, some fundamental information on concentrated H_3PO_4 solutions can be used as guidelines to construct the presolvation model as follows. According to experiments (Munson and Lazarus, 1967), the equilibriums in concentrated H_3PO_4 solution at 16.8 M can be represented by



and the fast proton transfer involves the self-dissociation and dehydration reactions in equations (2.1) and (2.2), respectively. Based on the equilibrium constants at 298 K, Chung *et al.* suggested that the dominant species in 85 wt.% (14.6 M) H_3PO_4 solution is undissociated H_3PO_4 (97.6%), the presence of condensed phosphates can be neglected, and the mechanism for anion (H_2PO_2^-) transport is vehicular type (Chung, Bajue, and Greenbaum, 2000). These findings are supplemented by the experimental results in Munson *et al.*, in which H_3PO_4 , H_4PO_4^+ , and H_3O^+ were concluded to play the most important roles in the structural diffusion in the liquid and concentrated solution (Munson and Lazarus, 1967). Therefore, the presolvation models for proton dissociation and transfer consist of H_3PO_4 , H_2O , H_4PO_4^+ , and H_3O^+ ; the protonated forms must be included to represent the acid conditions. The size of the presolvation

model was determined based on the theoretical study in Vilčiauskas, in which the extent of the Grotthuss chains in equimolar mixture of H_3PO_4 and H_2O (1:1 molar ratio) was examined using CPMD simulations. It appeared that the properties of the H-bonds in this system are virtually identical to those of pure H_3PO_4 (no resemblance to liquid water), and the weak solvent coupling and sufficient degree of configurational disorder result in fast proton transport. Based on the proton coupling correlation function as a function of H-bond connectivity, the probability of two quasicohherent proton transfer events within two neighboring H-bonds is about 4% when the relaxation of the H-bond network, $\tau_{\text{res}} = 0$ fs, about two times lower than in neat liquid H_3PO_4 . As the relay time parameter increased to $\tau_{\text{res}} = 50$ fs, the probabilities to form chains of three and four consecutive H-bonds are about 18 and 2%, respectively. Because the probability to form four consecutive H-bonds is significantly lower than that in neat liquid H_3PO_4 (about 10%), the authors concluded that the presence of water opposes the formation of extensive Grotthuss chains (Vilčiauskas, 2012; Vilčiauskas, Tuckerman, Bester, Paddison, and Kreuer, 2012), and one could anticipate that four consecutive H-bonds are sufficient to take into account the quasicohherent proton transfer events in the hydrated H_3PO_4 systems. Additionally, because the dynamics in short time and short length scales are of interest, and the cation in the present system is a protonated H_3PO_4 , which is considerably larger than proton and Mg^{2+} (Tielrooij, Timmer, Bakker, and Bonn, 2009), it is reasonable to anticipate that the number of affected water molecules are much less than these two cations. Based on the above discussions, and because the dynamics of protons in the intermediate complexes in a short-time scale are of interest, to implement the concept of presolvation, the H-bond clusters formed from

H_3PO_4 , H_3O^+ , and $n\text{H}_2\text{O}$ ($n = 1-3$) were proposed as a candidate presolvation model. The proposed presolvation model was confirmed by static and dynamic calculations, which revealed that the intermediate complexes of proton dissociation and transfer (with shared-proton structures) are formed only in the H-bond clusters with $n \leq 3$. In this study, H_4PO_4^+ and H_3PO_4 are considered the protonated and deprotonated forms, respectively.

2.2 Quantum chemical methods

Three basic steps that were applied successfully in the previous investigations were used in this work (Böhm and Ahlrichs, 1985; Sagarik, 1999; Sagarik and Dokmaisrijan, 2005): (1) searching for the intermediate complexes in the proton transfer pathway using the Test-particle model (T-model) potentials (Böhm and Ahlrichs, 1982; Böhm and Ahlrichs, 1985; Sagarik and Ahlrichs, 1987; Sagarik, Pongpituk, Chaiyapongs, and Sisot, 1991; Sagarik and Spohr, 1995; Sagarik and Asawakun, 1997; Sagarik, 1999; Sagarik and Rode, 2000; Sagarik, Chaiwongwattana, and Sisot, 2004; Sagarik and Chaiyapongs, 2005; Sagarik and Dokmaisrijan, 2005); (2) refining the T-model-optimized structures using an accurate quantum chemical method; and (3) performing BOMD simulations on the candidate intermediate complexes using the refined structures as the starting configurations. Because the effects of electron correlations may play important roles in the present model systems, the quantum chemical calculations were performed using the second-order Møller–Plesset perturbation theory (MP2) with the resolution of the identity (RI) approximation and the TZVP basis set (this process is abbreviated RIMP2/TZVP calculations) (Weigend and Häser, 1997). Additionally, due to the potential

applications of the density functional theory (DFT) methods in the study of proton transfer in larger H-bond systems and the fact that the previous theoretical results were reported based on B3LYP/TZVP calculations (Sagarik, Chaiwongwattana, Vchirawongkwin, and Prueksaaron, 2010; Lao-ngam, Asawakun, Wannarat, and Sagarik, 2011; Phonyiem, Chaiwongwattana, Lao-ngam, and Sagarik, 2011), quantum chemical calculations were also conducted at this level of theory. The applicability and performance of RIMP2/TZVP and B3LYP/TZVP calculations were compared and discussed. Additionally, to study the effects of a polar solvent on proton dissociation and transfer, a continuum aqueous solvent was included in the model calculations. Because the conductor-like screening model (COSMO) (Klamt and Schuurmann, 1993) was applied successfully in similar H-bond systems (Sagarik, Chaiwongwattana, Vchirawongkwin, and Prueksaaron, 2010; Lao-ngam, Asawakun, Wannarat, and Sagarik, 2011; Phonyiem, Chaiwongwattana, Lao-ngam, and Sagarik, 2011), the proton dissociation and transfer were studied both in the gas phase and in COSMO with $\epsilon = 78$. All of the theoretical calculations were performed using TURBOMOLE 6.4.

2.3 Static calculations

2.3.1 Structures and energies

The absolute and local minimum energy geometries of the $\text{H}_3\text{PO}_4\text{-H}_3\text{O}^+-n\text{H}_2\text{O}$ complexes ($n = 1-3$), which were obtained from the T-model potentials, were refined using both B3LYP/TZVP and RIMP2/TZVP geometry optimizations. The tendency of proton dissociation and transfer, as well as the structure of the smallest, most stable intermediate complex, in the presolvation model were primarily anticipated from the asymmetric stretching coordinate (Δd_{DA}), which was computed from

$$\Delta d_{\text{DA}} = |d_{\text{A-H}} - d_{\text{B}\cdots\text{H}}|, \quad (2.4)$$

where $d_{\text{A-H}}$ and $d_{\text{B}\cdots\text{H}}$ are the A-H and B \cdots H distances in the A-H \cdots B H-bond, respectively. The interaction energies (ΔE) of the H-bond complexes were computed from

$$\Delta E = E(\text{H}_3\text{PO}_4\text{-H}_3\text{O}^+-n\text{H}_2\text{O}) - [E(\text{H}_3\text{PO}_4) + E(\text{H}_3\text{O}^+) + nE(\text{H}_2\text{O})], \quad (2.5)$$

where $E(\text{H}_3\text{PO}_4\text{-H}_3\text{O}^+-n\text{H}_2\text{O})$ is the total energy of the optimized structure of the $\text{H}_3\text{PO}_4\text{-H}_3\text{O}^+-n\text{H}_2\text{O}$ complex; $E(\text{H}_3\text{PO}_4)$, and $E(\text{H}_3\text{O}^+)$ and $E(\text{H}_2\text{O})$ are the total energies of the optimized structures of the isolated species (Lao-ngam, Asawakun, Wannarat, and Sagarik, 2011; Phonyiem, Chaiwongwattana, Lao-ngam, and Sagarik, 2011). The solvation energies (COSMO with $\varepsilon = 78$) were approximated by

$$\Delta E^{\text{sol}} = E(\text{H}_3\text{PO}_4\text{-H}_3\text{O}^+\text{-}n\text{H}_2\text{O})^{\text{COSMO}} - E(\text{H}_3\text{PO}_4\text{-H}_3\text{O}^+\text{-}n\text{H}_2\text{O}), \quad (2.6)$$

where $E(\text{H}_3\text{PO}_4\text{-H}_3\text{O}^+\text{-}n\text{H}_2\text{O})^{\text{COSMO}}$ and $E(\text{H}_3\text{PO}_4\text{-H}_3\text{O}^+\text{-}n\text{H}_2\text{O})$ are the total energies of the optimized structures obtained with and without COSMO, respectively (Lao-ngam, Asawakun, Wannarat, and Sagarik, 2011; Phonyiem, Chaiwongwattana, Lao-ngam, and Sagarik, 2011). Because the dynamics of a proton are governed by the potential energy surface on which the transferring proton moves and the O-O and O-H⁺ vibrations in the O-H⁺...O H-bond are coupled (Sagarik, Phonyiem, Lao-ngam, and Chaiwongwattana, 2008), to provide energetic information for the discussion of the structural diffusion process, two-dimensional potential energy surfaces (2D-PES) of the transferring proton in the smallest, most stable intermediate complex were constructed both in the gas phase and in COSMO through the calculation of ΔE at various $R_{\text{O-O}}$ and $R_{\text{O-H}}$ distances (Lao-ngam, Phonyiem, Chaiwongwattana, Kawazoe, and Sagarik, 2013). Two sets of equally spaced grid points were generated from ΔE and 2D-PES and plotted as a function of $R_{\text{O-O}}$ and Δd_{DA} using the SURFER program ("SURFER for Window," 1997). The interaction energy path connecting the single- and double-well potentials, as well as the path with the highest energy barriers, were identified and studied in detail.

2.3.2 Vibrational and NMR spectra

To obtain vibrational signatures of the transferring protons which can be used as guidelines for the discussion of the dynamic results, the harmonic vibrational frequencies of molecules in the presolvation model were computed from the numerical second derivatives of the B3LYP/TZVP and RIMP2/TZVP total energies, from which analyses of the normal modes in terms of the internal

coordinates were made using the NUMFORCE and AOFORCE programs, respectively (TURBOMOLE Tutorial 6.4). The programs are included in TURBOMOLE 6.4 (TURBOMOLE Tutorial 6.4; Ahlrichs, Bär, Häser, Horn, and Kölmel, 1989; Treutler and Ahlrichs, 1995). Only the asymmetric O-H stretching frequencies of the H-bond protons (ν^{OH}) were analyzed and discussed in detail (Sagarik, Phonyiem, Lao-ngam, and Chaiwongwattana, 2008; Sagarik, Chaiwongwattana, Vchirawongkwin, and Prueksaaron, 2010; Lao-ngam, Asawakun, Wannarat, and Sagarik, 2011; Phonyiem, Chaiwongwattana, Lao-ngam, and Sagarik, 2011). The threshold asymmetric O-H stretching frequencies of proton dissociation from H_4PO_4^+ (ν^{OH^*}) were estimated from the plots of ν^{OH} and Δd_{DA} (Lao-ngam, Asawakun, Wannarat, and Sagarik, 2011; Phonyiem, Chaiwongwattana, Lao-ngam, and Sagarik, 2011). The relationships between ν^{OH} and Δd_{DA} were represented by the reflected normal distribution functions, the second derivatives of which are equal to zero at $\nu^{\text{OH}} = \nu^{\text{OH}^*}$ (Lao-ngam, Asawakun, Wannarat, and Sagarik, 2011; Phonyiem, Chaiwongwattana, Lao-ngam, and Sagarik, 2011). For the B3LYP/TZVP and RIMP2/TZVP calculations, the scaling factors of 0.9614 (Scott and Radom, 1996) and 0.9434 (TURBOMOLE Tutorial 6.4) were used in the calculations of the vibrational frequencies, respectively. Since proton transfers in H-bond are coupled with various degrees of freedom.

As an effective probe for H-bond formation (Konrat, Tollinger, Kontaxis, and Kräutler, 1999), isotropic shielding constants were computed at both the RIMP2/TZVP and the B3LYP/TZVP levels (Taubert, Konschin, and Sundholm, 2005) using the GIAO method (Ditchfield, 1974; Ditchfield, 1976). The ^1H NMR

shielding constants at the RIMP2/TZVP level ($\sigma_{\text{H}^+}^{\text{corr}}$) were derived from (Chesnut, 1995)

$$\sigma_{\text{H}^+}^{\text{corr}} = \sigma_{\text{H}^+}^{\text{HF}} + 2/3(\sigma_{\text{H}^+}^{\text{RIMP2}} - \sigma_{\text{H}^+}^{\text{HF}}), \quad (2.7)$$

where $\sigma_{\text{H}^+}^{\text{HF}}$ and $\sigma_{\text{H}^+}^{\text{RIMP2}}$ are the isotropic shielding constants obtained at the Hartree–Fock and RIMP2 levels, respectively. The ^1H NMR chemical shifts of the H-bond protons ($\delta_{\text{H}^+}^{\text{corr}}$) were derived from $\sigma_{\text{H}^+}^{\text{corr}}$ with respect to tetramethylsilane (Harris *et al.*, 2008), which was computed at the MP2/TZVP level to be 31.97 ppm (Taubert, Konschin, and Sundholm, 2005). Based on the observation that the isotropic shielding constants of protons in strong, protonated H-bonds depend only on the H-bond distance ($R_{\text{O-O}}$) and not the neighboring water molecules (Chesnut and Rusiloski, 1994) and the conclusion that the effects of a continuum solvent (reaction field) on the H-bond structures are small (Chesnut and Rusiloski, 1994; Chesnut, 2005; Taubert, Konschin, and Sundholm, 2005), it is reasonable to discuss only the ^1H NMR shielding constants of the smallest, most stable intermediate complex in the gas phase (Lao-ngam, Phonyiem, Chaiwongwattana, Kawazoe, and Sagarik, 2013). To correlate the ^1H NMR shielding constants with the structures of 2D-PES, the $\sigma_{\text{H}^+}^{\text{corr}}$ of the proton on the structural diffusion (the low-interaction energy path connecting the single- and double-well potentials) and oscillatory shuttling paths (the path with $\Delta d_{\text{DA}} \approx 0 \text{ \AA}$) were computed and plotted as a function $R_{\text{O-H}}$ (Lao-ngam, Phonyiem, Chaiwongwattana, Kawazoe, and Sagarik, 2013)

2.4 Dynamic calculations

2.4.1 BOMD simulations

The equilibrium structures of the model systems obtained from the RIMP2/TZVP calculations were used as the starting configurations in BOMD simulations. In the previous work (Lao-ngam, Asawakun, Wannarat, and Sagarik, 2011; Phonyiem, Chaiwongwattana, Lao-ngam, and Sagarik, 2011; Chaiwongwattana, Phonyiem, Vchirawongkwin, Prueksaaron, and Sagarik, 2012), the applicability and performance of the NVT ensemble for the study of the dynamics of proton transfer were examined in detail. Because the energy released and absorbed during the proton transfer process can be managed by a thermostat bath, the local temperature can be maintained throughout the course of the NVT-BOMD simulations provided that an appropriate thermostat relaxation time is chosen. In the previous and present work, a Nosé-Hoover chain thermostat (Nosé and Klein, 1983; Nosé, 1984; Hoover, 1985; Shuichi, 1991) was applied to each degree of freedom in the model systems, and a thermostat relaxation that was 20-fold larger than the time step was proven to be appropriate for the generation of reasonable local-energy fluctuations (Sagarik, Chaiwongwattana, Vchirawongkwin, and Prueksaaron, 2010; Lao-ngam, Asawakun, Wannarat, and Sagarik, 2011; Phonyiem, Chaiwongwattana, Lao-ngam, and Sagarik, 2011; Chaiwongwattana, Phonyiem, Vchirawongkwin, Prueksaaron, and Sagarik, 2012; Lao-ngam, Phonyiem, Chaiwongwattana, Kawazoe, and Sagarik, 2013). As an example (Lao-ngam, Phonyiem, Chaiwongwattana, Kawazoe, and Sagarik, 2013), the NVT-BOMD simulations of the Zundel complex at 350 K yielded local energy fluctuation of only approximately 0.4 kJ/mol/degree of freedom compared with the activation energy obtained from the ^1H NMR measurements of

approximately 10 kJ/mol (Luz and Meiboom, 1964). Additionally, to confirm that the energetics and dynamics are well represented, energy conservation and mean-square displacements (MSD) plots were constructed (Chaiwongwattana, Phonyiem, Vchirawongkwin, Prueksaaron, and Sagarik, 2012). Because the trend of the energy conservation plot showed no systematic drift and the correct linear relationship was obtained for the MSD plot, one can conclude that the dynamics of the transferring proton, which were obtained under the present NVT-BOMD simulations conditions, including the Nosé-Hoover thermostat, are reasonable and very well represented, especially in the case in which the structures of the model systems are at equilibrium and not substantially changed in the BOMD simulations. In this work, 2000 and 20000 BOMD steps of 1 fs were devoted to the equilibration and the property calculations, corresponding to 2 and 20 ps, respectively. The activation energies ($\Delta E^{\ddagger, \text{Arr}}$) of proton dissociation and transfer from the first hydration shell were determined from the Arrhenius equation by performing BOMD simulations over the temperature range of 298–430 K. The first-order rate constants (k) for the exchange between the shared-proton ($\text{O}\cdots\text{H}^+\cdots\text{O}$) and close-contact ($\text{O}-\text{H}^+\cdots\text{O}$) structures were approximated from the exponential relaxation behavior of the envelopes of the velocity autocorrelation functions (VACF) of the O-O vibrations (Lao-ngam, Asawakun, Wannarat, and Sagarik, 2011; Phonyiem, Chaiwongwattana, Lao-ngam, and Sagarik, 2011; Chaiwongwattana, Phonyiem, Vchirawongkwin, Prueksaaron, and Sagarik, 2012; Lao-ngam, Phonyiem, Chaiwongwattana, Kawazoe, and Sagarik, 2013) and the $\Delta E^{\ddagger, \text{Arr}}$ from the linear relationship between $\ln(k)$ and $1000/T$.

2.4.2 Vibrational and NMR spectra

Because the harmonic approximation yields reliable vibrational frequencies only at stationary points on the total energy surface, to completely understand the vibrational behaviors of the transferring protons, especially in distorted H-bond structures, BOMD simulations must be performed, from which the vibrational spectra were determined by Fourier transformation of the VACF. Because conventional vibrational analysis of the VACF of atoms cannot not yield the information on the types of motions associated with the frequencies of interest, attempt was made in Bopp (1986) to describe vibrational modes using an appropriate correlation function technique. In this approach, the velocity vectors associated with the vibrational modes were defined and used in the calculations of the VACF, from which the vibrational spectra and the lifetimes of the motions were computed. In the previous work (Lao-ngam, Asawakun, Wannarat, and Sagarik, 2011; Phonyiem, Chaiwongwattana, Lao-ngam, and Sagarik, 2011; Chaiwongwattana, Phonyiem, Vchirawongkwin, Prueksaaron, and Sagarik, 2012; Lao-ngam, Phonyiem, Chaiwongwattana, Kawazoe, and Sagarik, 2013), the symmetric and asymmetric O-H stretching frequencies, as well as the O-O vibrational frequencies, were computed using the predefined-velocity vectors in Figure 2.1. (Bopp, 1986)

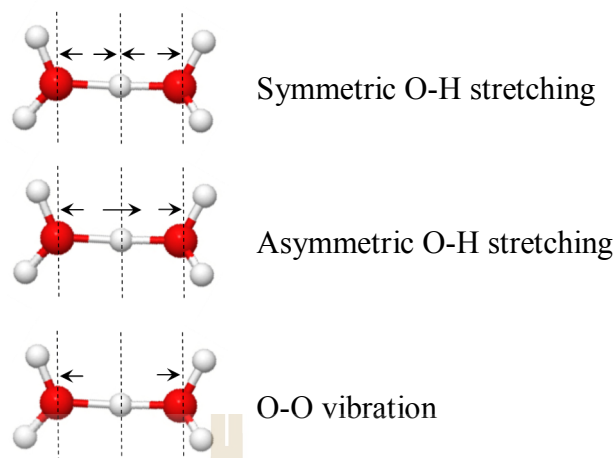


Figure 2.1 Definitions of the velocity vectors used in the calculations of the symmetric and asymmetric O-H stretching frequencies, as well as the O-O vibrational frequencies (Sagarik, Chaiwongwattana, Vchirawongkwin, and Prueksaaron, 2010).

As the definitions of the velocity vectors were different, the symmetric and asymmetric O-H stretching peaks were quite well separated (Figure 3.21). It should be noted that, due to similar definitions of the velocity vectors of the symmetric O-H stretching and the O-O vibration, some interferences (mixings) between these two modes can be observed. Due to the previous studies have shown (Lao-ngam, Asawakun, Wannarat, and Sagarik, 2011; Phonyiem, Chaiwongwattana, Lao-ngam, and Sagarik, 2011; Chaiwongwattana, Phonyiem, Vchirawongkwin, Prueksaaron, and Sagarik, 2012; Lao-ngam, Phonyiem, Chaiwongwattana, Kawazoe, and Sagarik, 2013) that the characteristic vibrational motions of the transferring protons discussed based on the asymmetric O-H stretching frequencies were very reasonable, the same approach was used in this work. Remarks should be made on the computational aspects of the vibrational spectra reported in this work, and the

absorption IR spectra obtained from ultrafast vibrational spectroscopy, for example, transient-hole burning, and vibrational echo techniques (Schmidt, Corcelli, and Skinner, 2005). In this work, vibrational spectra were computed from the Fourier transformation of the VACF, whereas the ultrafast absorption vibrational spectra can be obtained theoretically based on the Fourier transformation of the quantum dipole time-correlation function and response functions. Therefore, these two approaches do not yield exactly the same vibrational properties; the former are associated with the local vibrational modes, whereas the latter are connected to the vibrational transition frequencies of local oscillators. Because, in this study, the vibrational frequencies were used in the discussion of the characteristic vibrational motions of the transferring protons, and it was not the intention to calculate the absorption IR spectra *per se*, the Fourier transformation of the VACF was used. It should be added that, for strong H-bond systems such as liquid water, the ultrafast absorption IR spectra are complicated due to the pronounced non-Condon effects, defined as “the dependence of the vibrational transition dipole moment of a particular molecule on the rotational and translational coordinates of all the molecules in the liquid,” and conventional theoretical methods to calculate absorption IR spectra do not take into account these effects (Schmidt, Corcelli, and Skinner, 2005). It was demonstrated that inclusion of the non-Condon effects in the model calculations is important for an accurate calculation of the homodyned and heterodyned three-pulse echoes, which are not the objectives of this study. The vibrational energies for the interconversion between the oscillatory shuttling and structural diffusion motions ($\Delta v_{BA}^{\text{OH,MD}}$) were approximated from the difference between the structural diffusion ($v_B^{\text{OH,MD}}$) and oscillatory shuttling ($v_A^{\text{OH,MD}}$) frequencies (Phonyiem, Chaiwongwattana, Lao-ngam, and Sagarik, 2011).

In this study, the dynamics of the protons were also discussed using the ^1H NMR chemical shift spectra ($\delta_{\text{H}^+}^{\text{corr}}$) obtained from the BOMD simulations over the temperature range of 298–430 K (Lee *et al.*, 2007; Brunklaus *et al.*, 2009). In the calculations of the ^1H NMR chemical shift spectra, a statistical sampling of the structures of the smallest, most stable intermediate complex was performed every five BOMD steps (Lao-ngam, Phonyiem, Chaiwongwattana, Kawazoe, and Sagarik, 2013), and two thousand five hundred H-bond structures were used in the calculations of the instantaneous ^1H NMR shielding constants ($\sigma_{\text{H}^+}^{\text{corr,MD}}$) using the *ab initio* GIAO method at the RIMP2/TZVP level. The ^1H NMR chemical shift spectra were represented by Lorentzian peak functions (Murakhtina, Heuft, Meijer, and Sebastiani, 2006), from which the activation energies ($\Delta E^{\ddagger,\text{NMR}}$) for the exchange between the shared-proton and close-contact structures were obtained through a simple line shape analysis. Based on the assumption that the change in the ^1H NMR line width ($\Delta\delta_{\text{H}^+}^{\text{corr,MD}}$) as a function of temperature is correlated with the exchange rate, which can be used to determine $\Delta E^{\ddagger,\text{NMR}}$ through the Arrhenius equation (Lee *et al.*, 2007), $\Delta\delta_{\text{H}^+}^{\text{corr,MD}}$ was approximated as the FWHM of the ^1H NMR chemical shift spectra (Narayanan, Yen, Liu, and Greenbaum, 2006). In this study, the effective transverse relaxation times (T_2^*) were calculated from $\Delta\delta_{\text{H}^+}^{\text{corr,MD}}$ using

$$T_2^* = 1/(\pi\Delta\delta_{\text{H}^+}^{\text{corr,MD}}) \quad (2.8)$$

and the $\Delta E^{\ddagger,\text{NMR}}$ from the plots of $\ln(T_2^*)$ and $1000/T$ (Lee *et al.*, 2007).

2.5 References

- Ahlrichs, R., Bär, M., Häser, M., Horn, H., and Kölmel, C. (1989). Electronic structure calculations on workstation computers: The program system turbomole. **Chemical Physics Letters**. 162: 165-169.
- Böhm, H.-J., and Ahlrichs, R. (1985). The N₂-N₂ interaction. **Molecular Physics**. 55: 1159-1169.
- Böhm, H. J., and Ahlrichs, R. (1982). A study of short-range repulsions. **The Journal of Chemical Physics**. 77: 2028-2034.
- Bopp, P. (1986). A study of the vibrational motions of water in an aqueous CaCl₂ solution. **Chemical Physics**. 106: 205-212.
- Brunklaus, G., Schauff, S., Markova, D., Klapper, M., Müllen, K., and Spiess, H.-W. (2009). Proton Mobilities in Phosphonic Acid-Based Proton Exchange Membranes Probed by ¹H and ²H Solid-State NMR Spectroscopy. **The Journal of Physical Chemistry B**. 113: 6674-6681.
- Chaiwongwattana, S., Phonyiem, M., Vchirawongkwin, V., Prueksaaron, S., and Sagarik, K. (2012). Dynamics and mechanism of structural diffusion in linear hydrogen bond. **Journal of Computational Chemistry**. 33: 175-188.
- Chesnut, D. B. (1995). An approximate infinite order perturbation theory prescription for isotropic NMR chemical shieldings. **Chemical Physics Letters**. 246: 235-238.
- Chesnut, D. B. (2005). A Theoretical Study of ³¹P NMR Chemical Shielding Models for Concentrated Phosphoric Acid Solution. **The Journal of Physical Chemistry A**. 109: 11962-11966.

- Chesnut, D. B., and Rusiloski, B. E. (1994). A study of NMR chemical shielding in water clusters derived from molecular dynamics simulations. **Journal of Molecular Structure: THEOCHEM**. 314: 19-30.
- Chung, S. H., Bajue, S., and Greenbaum, S. G. (2000). Mass transport of phosphoric acid in water: A ^1H and ^{31}P pulsed gradient spin-echo nuclear magnetic resonance study. **The Journal of Chemical Physics**. 112: 8515-8521.
- Ditchfield, R. (1974). Self-consistent perturbation theory of diamagnetism. **Molecular Physics**. 27: 789-807.
- Ditchfield, R. (1976). Theoretical studies of magnetic shielding in H_2O and $(\text{H}_2\text{O})_2$. **The Journal of Chemical Physics**. 65: 3123-3133.
- Glezakou, V.-A., Dupuis, M., and Mundy, C. J. (2007). Acid/base equilibria in clusters and their role in proton exchange membranes: computational insight. **Physical Chemistry Chemical Physics**. 9: 5752-5760.
- Greenwood, N. N., and Thompson, A. (1959). 701. The mechanism of electrical conduction in fused phosphoric and trideuterophosphoric acids. **Journal of the Chemical Society (Resumed)**: 3485-3492.
- Hoover, W. G. (1985). Canonical dynamics: Equilibrium phase-space distributions. **Physical Review A**. 31: 1695-1697.
- Klamt, A., and Schuurmann, G. (1993). COSMO: a new approach to dielectric screening in solvents with explicit expressions for the screening energy and its gradient. **Journal of the Chemical Society, Perkin Transactions 2**: 799-805.
- Konrat, R., Tollinger, M., Kontaxis, G., and Kräutler, B. (1999). NMR Techniques to Study Hydrogen Bonding in Aqueous Solution. **Monatshefte für Chemie / Chemical Monthly**. 130: 961-982.

- Lao-ngam, C., Asawakun, P., Wannarat, S., and Sagarik, K. (2011). Proton transfer reactions and dynamics in protonated water clusters. **Physical Chemistry Chemical Physics**. 13: 4562-4575.
- Lao-ngam, C., Phonyiem, M., Chaiwongwattana, S., Kawazoe, Y., and Sagarik, K. (2013). Characteristic NMR spectra of proton transfer in protonated water clusters. **Chemical Physics**. 420: 50-61.
- Lee, Y. J., Bingöl, B., Murakhtina, T., Sebastiani, D., Meyer, W. H., Wegner, G., and Spiess, H. W. (2007). High-Resolution Solid-State NMR Studies of Poly(vinyl phosphonic acid) Proton-Conducting Polymer: Molecular Structure and Proton Dynamics. **The Journal of Physical Chemistry B**. 111: 9711-9721.
- Luz, Z., and Meiboom, S. (1964). The Activation Energies of Proton Transfer Reactions in Water. **Journal of the American Chemical Society**. 86: 4768-4769.
- Munson, R. A., and Lazarus, M. E. (1967). Influence of ionic solutes upon the conductivity of molten phosphoric acid. **The Journal of Physical Chemistry**. 71: 3245-3248.
- Murakhtina, T., Heuft, J., Meijer, E. J., and Sebastiani, D. (2006). First Principles and Experimental ^1H NMR Signatures of Solvated Ions: The Case of $\text{HCl}(\text{aq})$. **ChemPhysChem**. 7: 2578-2584.
- Narayanan, S. R., Yen, S.-P., Liu, L., and Greenbaum, S. G. (2006). Anhydrous Proton-Conducting Polymeric Electrolytes for Fuel Cells. **The Journal of Physical Chemistry B**. 110: 3942-3948.
- Nosé, S. (1984). A unified formulation of the constant temperature molecular dynamics methods. **The Journal of Chemical Physics**. 81: 511-519.

- Nosé, S., and Klein, M. L. (1983). Constant pressure molecular dynamics for molecular systems. **Molecular Physics**. 50: 1055-1076.
- Phonyiem, M., Chaiwongwattana, S., Lao-ngam, C., and Sagarik, K. (2011). Proton transfer reactions and dynamics of sulfonic acid group in Nafion[®]. **Physical Chemistry Chemical Physics**. 13: 10923-10939.
- Harris, R. K., Becker, E. D., Cabral de Menezes, S. M., Granger, P., Hoffman, R. E., and Zilm, K. W. (2008). Further conventions for NMR shielding and chemical shifts (IUPAC Recommendations 2008). **Pure and Applied Chemistry**. 80: 59-58.
- Sagarik, K., and Asawakun, P. (1997). Intermolecular potential for phenol based on the test particle model. **Chemical Physics**. 219: 173-191.
- Sagarik, K., Chaiwongwattana, S., and Sisot, P. (2004). A theoretical study on clusters of benzoic acid–water in benzene solutions. **Chemical Physics**. 306: 1-12.
- Sagarik, K., Chaiwongwattana, S., Vchirawongkwin, V., and Prueksaaron, S. (2010). Proton transfer reactions and dynamics in CH₃OH-H₃O⁺-H₂O complexes. **Physical Chemistry Chemical Physics**. 12: 918-929.
- Sagarik, K., and Chaiyapongs, S. (2005). Structures and stability of salt-bridge in aqueous solution. **Biophysical Chemistry**. 117: 119-140.
- Sagarik, K., and Dokmaisrijan, S. (2005). A theoretical study on hydration of alanine zwitterions. **Journal of Molecular Structure: THEOCHEM**. 718: 31-47.
- Sagarik, K., Phonyiem, M., Lao-ngam, C., and Chaiwongwattana, S. (2008). Mechanisms of proton transfer in Nafion[registered sign]: elementary

- reactions at the sulfonic acid groups. **Physical Chemistry Chemical Physics**. 10: 2098-2112.
- Sagarik, K., and Rode, B. M. (2000). Intermolecular potential for benzoic acid–water based on the test-particle model and statistical mechanical simulations of benzoic acid in aqueous solutions. **Chemical Physics**. 260: 159-182.
- Sagarik, K., and Spohr, E. (1995). Statistical mechanical simulations on properties of liquid pyridine. **Chemical Physics**. 199: 73-82.
- Sagarik, K. P. (1999) Theoretical studies on hydrogen bonding in hydroxylamine clusters and liquid. **Journal of Molecular Structure: THEOCHEM**. 465: 141.
- Sagarik, K. P., and Ahlrichs, R. (1987). A test particle model potential for formamide and molecular dynamics simulations of the liquid. **The Journal of Chemical Physics**. 86: 5117-5126.
- Sagarik, K. P., Pongpituk, V., Chaiyapongs, S., and Sisot, P. (1991). Test-particle model potentials for hydrogen-bonded complexes: Complexes formed from HCN, HF, H₂O, NH₃, HCONH₂, HCONHCH₃, guanine and cytosine. **Chemical Physics**. 156: 439-456.
- Schmidt, J. R., Corcelli, S. A., and Skinner, J. L. (2005). Pronounced non-Condon effects in the ultrafast infrared spectroscopy of water. **The Journal of Chemical Physics**. 123: 044513.
- Scott, A. P., and Radom, L. (1996). Harmonic Vibrational Frequencies: An Evaluation of Hartree–Fock, Møller–Plesset, Quadratic Configuration Interaction, Density Functional Theory, and Semiempirical Scale Factors. **The Journal of Physical Chemistry**. 100: 16502-16513.

- Shuichi, N. (1991). Constant Temperature Molecular Dynamics Methods. **Progress of Theoretical Physics Supplement**. 103: 1-46.
- SURFER for Window (Version 6.04). (1997): Golden Software Inc., USA.
- Taubert, S., Konschin, H., and Sundholm, D. (2005). Computational studies of ^{13}C NMR chemical shifts of saccharides. **Physical Chemistry Chemical Physics**. 7: 2561-2569.
- Tielrooij, K. J., Timmer, R. L. A., Bakker, H. J., and Bonn, M. (2009). Structure Dynamics of the Proton in Liquid Water Probed with Terahertz Time-Domain Spectroscopy. **Physical Review Letters**. 102: 198303.
- Treutler, O., and Ahlrichs, R. (1995). Efficient molecular numerical integration schemes. **The Journal of Chemical Physics**. 102: 346-354.
- TURBOMOLE Tutorial 6.4, 1989-2007, TURBOMOLE GmbH, since 2007; available online <http://www.turbomole.com>.
- Vilčiauskas, L. (2012). Ph.D. thesis, Universität Stuttgart.
- Vilčiauskas, L., Tuckerman, M. E., Bester, G., Paddison, S. J., and Kreuer, K.-D. (2012). The mechanism of proton conduction in phosphoric acid. **Nature Chemistry**. 4: 461-466.
- Watts, R. O., and McGee, I. J. (1976). *Liquid State Chemical Physics*. New York: John Wiley & Sons.
- Weigend, F., and Häser, M. (1997). RI-MP2: first derivatives and global consistency. **Theoretical Chemistry Accounts**. 97: 331-340.

CHAPTER III

RESULTS AND DISCUSSION

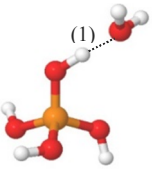
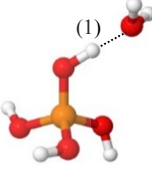
In order to simplify the discussion, the H-bond structures were labelled with a three-character code, the **G_n-[m]** or **C_n-[m]**: **G** = H-bond structure in the gas phase, and the **C** = H-bond structure in continuum aqueous solution, where **n** is the number of water molecules. Different H-bond structures with the same number of water molecules are distinguished by **[m]**. For example, according to the three-character code, **G3-[1]** and **G3-[2]** are different H-bond structures (**[1]** and **[2]**, respectively) with the same number of water molecules (**n = 3**) in the gas phase (**G**). In contrast, **G2-[1]** and **C2-[1]** are the same H-bond structure (**n = 2, m = 1**) in the gas phase (**G**) and continuum aqueous solution (**C**), respectively.

3.1 Static results

3.1.1 B3LYP and RIMP2 calculations

Tables 3.1 and 3.2 show the static results obtained from the B3LYP/TZVP and RIMP2/TZVP calculations, respectively. The equilibrium structures that may be involved in proton dissociation and transfer, which were obtained from the RIMP2/TZVP calculations in the gas phase and continuum aqueous solution, are shown in Figure 3.1, with the dipole moment (μ).

Table 3.1 Static results of the $\text{H}_3\text{PO}_4\text{-H}_3\text{O}^+-n\text{H}_2\text{O}$ complexes, $n = 1-3$, obtained from B3LYP/TZVP calculations, both in the gas phase and continuum aqueous solution. Energies, distances and vibrational frequencies are in kJ/mol, Å and cm^{-1} , respectively. ^1H NMR shielding constants and chemical shift are in ppm.

		G1			C1	
						
		ΔE	ΔE^{sol}	ΔE		
		-97.7	-278.9	-43.3		
H-bond	$R_{\text{O-O}}$	Δd_{DA}	ν^{OH}	σ_{H^+}	δ_{H^+}	
(1)	2.50	0.44	2306	16.67	15.25	
	(2.46)	(0.33)	(1862)	(15.54)	(16.38)	

ΔE = interaction energy; ΔE^{sol} = solvation energy; $R_{\text{O-O}}$ = H-bond distance; Δd_{DA} = asymmetric stretching coordinate; ν^{OH} = asymmetric O-H stretching frequency; σ_{H^+} = isotropic shielding constant; δ_{H^+} = ^1H NMR chemical shift; (..) = continuum aqueous solvent.

Table 3.1 (Continued).

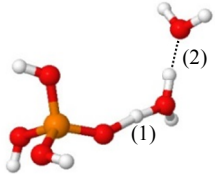
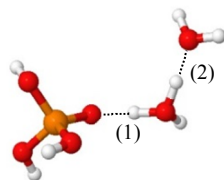
G2-[1]		C2-[1]			
					
ΔE	ΔE^{sol}	ΔE			
-171.5	-278.2	-80.6			
H-bond	$R_{\text{O-O}}$	Δd_{DA}	ν^{OH}	σ_{H^+}	δ_{H^+}
(1)	2.41 (2.49)	0.22 (0.41)	1792 (2350)	14.34 (17.01)	17.58 (5.67)
(2)	2.55 (2.50)	0.51 (0.39)	2749 (2106)	19.05 (16.61)	12.87 (5.53)

Table 3.1 (Continued).

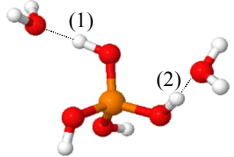
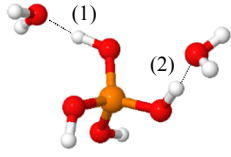
G2-[2]		C2-[2]			
					
ΔE	ΔE^{sol}	ΔE			
-186.1	-266.1	-83.1			
H-bond	$R_{\text{O-O}}$	Δd_{DA}	ν^{OH}	σ_{H^+}	δ_{H^+}
(1)	2.54 (2.50)	0.49 (0.42)	2573 (2243)	18.43 (17.19)	13.49 (5.73)
(2)	2.54 (2.49)	0.48 (0.39)	2640 (2115)	18.33 (16.79)	13.59 (5.59)

Table 3.1 (Continued).

		G3-[1]			C3-[1]	
		ΔE	ΔE^{sol}	ΔE		
		-250.2	-260.5	-107.9		
H-bond	$R_{\text{O-O}}$	Δd_{DA}	ν^{OH}	σ_{H^+}	δ_{H^+}	
(1)	2.43 (2.47)	0.23 (0.35)	1735 (1987)	14.09 (15.91)	17.83 (16.01)	
(2)	2.57 (2.57)	0.53 (0.53)	2747 (2617)	19.32 (19.51)	12.60 (12.41)	
(3)	2.65 (2.52)	0.67 (0.44)	3155 (2357)	22.69 (17.54)	9.23 (14.38)	

Table 3.1 (Continued).

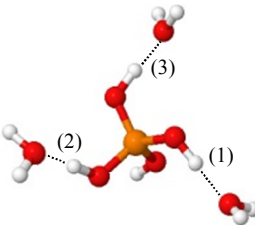
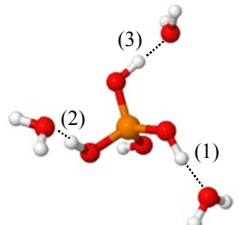
G3-[2]		C3-[2]			
					
ΔE	ΔE^{sol}	ΔE			
-263.0	-259.2	-119.4			
H-bond	$R_{\text{O} \cdots \text{O}}$	Δd_{DA}	ν^{OH}	σ_{H^+}	δ_{H^+}
(1)	2.58 (2.53)	0.55 (0.47)	2842 (2455)	19.66 (18.35)	12.26 (13.57)
(2)	2.57 (2.52)	0.53 (0.44)	2758 (2318)	19.50 (17.95)	12.42 (13.97)
(3)	2.58 (2.53)	0.55 (0.45)	2778 (2368)	19.69 (17.95)	12.23 (13.83)

Table 3.1 (Continued).

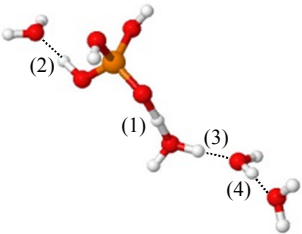
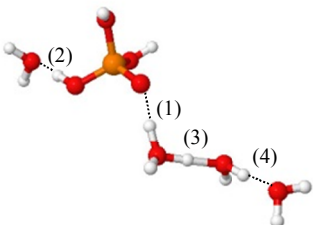
		G4-[1]		C4-[1]	
					
		ΔE	ΔE^{sol}	ΔE	
		-305.3	-265.1	-133.8	
H-bond	$R_{\text{O-O}}$	Δd_{DA}	ν^{OH}	σ_{H^+}	δ_{H^+}
(1)	2.41 (2.51)	0.19 (0.45)	1694 (2439)	13.84 (17.68)	18.08 (14.24)
(2)	2.61 (2.58)	0.60 (0.54)	2938 (2691)	20.63 (19.94)	11.29 (11.98)
(3)	2.49 (2.44)	0.41 (0.24)	2430 (1673)	17.16 (14.10)	14.76 (17.82)
(4)	2.69 (2.66)	0.72 (0.66)	3270 (3016)	23.89 (22.49)	8.03 (9.43)

Table 3.1 (Continued).

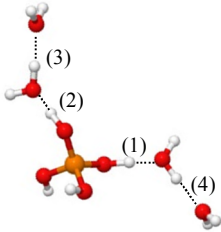
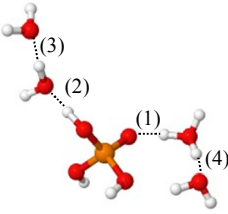
		G4-[2]		C4-[2]	
					
		ΔE	ΔE^{sol}	ΔE	
		-309.4	-260.2	-133.0	
H-bond	$R_{\text{O-O}}$	Δd_{DA}	ν^{OH}	σ_{H^+}	δ_{H^+}
(1)	2.46	0.32	2062	15.46	16.46
	(2.49)	(0.39)	(2088)	(16.90)	(15.02)
(2)	2.46	0.33	1971	15.59	16.33
	(2.51)	(0.43)	(2225)	(17.14)	(14.78)
(3)	2.68	0.70	3232	23.52	8.40
	(2.69)	(0.71)	(3145)	(23.69)	(8.23)
(4)	2.68	0.70	3230	23.47	8.45
	(2.50)	(0.41)	(2319)	(16.89)	(15.03)

Table 3.1 (Continued).

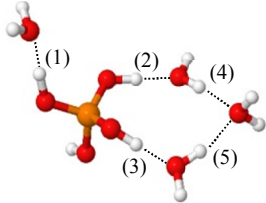
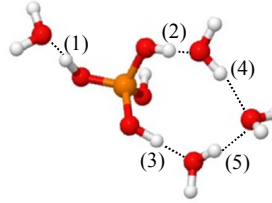
		G4-[3]		C4-[3]	
					
		ΔE	ΔE^{sol}	ΔE	
		-320.0	-267.6	-150.9	
H-bond	$R_{\text{O-O}}$	Δd_{DA}	ν^{OH}	σ_{H^+}	δ_{H^+}
(1)	2.58 (2.53)	0.56 (0.47)	2795 (2428)	19.84 (18.45)	12.08 (13.47)
(2)	2.58 (2.50)	0.56 (0.41)	2856 (2187)	19.81 (17.28)	12.11 (14.64)
(3)	2.54 (2.48)	0.50 (0.37)	2648 (1991)	18.78 (16.61)	13.14 (15.31)
(4)	2.88 (2.76)	0.94 (0.80)	3464 (3254)	26.79 (25.55)	5.13 (6.37)
(5)	2.84 (2.73)	0.92 (0.78)	3464 (3254)	26.51 (25.33)	5.41 (6.59)

Table 3.1 (Continued).

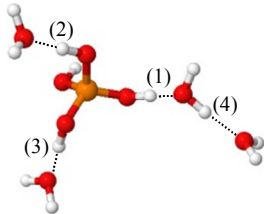
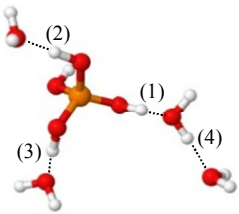
		G4-[4]		C4-[4]	
					
		ΔE	ΔE^{sol}	ΔE	
		-321.0	-258.0	-142.4	
H-bond	$R_{\text{O-O}}$	Δd_{DA}	ν^{OH}	σ_{H^+}	δ_{H^+}
(1)	2.48	0.36	2167	16.27	15.65
	(2.46)	(0.30)	(1741)	(15.32)	(16.60)
(2)	2.59	0.57	2856	20.21	11.71
	(2.54)	(0.48)	(2426)	(18.63)	(13.29)
(3)	2.59	0.57	2856	20.23	11.69
	(2.54)	(0.48)	(2426)	(18.63)	(13.29)
(4)	2.69	0.72	3264	23.87	8.05
	(2.67)	(0.67)	(3067)	(22.97)	(8.95)

Table 3.1 (Continued).

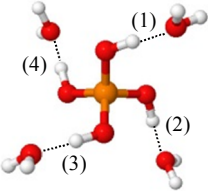
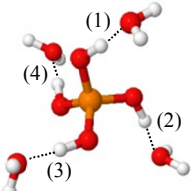
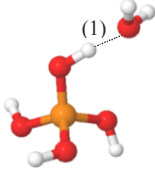
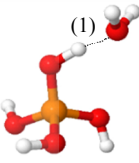
		G4-[5]			C4-[5]	
						
		ΔE	ΔE^{sol}	ΔE		
		-331.7	-257.8	-152.9		
H-bond	$R_{\text{O-O}}$	Δd_{DA}	ν^{OH}	σ_{H^+}	δ_{H^+}	
(1)	2.61 (2.55)	0.59 (0.51)	2911 (2515)	20.60 (19.22)	11.32 (12.70)	
(2)	2.61 (2.55)	0.59 (0.51)	2914 (2480)	20.63 (19.02)	11.29 (12.90)	
(3)	2.61 (2.54)	0.59 (0.51)	2905 (2467)	20.60 (18.89)	11.32 (13.30)	
(4)	2.60 (2.55)	0.59 (0.51)	2914 (2480)	20.60 (18.95)	11.32 (12.97)	

Table 3.2 Static results of the $\text{H}_3\text{PO}_4\text{-H}_3\text{O}^+ - n\text{H}_2\text{O}$ complexes, $n = 1-3$, obtained from RIMP2/TZVP calculations, both in the gas phase and continuum aqueous solution. Energies, distances and vibrational frequencies are in kJ/mol, Å and cm^{-1} , respectively. ^1H NMR shielding constants and chemical shift are in ppm.

G1		C1			
					
ΔE		ΔE^{sol}		ΔE	
-100.6		-282.1		-44.9	
H-bond	$R_{\text{O-O}}$	Δd_{DA}	ν^{OH}	$\sigma_{\text{H}^+}^{\text{corr}}$	$\delta_{\text{H}^+}^{\text{corr}}$
(1)	2.49	0.41	2363	16.33	15.63
	(2.45)	(0.32)	(1866)	(14.85)	(17.11)

ΔE = interaction energy; ΔE^{sol} = solvation energy; $R_{\text{O-O}}$ = H-bond distance; Δd_{DA} = asymmetric stretching coordinate; ν^{OH} = asymmetric O-H stretching frequency; $\sigma_{\text{H}^+}^{\text{corr}}$ = isotropic shielding constant; $\delta_{\text{H}^+}^{\text{corr}}$ = ^1H NMR chemical shift; (..) = continuum aqueous solvent.

Table 3.2 (Continued).

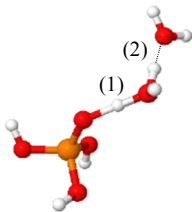
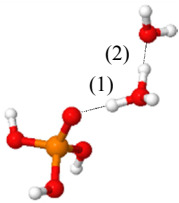
G2-[1]		C2-[1]			
					
ΔE	ΔE^{sol}	ΔE			
-174.0	-279.2	-81.1			
H-bond	$R_{\text{O} \cdots \text{O}}$	Δd_{DA}	ν^{OH}	$\sigma_{\text{H}^+}^{\text{corr}}$	$\delta_{\text{H}^+}^{\text{corr}}$
(1)	2.40 (2.49)	0.20 (0.43)	1746 (2424)	13.01 (16.55)	18.95 (15.41)
(2)	2.55 (2.48)	0.53 (0.40)	2832 (2192)	18.98 (15.97)	12.98 (15.99)

Table 3.2 (Continued).

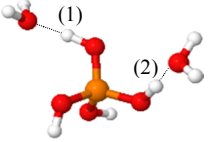
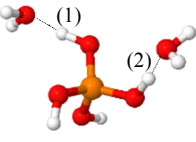
G2-[2]		C2-[2]			
					
ΔE		ΔE^{sol}			
-188.7		-266.9			
ΔE		ΔE			
-188.7		-83.5			
H-bond	$R_{\text{O-O}}$	Δd_{DA}	ν^{OH}	$\sigma_{\text{H}^+}^{\text{corr}}$	$\delta_{\text{H}^+}^{\text{corr}}$
(1)	2.53 (2.50)	0.49 (0.42)	2682 (2319)	18.19 (16.89)	13.77 (15.07)
(2)	2.53 (2.49)	0.49 (0.40)	2618 (2198)	18.03 (16.49)	13.93 (15.47)

Table 3.2 (Continued).

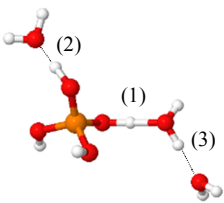
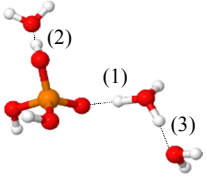
G3-[1]		C3-[1]			
					
ΔE		ΔE^{sol}		ΔE	
-252.0		-267.9		-113.6	
H-bond	$R_{\text{O-O}}$	Δd_{DA}	ν^{OH}	$\sigma_{\text{H}^+}^{\text{corr}}$	$\delta_{\text{H}^+}^{\text{corr}}$
(1)	2.43 (2.47)	0.25 (0.37)	1784 (2151)	13.56 (15.49)	18.40 (16.47)
(2)	2.55 (2.56)	0.53 (0.52)	2777 (2680)	19.03 (19.45)	12.93 (12.51)
(3)	2.65 (2.49)	0.68 (0.42)	3206 (2369)	22.66 (16.45)	9.30 (15.51)

Table 3.2 (Continued).

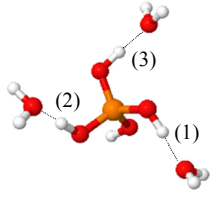
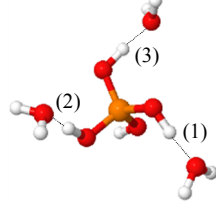
		G3-[2]		C3-[2]			
							
		ΔE	ΔE^{sol}	ΔE			
		-267.9	-259.3	-121.0			
H-bond	$R_{\text{O-O}}$	Δd_{DA}	ν^{OH}	$\sigma_{\text{H}^+}^{\text{corr}}$	$\delta_{\text{H}^+}^{\text{corr}}$		
(1)	2.57 (2.52)	0.55 (0.46)	2810 (2504)	19.45 (18.02)	12.51 (13.94)		
(2)	2.56 (2.51)	0.54 (0.45)	2794 (2379)	19.27 (17.67)	12.69 (14.29)		
(3)	2.56 (2.51)	0.54 (0.45)	2868 (2420)	19.38 (17.71)	12.69 (14.25)		

Table 3.2 (Continued).

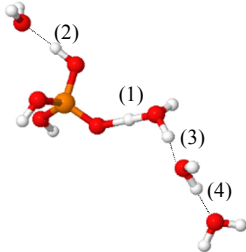
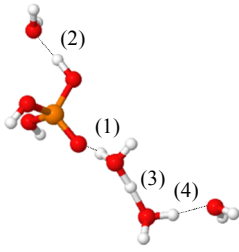
		G4-[1]		C4-[1]	
					
		ΔE	ΔE^{sol}	ΔE	
		-306.0	-267.3	-132.9	
H-bond	$R_{\text{O-O}}$	Δd_{DA}	ν^{OH}	$\sigma_{\text{H}^+}^{\text{corr}}$	$\delta_{\text{H}^+}^{\text{corr}}$
(1)	2.41 (2.50)	0.21 (0.45)	1757 (2527)	13.28 (17.31)	18.68 (14.65)
(2)	2.60 (2.57)	0.60 (0.55)	2979 (2738)	20.52 (19.74)	11.44 (13.75)
(3)	2.48 (2.43)	0.41 (0.26)	2447 (1703)	16.39 (13.28)	15.57 (18.68)
(4)	2.69 (2.65)	0.72 (0.67)	3295 (3094)	23.71 (22.44)	8.25 (9.52)

Table 3.2 (Continued).

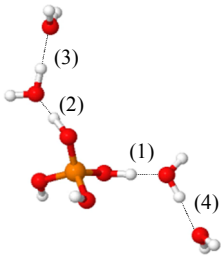
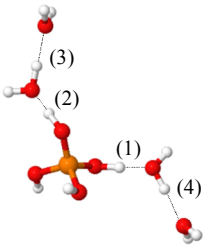
		G4-[2]		C4-[2]	
					
		ΔE	ΔE^{sol}	ΔE	
		-310.4	-258.6	-128.6	
H-bond	$R_{\text{O-O}}$	Δd_{DA}	ν^{OH}	$\sigma_{\text{H}^+}^{\text{corr}}$	$\delta_{\text{H}^+}^{\text{corr}}$
(1)	2.45 (2.43)	0.34 (0.25)	2043 (1616)	15.03 (13.68)	16.93 (18.28)
(2)	2.46 (2.43)	0.34 (0.27)	2124 (1669)	15.11 (14.03)	16.85 (17.93)
(3)	2.68 (2.65)	0.71 (0.67)	3274 (3089)	23.66 (22.44)	8.30 (9.52)
(4)	2.68 (2.64)	0.70 (0.66)	3268 (3076)	23.37 (22.16)	8.59 (9.80)

Table 3.2 (Continued).

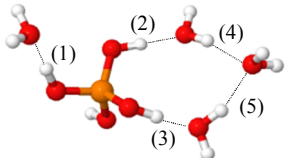
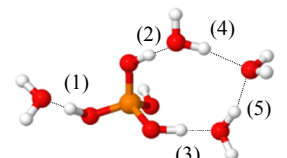
		G4-[3]		C4-[3]	
					
		ΔE	ΔE^{sol}	ΔE	
		-323.4	-266.8	-149.8	
H-bond	$R_{\text{O-O}}$	Δd_{DA}	ν^{OH}	$\sigma_{\text{H}^+}^{\text{corr}}$	$\delta_{\text{H}^+}^{\text{corr}}$
(1)	2.57 (2.52)	0.55 (0.47)	2880 (2485)	19.54 (18.18)	12.42 (13.78)
(2)	2.57 (2.49)	0.55 (0.42)	2824 (2247)	19.60 (16.96)	12.36 (15.00)
(3)	2.53 (2.46)	0.49 (0.35)	2659 (1960)	18.36 (15.73)	13.60 (16.23)
(4)	2.88 (2.74)	0.95 (0.80)	3476 (3286)	26.69 (25.35)	3.37 (6.61)
(5)	2.82 (2.72)	0.92 (0.78)	3502 (3522)	26.33 (25.06)	5.63 (6.90)

Table 3.2 (Continued).

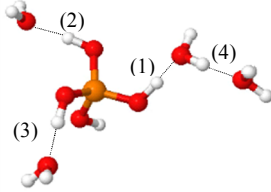
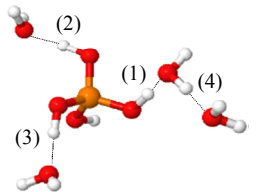
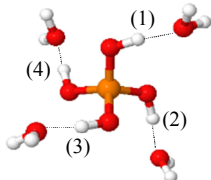
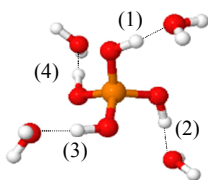
G4-[4]		C4-[4]			
					
ΔE		ΔE^{sol}			
-325.2		-258.5			
		ΔE			
		-143.2			
H-bond	$R_{\text{O-O}}$	Δd_{DA}	ν^{OH}	$\sigma_{\text{H}^+}^{\text{corr}}$	$\delta_{\text{H}^+}^{\text{corr}}$
(1)	2.47	0.37	2208	15.75	16.21
	(2.45)	(0.31)	(1840)	(14.92)	(17.04)
(2)	2.58	0.57	2885	19.96	12.01
	(2.52)	(0.47)	(2466)	(18.22)	(13.74)
(3)	2.58	0.57	2927	20.00	11.96
	(2.53)	(0.47)	(2525)	(18.28)	(13.68)
(4)	2.69	0.72	3294	23.70	8.26
	(2.66)	(0.68)	(3128)	(22.84)	(9.12)

Table 3.2 (Continued).

		G4-[5]		C4-[5]	
					
		ΔE	ΔE^{sol}	ΔE	
		-339.3	-257.9	-156.7	
H-bond	$R_{\text{O-O}}$	Δd_{DA}	ν^{OH}	$\sigma_{\text{H}^+}^{\text{corr}}$	$\delta_{\text{H}^+}^{\text{corr}}$
(1)	2.59 (2.54)	0.59 (0.50)	2931 (2559)	20.32 (18.87)	11.64 (13.09)
(2)	2.59 (2.53)	0.59 (0.49)	2932 (2520)	20.34 (18.69)	11.63 (13.27)
(3)	2.59 (2.53)	0.59 (0.49)	2931 (2520)	20.34 (18.61)	11.62 (13.35)
(4)	2.59 (2.53)	0.59 (0.49)	2932 (2531)	20.34 (18.67)	11.63 (13.29)

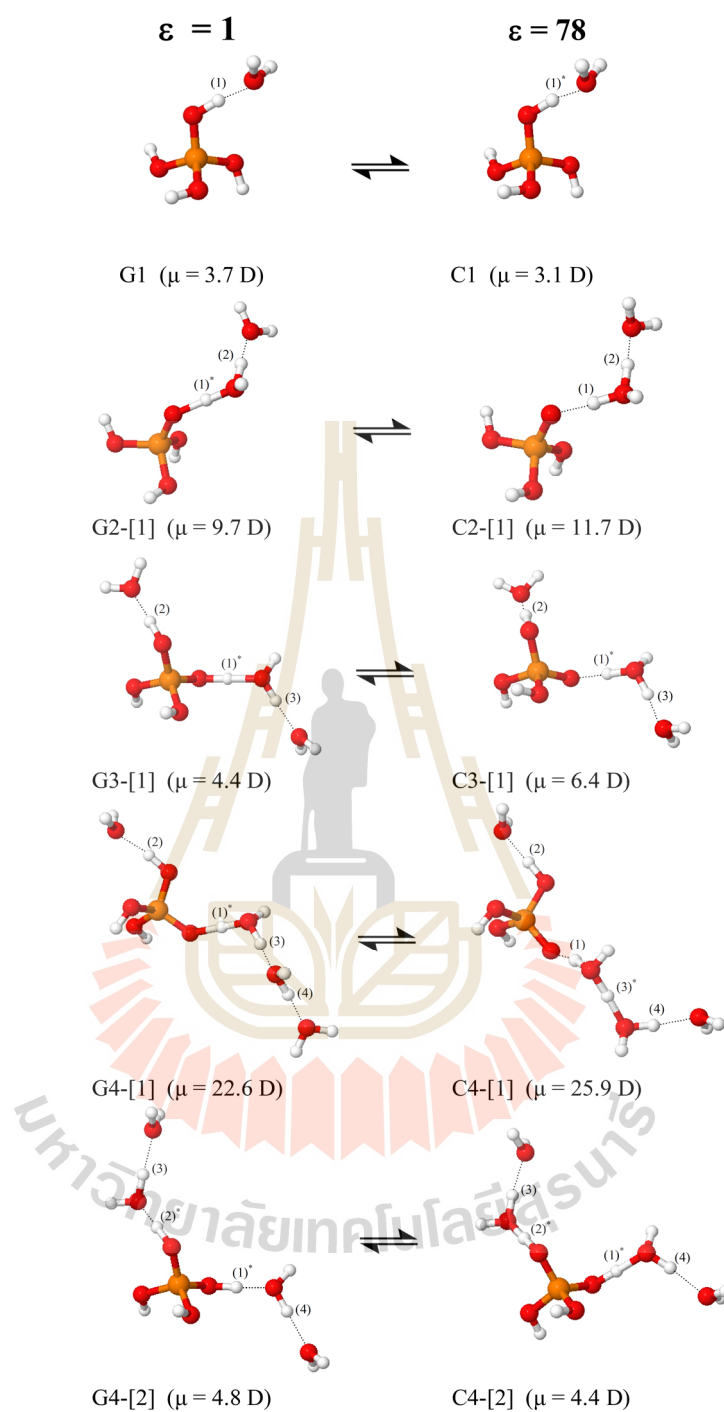
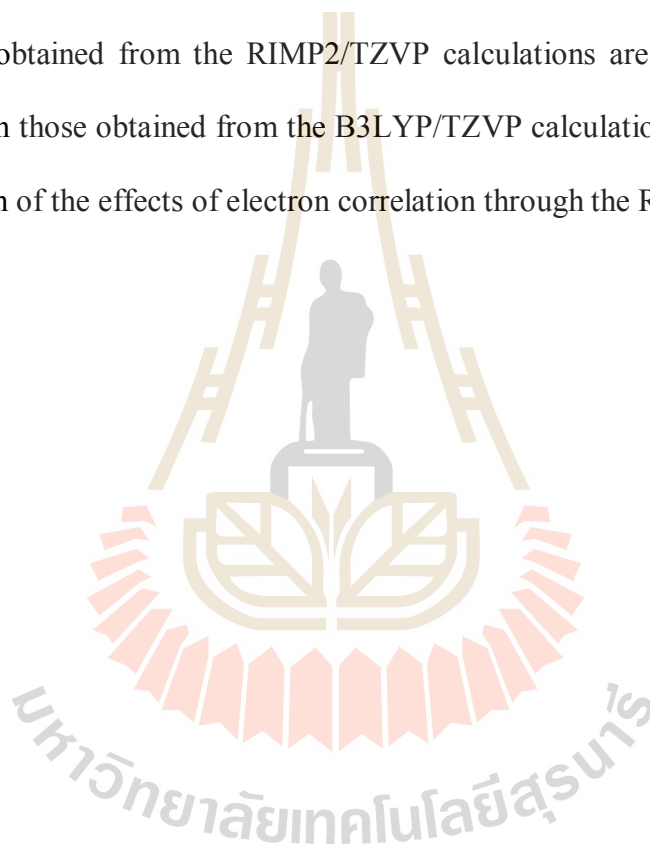


Figure 3.1 Linear H-bond structures of the $\text{H}_3\text{PO}_4\text{-H}_3\text{O}^+ - n\text{H}_2\text{O}$ complexes ($n = 1\text{--}3$) potentially involved in proton dissociation and transfer. These were obtained from the RIMP2/TZVP calculations in the gas phase and continuum aqueous solvent.

* = H-bond susceptible to proton transfer; μ = dipole moment.

The correlations between the RIMP2/TZVP and B3LYP/TZVP results are shown in Figures 3.2–3.6. These are represented by linear functions with R^2 values in the range of 0.986 to 0.999, reflecting excellent agreement between the two methods, *e.g.*, $R^2 = 0.999$ for the interaction (ΔE) and solvation energies (ΔE^{sol}). The investigation of the protonated H-bond structures in Tables 3.1 and 3.2 showed that the equilibrium structures obtained from both methods are generally the same and that the ΔE obtained from the RIMP2/TZVP calculations are slightly lower (more negative) than those obtained from the B3LYP/TZVP calculations, indicating a better representation of the effects of electron correlation through the RIMP2/TZVP method.



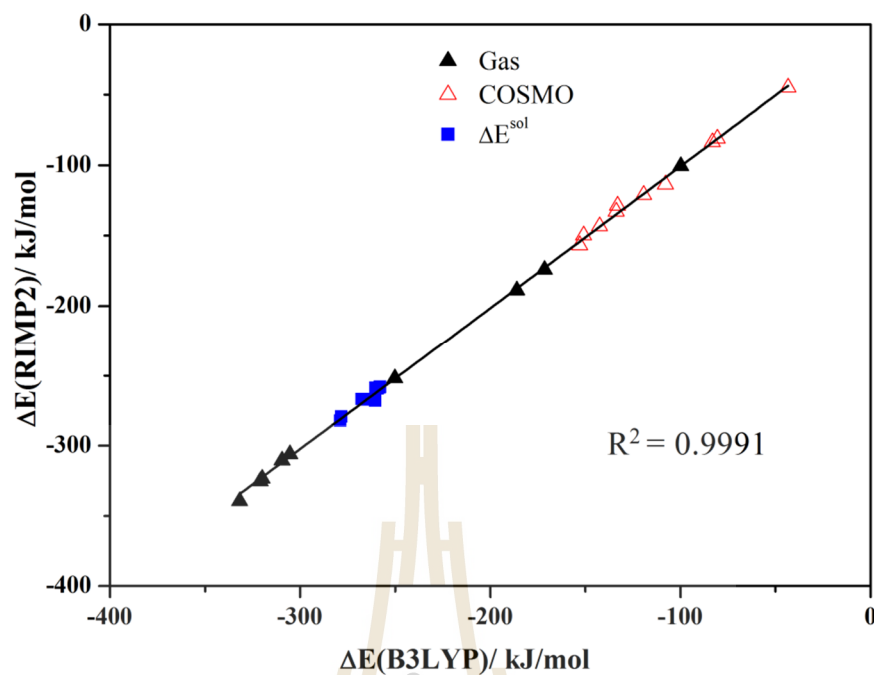


Figure 3.2 Correlations between the results obtained from the RIMP2/TZVP and B3LYP/TZVP calculations. ΔE and ΔE^{sol} are interaction and solvation energies, respectively; Gas = gas phase; COSMO = continuum aqueous solvent.

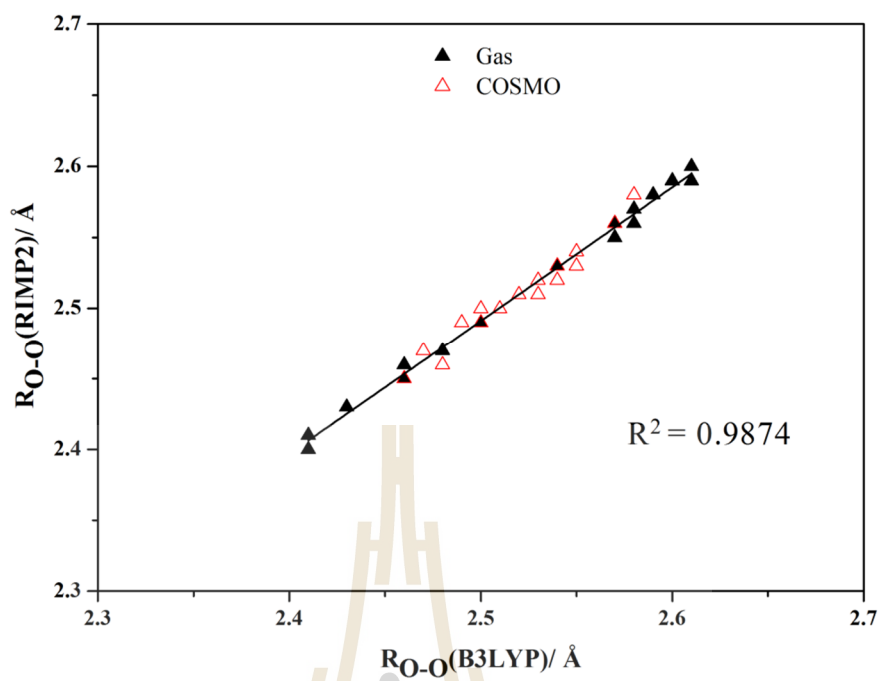


Figure 3.3 Correlations between the results obtained from the RIMP2/TZVP and B3LYP/TZVP calculations. R_{O-O} = H-bond distances; Gas = gas phase; COSMO = continuum aqueous solvent.

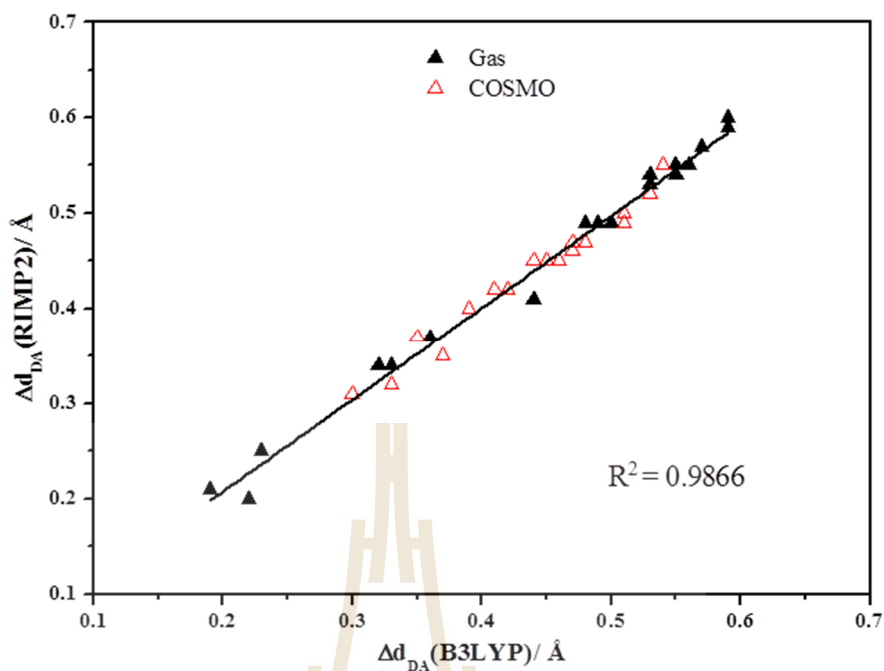


Figure 3.4 Correlations between the results obtained from the RIMP2/TZVP and B3LYP/TZVP calculations. Δd_{DA} = asymmetric stretching coordinates; Gas = gas phase; COSMO = continuum aqueous solvent.

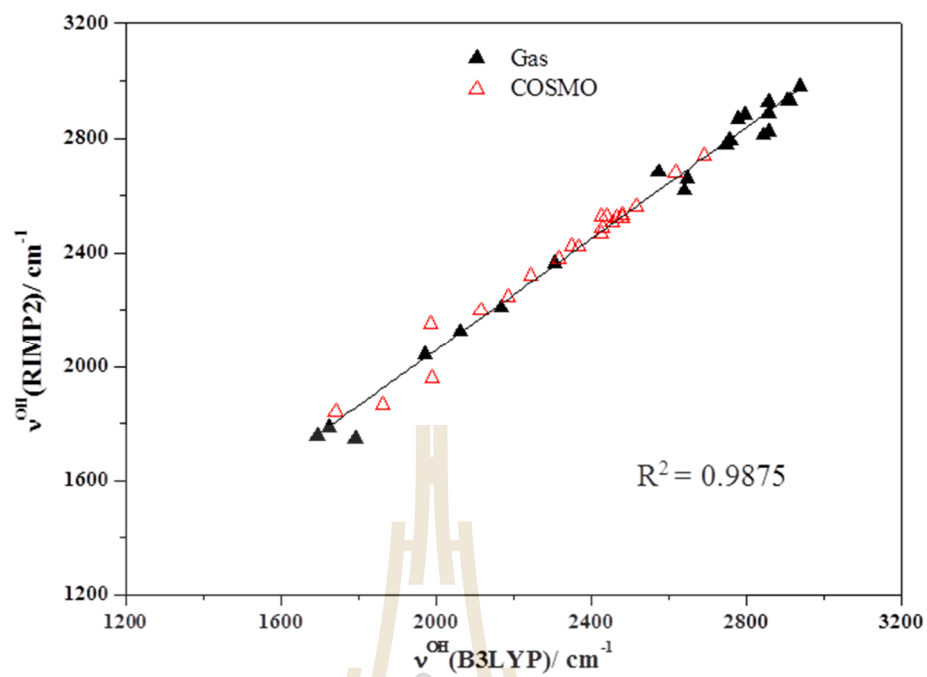


Figure 3.5 Correlations between the results obtained from the RIMP2/TZVP and B3LYP/TZVP calculations. ν^{OH} = asymmetric O-H stretching frequencies; Gas = gas phase; COSMO = continuum aqueous solvent.

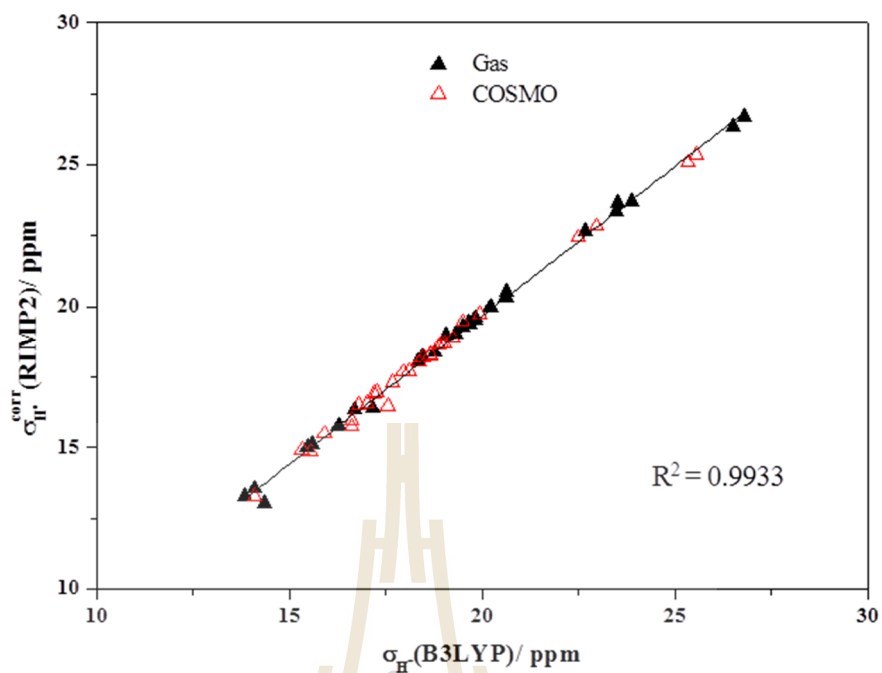


Figure 3.6 Correlations between the results obtained from the RIMP2/TZVP and B3LYP/TZVP calculations. $\sigma_{\text{H}}^{\text{corr}}$ = ^1H NMR shielding constants; Gas = gas phase; COSMO = continuum aqueous solvent.

The trends of the vibrational and NMR results are quite similar at both levels of theory. For the RIMP2/TZVP calculations, the plots of ν^{OH} and Δd_{DA} shown in Figure 3.7 yielded threshold asymmetric O-H stretching frequencies ($\nu^{\text{OH}*}$) for deprotonation in H-bond (**1**) at 2295 cm^{-1} in the gas phase and at 2078 cm^{-1} in continuum aqueous solution. These values are slightly lower than those obtained from the B3LYP/TZVP calculations: $\nu^{\text{OH}*} = 2306$ and 2136 cm^{-1} , respectively. The ^1H NMR shielding constants obtained from the RIMP2/TZVP calculations ($\sigma_{\text{H}^+}^{\text{corr}}$) are slightly smaller than those obtained from the B3LYP/TZVP calculations (σ_{H^+}), confirming that more associated H-bond complexes are obtained with the RIMP2/TZVP method. The plots of $\sigma_{\text{H}^+}^{\text{corr}}$ and Δd_{DA} and of ν^{OH} and $\sigma_{\text{H}^+}^{\text{corr}}$ shown in Figures 3.8–3.9 yielded threshold ^1H NMR shielding constant ($\sigma_{\text{H}^+}^{\text{corr}*}$) for deprotonation in H-bond (**1**) of 16 ppm in the gas phase, whereas the protonated forms (H_4PO_4^+ and H_3O^+) in the linear H-bond chains possess $\sigma_{\text{H}^+}^{\text{corr}}$ values in the ranges of 15 to 17 ppm and of 13 to 14 ppm, respectively, corresponding to ^1H NMR chemical shifts ($\sigma_{\text{H}^+}^{\text{corr}}$) of 17 to 15 ppm and of 19 to 18 ppm, respectively.

Because the RIMP2/TZVP and B3LYP/TZVP calculations yielded the same trends in the structural, energetic, and spectroscopic properties, the present study concluded that, in the case of restricted computational resources, the B3LYP/TZVP method can be applied in the study of hydrated H_3PO_4 under excess proton conditions. However, because the sizes of the model systems considered here are moderate, BOMD simulations can be performed based on the RIMP2/TZVP calculations.

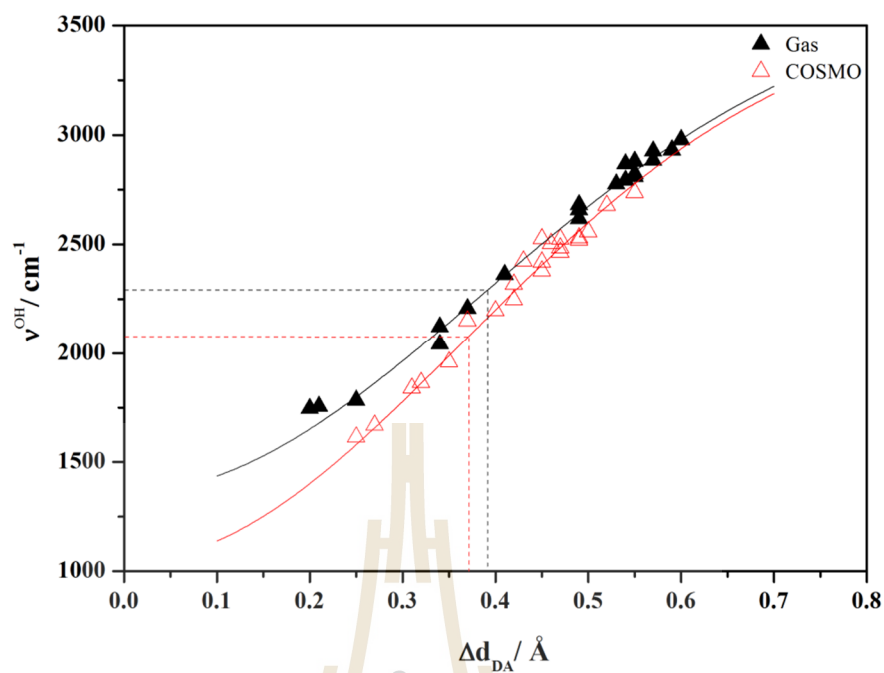


Figure 3.7 Plots of the asymmetric O-H stretching frequency (ν^{OH}) as a function of the asymmetric stretching coordinate (Δd_{DA}) in the gas phase and continuum aqueous solvent.

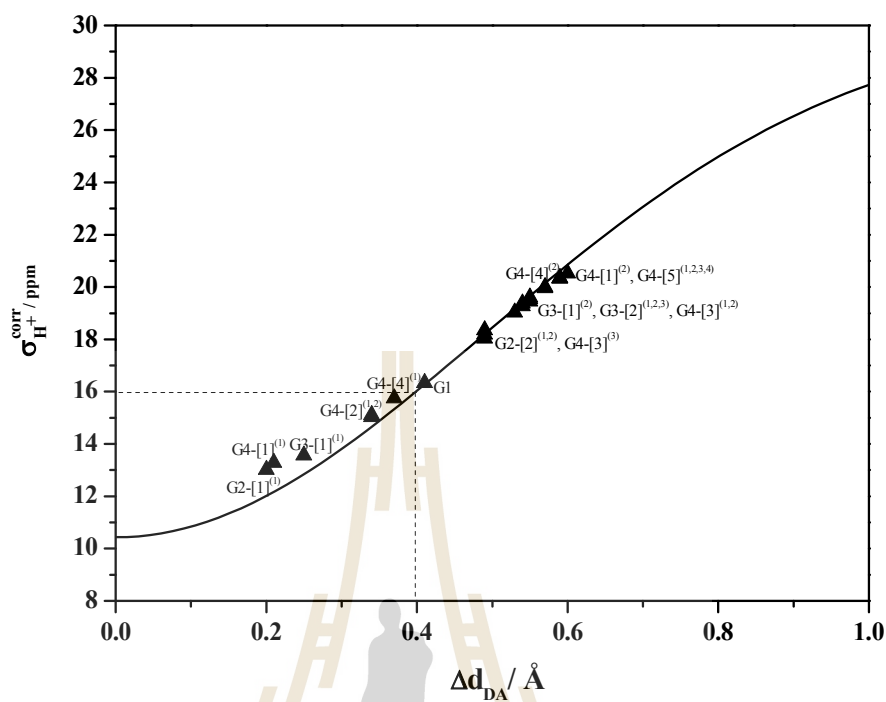


Figure 3.8 Plot of ^1H NMR shielding constant ($\sigma_{H^+}^{corr}$) and asymmetric stretching coordinate (Δd_{DA}) in the gas phase.

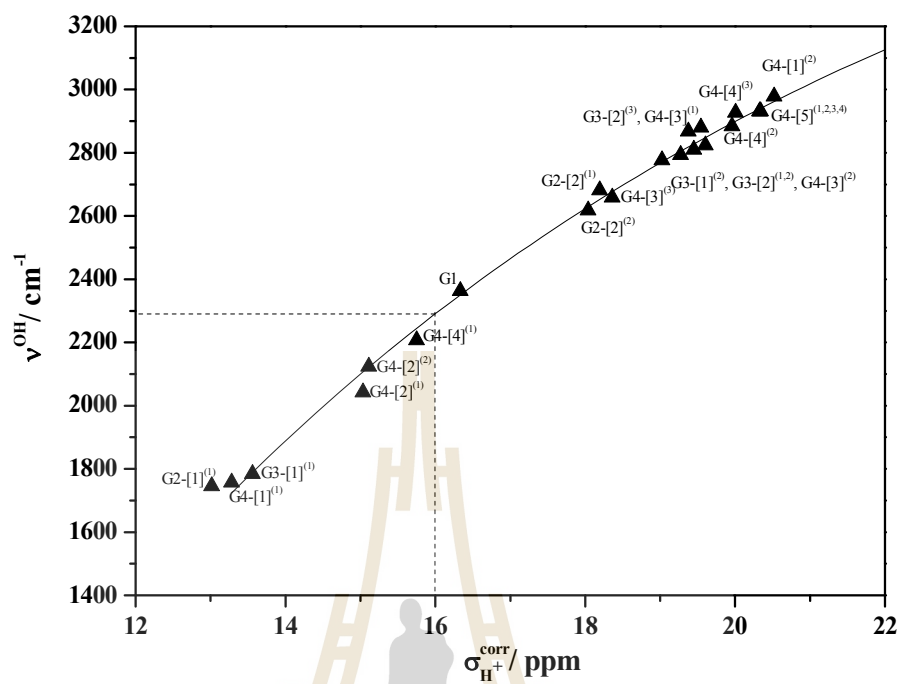


Figure 3.9 Correlation between the asymmetric O-H stretching frequency (ν^{OH}) and the ^1H NMR shielding constant ($\sigma_{\text{H}^+}^{\text{corr}}$) in the gas phase.

3.1.2 Structures and solvent effects

The equilibrium structures of the $\text{H}_3\text{PO}_4\text{-H}_3\text{O}^+-n\text{H}_2\text{O}$ complexes ($n = 1\text{-}3$) shown in Tables 3.1 and 3.2 can be divided into two groups, namely linear H-bond chains, *e.g.*, structures **G1**, **C1**, **G2-[1]**, **C2-[1]**, **G4-[1]**, and **C4-[1]**, and embedded H_4PO_4^+ clusters, *e.g.*, structures **G3-[2]**, **C3-[2]**, **G4-[4]**, and **C4-[4]**. According to the asymmetric O-H stretching frequencies (ν^{OH}), linear H-bond chains with asymmetric hydration at H_4PO_4^+ , as shown in Figure 3.2, are potentially involved in proton dissociation and transfer ($\nu^{\text{OH}} < \nu^{\text{OH}*}$), and this finding supports the protonic-chain conduction mechanism, as in the case of liquid phosphoric acid (Greenwood and Thompson, 1959; Munson and Lazarus, 1967) and methanol (Chaiwongwattana, Phonyiem, Vchirawongkwin, Prueksaaron, and Sagarik, 2012). The values of ν^{OH} in Table 3.2 and the H-bond structures in Figure 3.1 also suggest that the shared-proton structures, in which protons stay almost at the centre of the H-bond (**1**), are favorable in the gas phase, *e.g.*, structures **G2-[1]**, **G4-[1]**, and **G3-[1]**, and that structure **G2-[1]** may represent the smallest, most stable intermediate complex in the proton dissociation pathway ($\Delta d_{\text{DA}} = 0.20 \text{ \AA}$). Most importantly, in the gas phase, the extension of the linear H-bond chains does not increase the tendency of proton transfer from the first to the second hydration shell, *e.g.*, protons in the H-bond (**2**) of structure **G2-[1]** and the H-bond (**3**) of structures **G3-[1]** and **G4-[1]** exhibit $\nu^{\text{OH}} > \nu^{\text{OH}*}$.

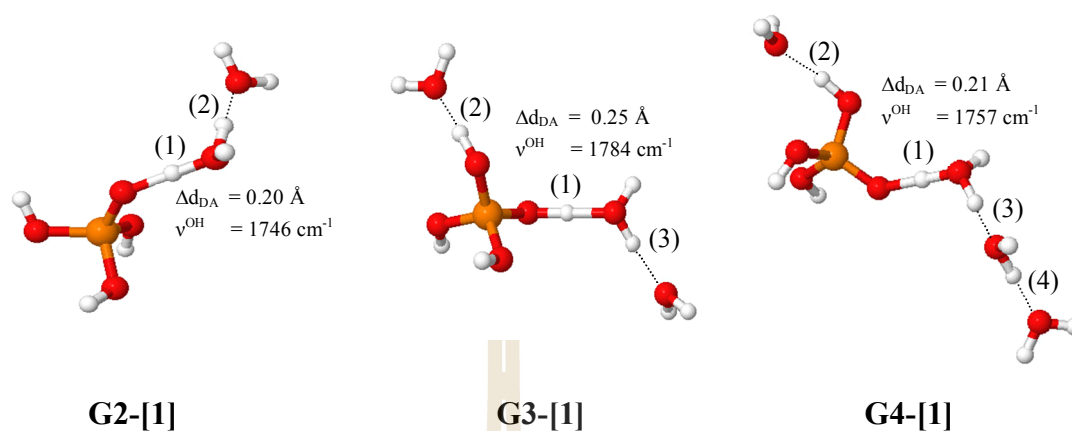


Figure 3.10 Effects of extension of the linear H-bond chains in the gas phase. ν^{OH} = asymmetric O-H stretching frequencies; Δd_{DA} = asymmetric stretching coordinates.

The RIMP2/TZVP results shown in Table 3.2 demonstrate that the ν^{OH} of protons in H-bond (1) of the protonated forms (H_4PO_4^+ and H_3O^+) are in the range of 2040 (linear H-bond structure, structure **G4-[2]**) to 2940 cm^{-1} (fully hydrated H_4PO_4^+ , structure **G4-[5]**) and of 1740 (structure **G2-[1]**) to 1790 cm^{-1} (structure **G3-[1]**), respectively. These characteristic vibrational frequencies could be used to differentiate between the protonated and deprotonated forms in BOMD simulations.

The comparison of the structures of the linear H-bond chains and the dipole moments in the gas phase and continuum aqueous solvent shown in Figure 3.1, e.g., structures **G2-[1]** ($\mu = 9.2$ D) and **C2-[1]** ($\mu = 11.8$ D), revealed prominent effects of solvent polarity on proton dissociation. In the present case, an increase in solvent polarity from $\epsilon = 1$ to $\epsilon = 78$ leads to strong charge redistributions (observed from an increase in the dipole moment), more effective interaction with the electrostatic field of the

solvent, and the shift in the proton in the H-bond **(1)** toward H₂O. The influence of solvent polarity on proton dissociation is in accordance with the localised-charge solvation (LCS) concept, in which “a polar solvent solvates species with localised charges more efficiently than species with more delocalised charges” (Koeppel, Guo, Tolstoy, Denisov, and Limbach, 2013). Therefore, in this case, the protonated forms (H₃O⁺), *e.g.*, structures **C2-[1]** and **C3-[1]**, are more favourable than the shared-proton forms (*e.g.*, structures **G2-[1]** and **G3-[1]**) in continuum aqueous solvent. Based on the localised-charge solvation concept, the possibility of proton transfer from the first hydration shell could be envisaged from structures **G4-[1]** ($\mu = 22.7$ D) and **C4-[1]** ($\mu = 25.9$ D); when COSMO is switched on, the dipole moment of the linear H-bond chain increases, and the shared-proton structure is moved from H-bond **(1)** to **(3)**, generating a Zundel complex attached to H₃PO₄ with a ν^{OH} lower than the ν^{OH^*} of the protonated water clusters (1703 and 1987 cm⁻¹, respectively) (Lao-ngam, Phonyiem, Chaiwongwattana, Kawazoe, and Sagarik, 2013). Therefore, structure **C4-[1]** maybe an intermediate complex for proton transfer from the first to the second hydration shell and should be further studied in BOMD simulations.

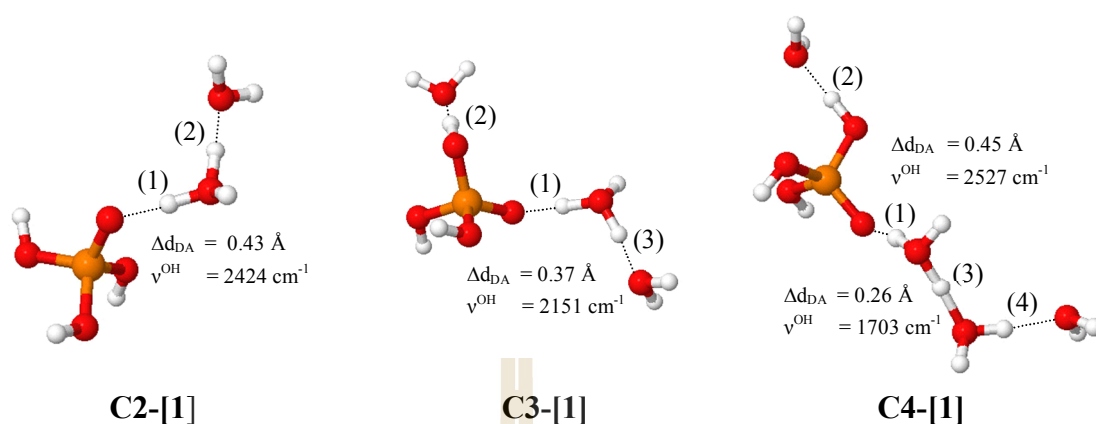
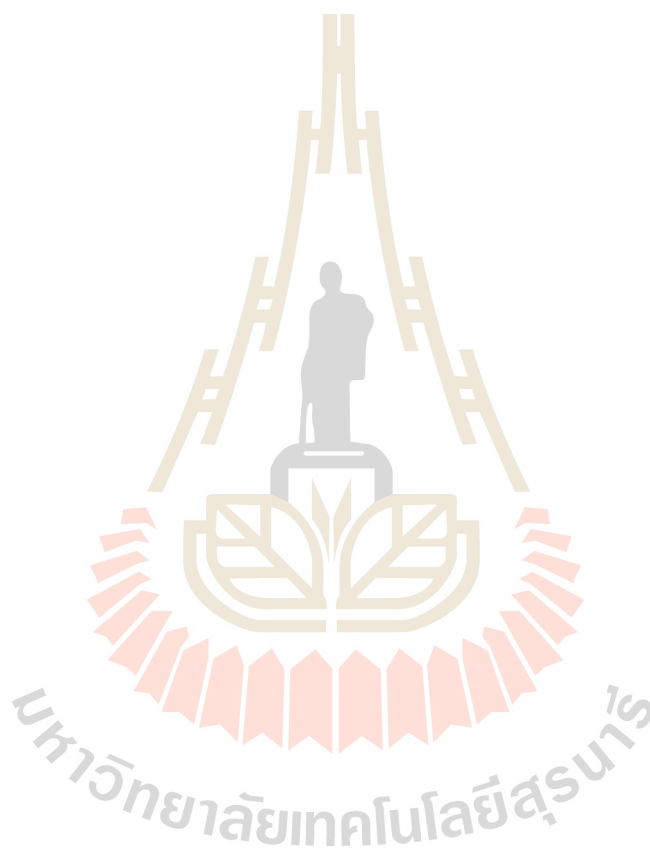


Figure 3.11 Effects of extension of the linear H-bond chains in continuum aqueous solvent. ν^{OH} = asymmetric O-H stretching frequencies; Δd_{DA} = asymmetric stretching coordinates.

Because the linear H-bond chains in a low local-dielectric constant environment ($\epsilon = 1$) represent effective intermediate complexes in the proton dissociation process, *e.g.*, structures **G2-[1]** and **G4-[1]**, because structure **C4-[1]** in a high local-dielectric constant environment ($\epsilon = 78$) is the intermediate complex for proton transfer from the first to the second hydration shell, and because H_3O^+ and H_5O_2^+ , are stabilized in COSMO, one could anticipate that fluctuations in the number of water molecules and the local-dielectric constant play essential roles in the proton dissociation and transfer processes, and the elementary steps could be formulated from the H-bond structures shown in Figure 3.1. Examples of the proposed elementary steps are shown schematically in Figure 3.12. In this scheme, structures **G2-[1]** and **G3-[1]** in a low local-dielectric constant environment ($\epsilon = 1$) are the intermediate complexes of proton dissociation and are produced through elementary

steps **(I)** and **(II)**, respectively. In addition, for proton transfer from the first to the second hydration shell, structure **C4-[1]** in a high local-dielectric constant environment ($\epsilon = 78$) is the most stable intermediate complex and is produced through elementary step **(III)**. All of the proposed elementary steps were verified and studied in detail through BOMD simulations.



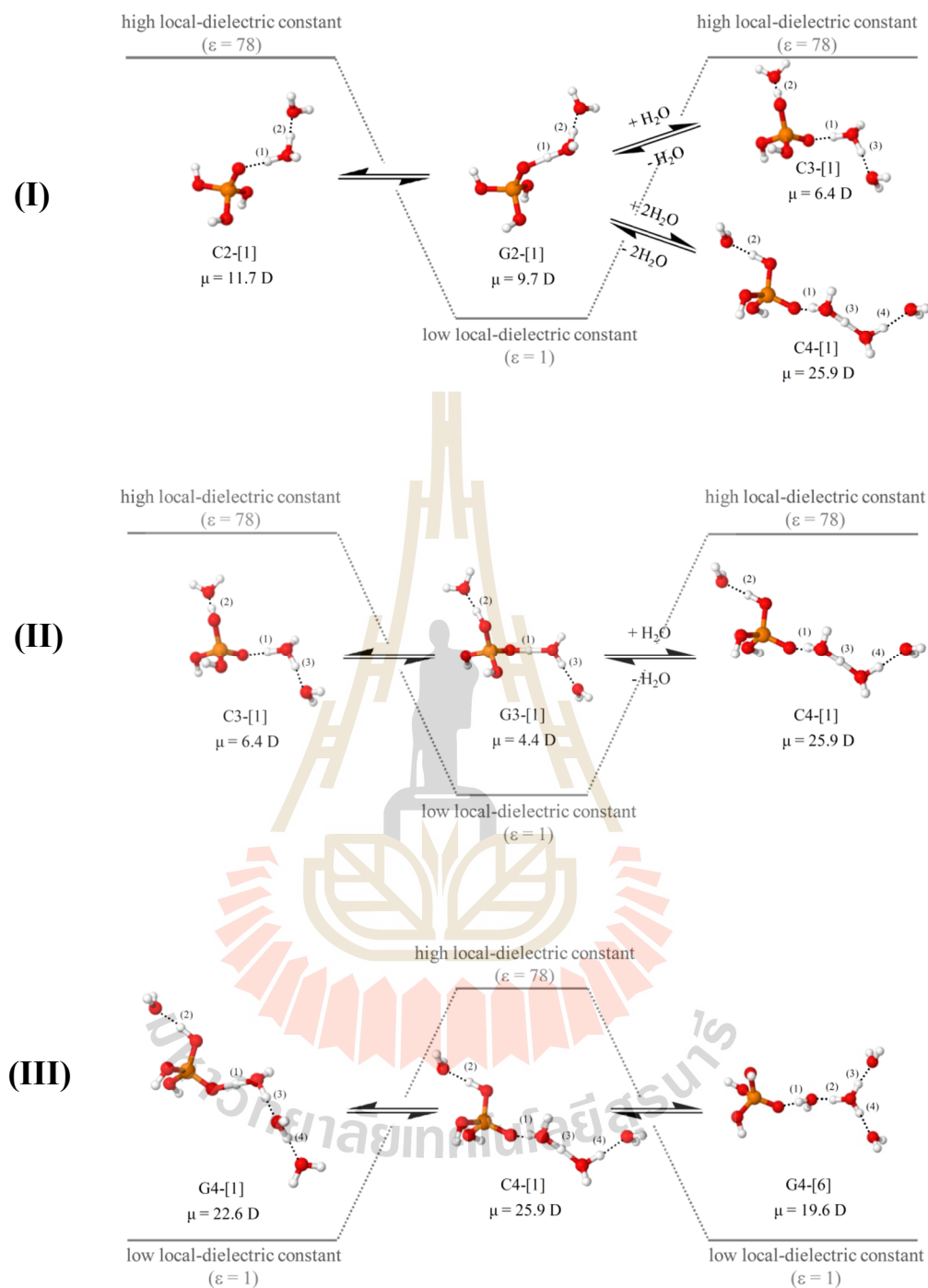


Figure 3.12 Examples of the elementary steps of proton dissociation (**I** and **II**) and transfer (**III**) in $\text{H}_3\text{PO}_4\text{-H}_3\text{O}^+ - n\text{H}_2\text{O}$ complexes ($n = 1\text{-}3$). These steps involve fluctuations in the number of water molecules and in the local-dielectric constant. μ = dipole moment.

3.1.3 Two-dimensional potential energy surfaces

The two-dimensional potential energy surfaces (2D-PES) for proton exchange in the smallest, most stable intermediate complexes in the gas phase and continuum aqueous solvent are illustrated in Figures 3.13 and 3.14, the protons in H-bond (**1**) of structures **G2-[1]** and **C2-[1]**, respectively. Figure 3.13 shows that the absolute minimum on the 2D-PES of structure **G2-[1]** is represented by an asymmetric single-well potential at $R_{O-O} \approx 2.4 \text{ \AA}$ and $\Delta d_{DA} \approx 0.1 \text{ \AA}$. At a longer R_{O-O} distance, a double-well potential appears with an increase in the energy barrier ($\Delta E^{\ddagger, \text{RIMP2/TZVP}}$) as R_{O-O} increases. Two low-interaction energy paths (“energy valleys”) connecting the single- and double-well potentials span from **A** to **C** and from **A** to **B**, whereas the path with the highest $\Delta E^{\ddagger, \text{RIMP2/TZVP}}$ (“energy crest” at $\Delta d_{DA} \approx 0 \text{ \AA}$) is from **D** to **E**. The low-interaction energy paths are regarded hereafter as the structural diffusion paths (also denoted paths **AC** and **AB**), and the path with the highest $\Delta E^{\ddagger, \text{RIMP2/TZVP}}$ is regarded as the transition state path (also denoted path **DE**). The cross-sectional plots of the 2D-PES in Figure 3.13 suggest that the structural diffusion path **AC** is preferred compared with **AB**. Due to the presence of continuum aqueous solvent, the detailed 2D-PES of structure **C2-[1]** is different from that of structure **G2-[1]**. In a high local-dielectric constant environment, such as COSMO with $\epsilon = 78$, the single-well potential becomes more asymmetrical and shifts even closer to H_2O , confirming the previously discussed effects of continuum aqueous solvent, namely increases in the solvent polarity and in the length of the H-bond chain that induce proton displacement from the solute. The shapes of the single-well potentials of structures **G2-[1]** and **C2-[1]** are consistent with the asymmetric O-H stretching frequencies (ν^{OH}) and the ^1H NMR shielding constants ($\sigma_{\text{H}^+}^{\text{corr}}$) listed in

Table 3.2; ν^{OH} of H-bond (**1**) in the gas phase is 1746 cm^{-1} , whereas in continuum aqueous solution, ν^{OH} blue shifts to 2424 cm^{-1} , and $\sigma_{\text{H}^+}^{\text{corr}}$ is 13.0 ppm in the gas phase and increases to 16.6 ppm in continuum aqueous solvent. These values reflect the slightly higher covalent bond character and shielding of a proton in continuum aqueous solvent, which results in the proton staying closer to H_2O .



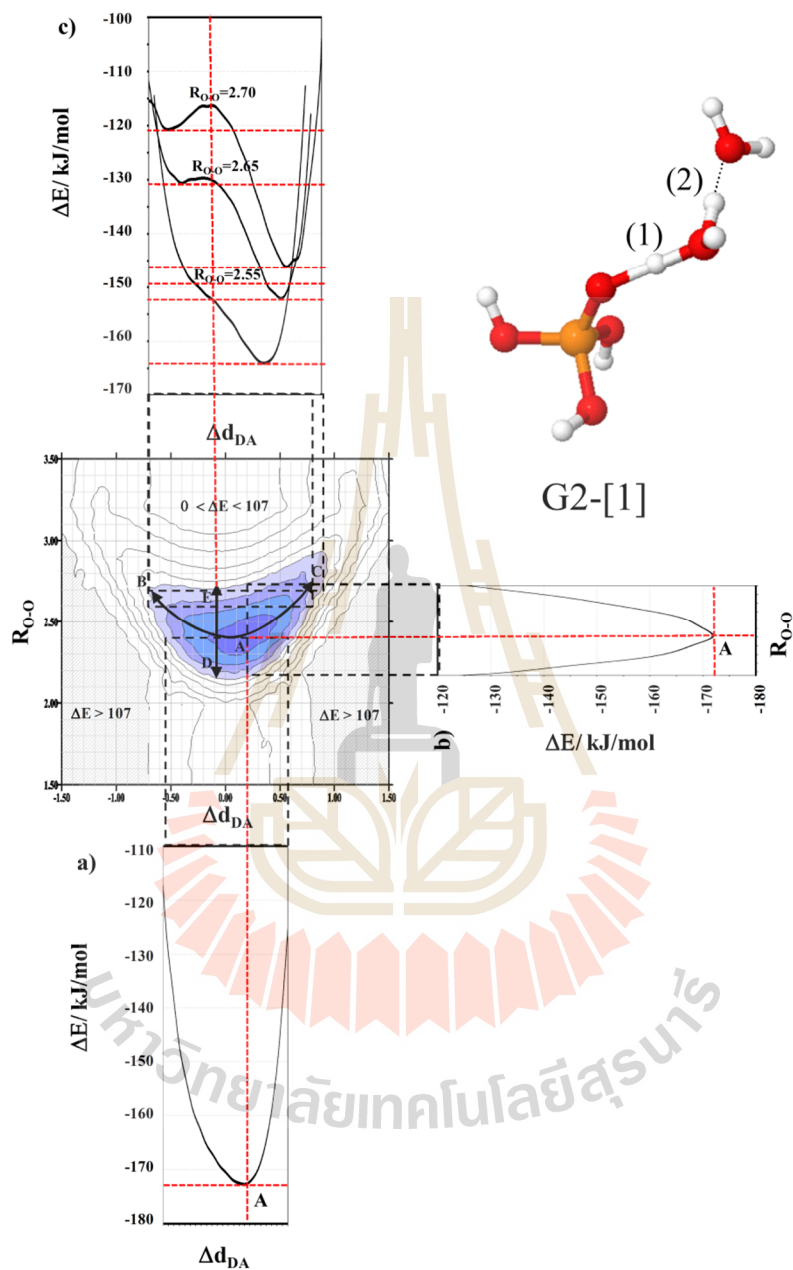


Figure 3.13 Two-dimensional potential energy surface (2D-PES) of a proton in H-bond (1) of structure G2-[1] as a function of H-bond distances (R_{O-O}) and asymmetric O-H stretching frequencies (Δd_{DA}).

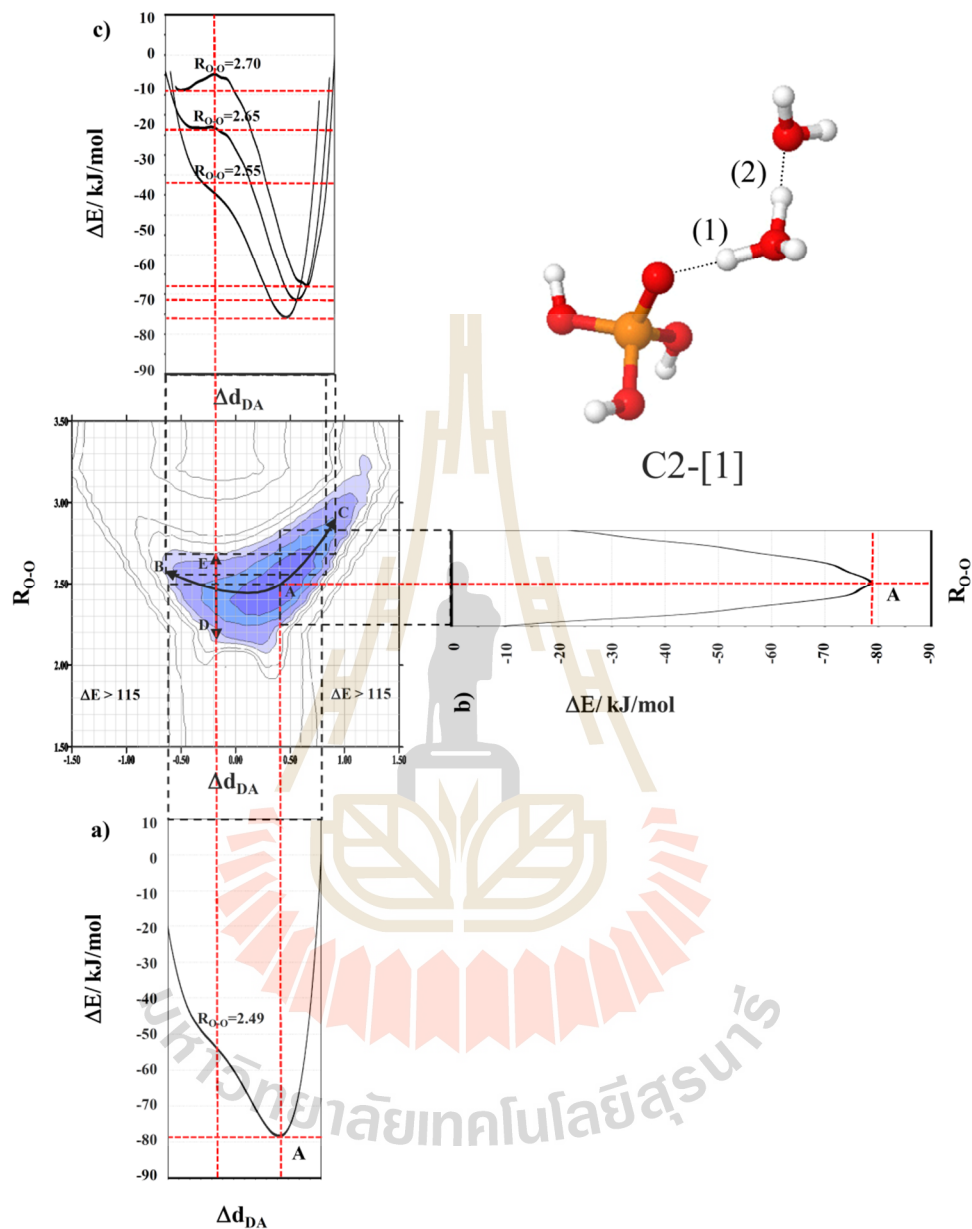


Figure 3.14 Two-dimensional potential energy surface (2D-PES) of a proton in H-bond (1) of structure C2-[1] as a function of H-bond distances (R_{O-O}) and asymmetric O-H stretching frequencies (Δd_{DA}).

3.1.4 Characteristic NMR spectra on 2D-PES

To study the dynamics of proton dissociation through BOMD simulations, the ^1H NMR shielding constants ($\sigma_{\text{H}^+}^{\text{corr}}$) of a proton on the preferential structural diffusion path (path **AC**) and the transition state path (path **DE**) in the gas phase and continuum aqueous solvent were computed and plotted as a function of $R_{\text{O-H}}$ in Figure 3.15–3.16. The $\sigma_{\text{H}^+}^{\text{corr}}$ of the H-bond protons in the $\text{H}_3\text{PO}_4\text{-H}_3\text{O}^+-n\text{H}_2\text{O}$ complexes ($n = 1\text{-}3$) were also included in Figure 3.15–3.16 for comparison. It appears that the trends of $\sigma_{\text{H}^+}^{\text{corr}}$ in the gas phase and continuum aqueous solvent are similar; on the energy crest, $\sigma_{\text{H}^+}^{\text{corr}}$ varies over a narrow range (almost constant at approximately 12 ppm), whereas in the energy valley, $\sigma_{\text{H}^+}^{\text{corr}}$ changes exponentially with $R_{\text{O-H}}$ (from 14 ppm to 12 ppm as $R_{\text{O-H}}$ is increased from 1.10 Å to 1.15 Å). The latter correspond to ^1H NMR chemical shifts ($\delta_{\text{H}^+}^{\text{corr}}$) of 18 and 20 ppm, respectively.

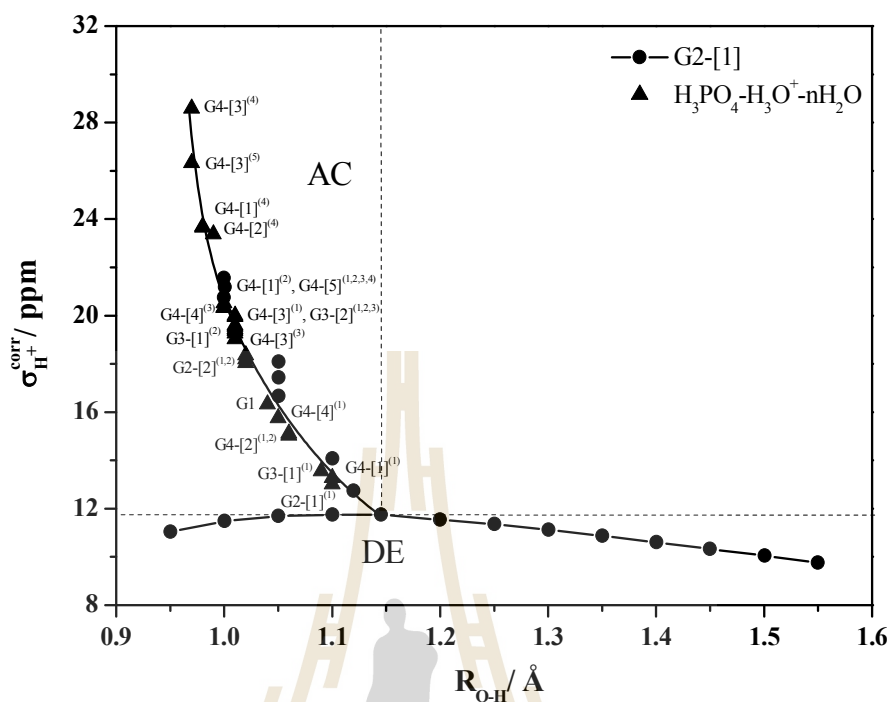


Figure 3.15 Plots of the ^1H NMR shielding constant ($\sigma_{\text{H}^+}^{\text{corr}}$) and $R_{\text{O-H}}$ of a proton on the low-interaction energy path (structural diffusion path, AC) and on the path with the highest $\Delta E^{\ddagger, \text{RIMP2/TZVP}}$ (transition state path, DE), obtained from the RIMP2/TZVP calculations in the gas phase.

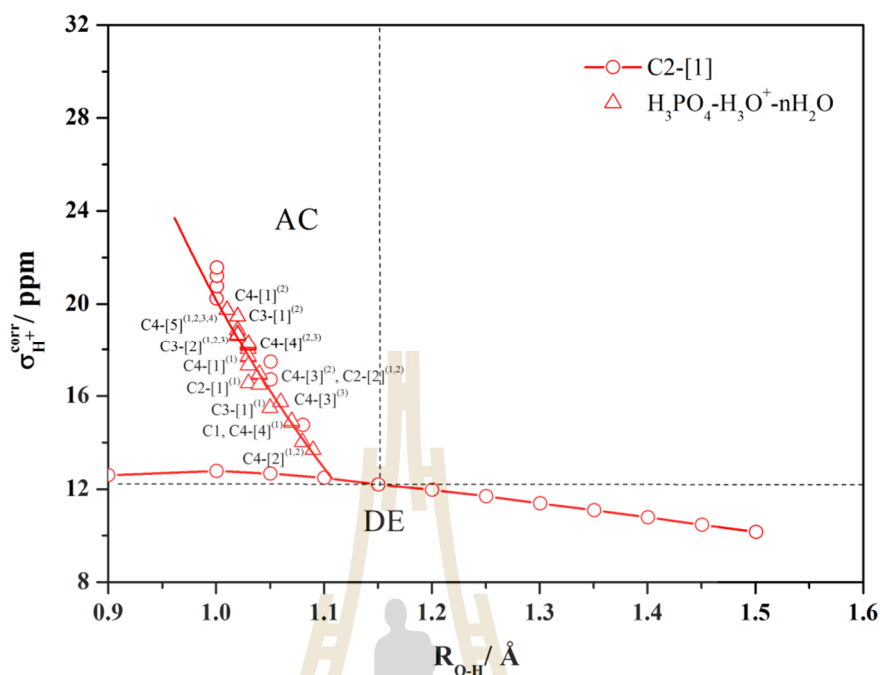


Figure 3.16 Plots of the ^1H NMR shielding constant ($\sigma_{\text{H}^+}^{\text{corr}}$) and $R_{\text{O-H}}$ of a proton on the low-interaction energy path (structural diffusion path, **AC**) and on the path with the highest $\Delta E^{\ddagger, \text{RIMP2/TZVP}}$ (transition state path, **DE**), obtained from the RIMP2/TZVP calculations in continuum aqueous solvent.

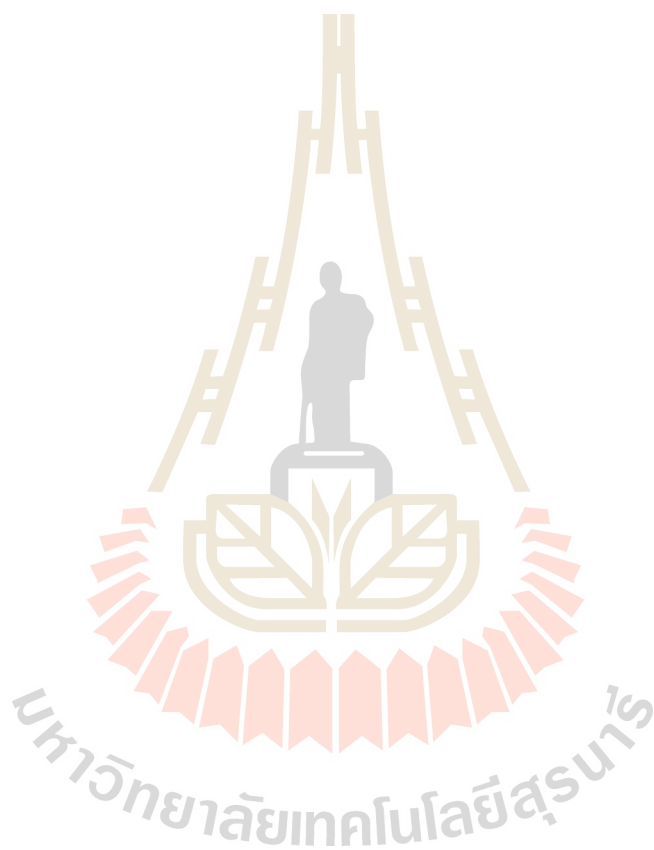
3.2 Dynamic results

3.2.1 Structures and energies

The BOMD simulations confirmed that only the linear H-bond chains with asymmetric hydration at H_4PO_4^+ are susceptible to proton dissociation and transfer and that the structures **G2-[1]** and **C4-[1]** are the most stable intermediate complexes in these processes, respectively. To further study the effects of a polar solvent and verify the proposed elementary steps shown in Figure 3.12, the proton transfer profiles (Sagarik, Phonyiem, Lao-ngam, and Chaiwongwattana, 2008) of H-bonds **(1)** and **(2)** in structures **G2-[1]** and **C2-[1]** and H-bonds **(1)** and **(3)** in structures **G4-[1]** and **C4-[1]** at 298 K were constructed and are shown in Figures 3.17 (a) and (b) and 3.18 (a) and (b), respectively.

For proton dissociation in H-bond **(1)**, the oscillatory shuttling motion, which is a characteristic of the intermediate complex and determines the rate of proton dissociation, was observed only in structures **G2-[1]** and **G4-[1]** (see panel **(II)** of Figures 3.17 (a) and 3.18 (a), respectively). Because the oscillatory shuttling vibrational frequencies of a proton in H-bond **(1)** of structure **G2-[1]**, which were obtained from both static and dynamic calculations, are lower than those obtained for structure **G4-[1]**, structure **G2-[1]** was confirmed to be the smallest, most stable intermediate complex. In continuum aqueous solvent, the proton transfer profiles of H-bond **(1)** in structures **C2-[1]** and **C4-[1]** (see panel **(II)** of Figures 3.17 (b) and 3.18 (b)) indicated that a proton prefers to stay close to H_2O , which rules out the possibility that both structures are intermediate complexes in the proton dissociation process. The proton transfer profile in panel **(VI)** of Figure 3.18 (b) confirmed that structure **C4-[1]** is the intermediate complex for proton

transfer from the first to the second hydration shell, which implies that continuum aqueous solvent is required to induce and stabilize the shared-proton structure in H-bond (3).



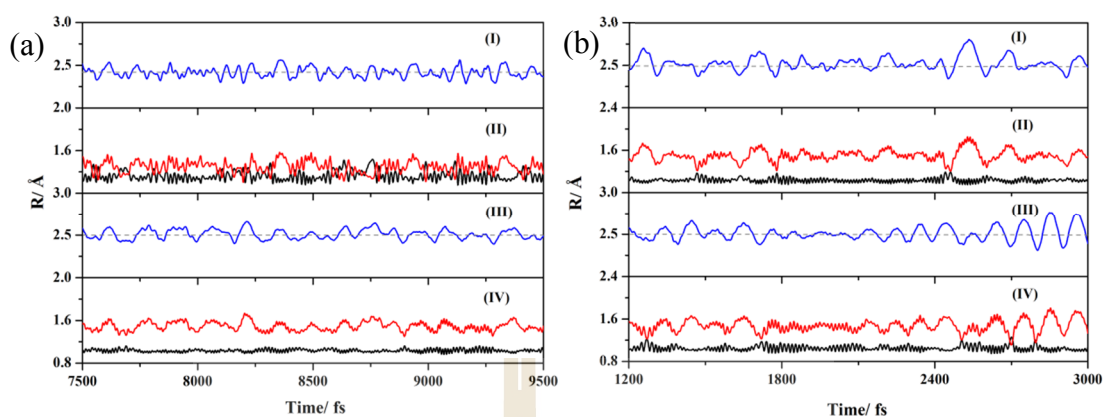


Figure 3.17 Variations in the R_{O-O} and R_{O-H} distances in H-bonds determined through BOMD simulations at 298 K. (a) and (b) Structures **G2-[1]** and **C2-[1]**, respectively. Panels **(I)** and **(II)** are the R_{O-O} and R_{O-H} of H-bond **(1)**. Panels **(III)** and **(IV)** are the R_{O-O} and R_{O-H} of H-bond **(2)**.

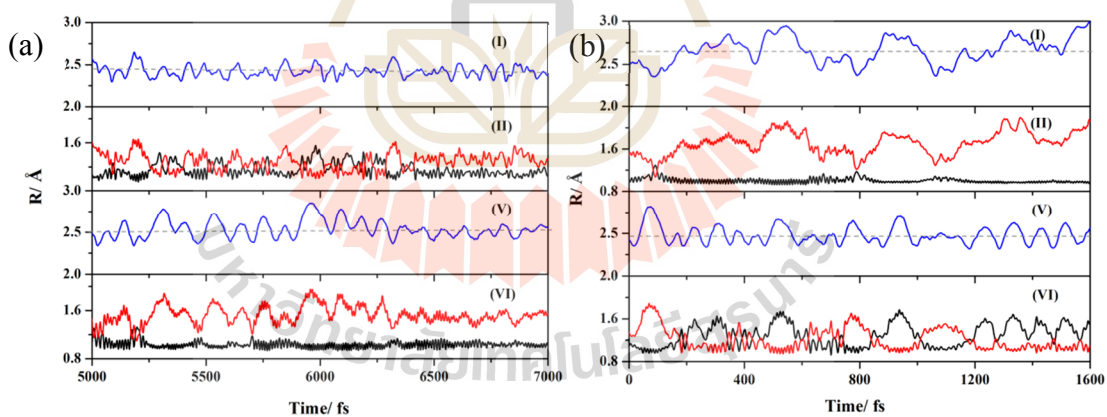


Figure 3.18 Variations in the R_{O-O} and R_{O-H} distances in H-bonds determined through BOMD simulations at 298 K. (a) and (b) Structures **G4-[1]** and **C4-[1]**, respectively. Panels **(I)** and **(II)** are the R_{O-O} and R_{O-H} of H-bond **(1)**. Panels **(V)** and **(VI)** are the R_{O-O} and R_{O-H} of H-bond **(3)**.

3.2.2 Activation energies of proton dissociation and transfer

The activation energies ($\Delta E^{\ddagger, \text{Arr}}$) of the rate-determining processes in proton dissociation and transfer in the $\text{H}_3\text{PO}_4\text{-H}_3\text{O}^+ - n\text{H}_2\text{O}$ complexes ($n = 1\text{-}3$) were obtained from BOMD simulations of the most stable intermediate complexes over the temperature range of 298 to 430 K. The Arrhenius plot in Figure 3.19 yielded an $\Delta E^{\ddagger, \text{Arr}}$ of proton dissociation for H-bond **(1)** of structure **G2-[1]** of 13.1 kJ/mol, whereas the Arrhenius plot of H-bond **(3)** in structure **C4-[1]**, which is shown in Figure 3.20, suggests an $\Delta E^{\ddagger, \text{Arr}}$ of proton transfer from the first to the second hydration shell of 9.9 kJ/mol. The latter is slightly lower than the $\Delta E^{\ddagger, \text{Arr}}$ of proton exchange in the Zundel complex of 10.2 kJ/mol (Lao-ngam, Phonyiem, Chaiwongwattana, Kawazoe, and Sagarik, 2013) and is compatible with the activation energies obtained from ion conductivity measurements of 85–100 wt.% H_3PO_4 solutions at 293 K, which were reported to be in the range of 7.8 to 14 kJ/mol (He, Li, Xiao, and Bjerrum, 2003), and ^1H NMR line width analyses over the temperature range of 293 to 353 K of 11 kJ/mol (Chung, Bajue, and Greenbaum, 2000). Therefore, the activation energies obtained from the BOMD simulations confirmed elementary step **(III)** in Figure 3.12, in which structure **C4-[1]** is proposed to be the most stable intermediate complex for proton transfer from the first to the second hydration shell.

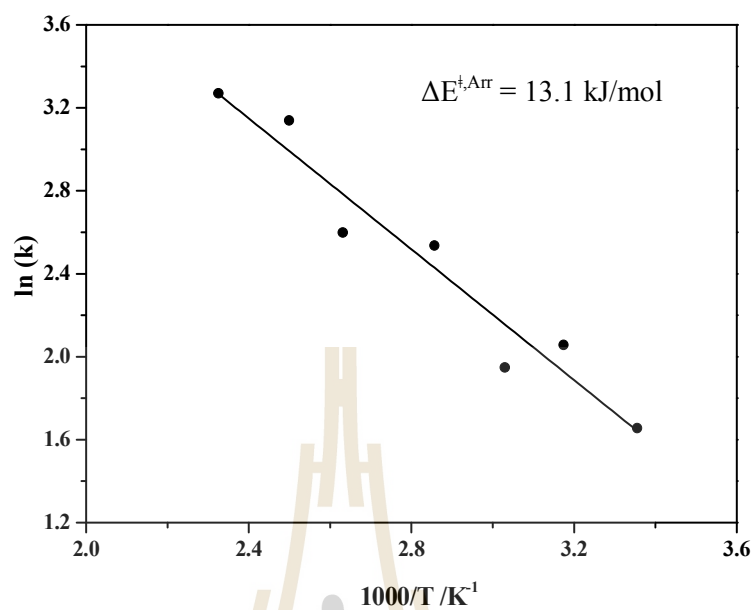


Figure 3.19 Arrhenius plots obtained from the BOMD simulations over the temperature range of 298–430 K for proton dissociation in H-bond (**1**) of structure G2-[1].

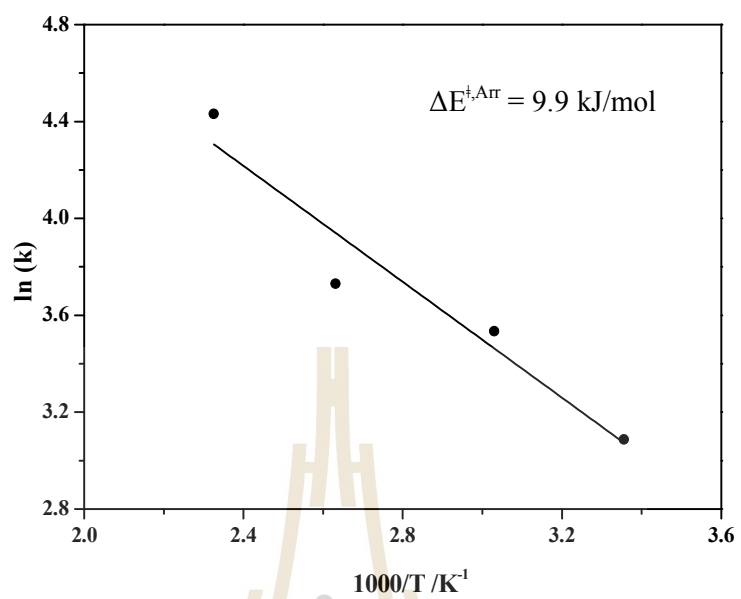


Figure 3.20 Arrhenius plots obtained from the BOMD simulations over the temperature range of 298–430 K for proton transfer in H-bond (3) of structure C4-[1].

3.2.3 Vibrational and NMR spectra

Before the vibrational spectra of proton dissociation and transfer are discussed, remarks should be made on the characteristic vibrational motions in protonated H-bonds. For a symmetric donor-acceptor pair, such as in the Zundel complex, the dynamics of the transferring proton are characterized by two vibrational modes, namely the oscillatory shuttling motion, in which the proton shuttles at the centre of the H-bond (proton moves in a symmetric single-well potential), and the structural diffusion motion, in which the centre of the vibration is slightly shifted toward an oxygen atom (proton moves on the structural diffusion path). However, for an asymmetric donor-acceptor pair, such as in H-bond **(1)** of structure **G2-[1]**, the cross-sectional plots in Figure 3.13 suggested three different modes of vibration, namely a vibrational mode associated with the proton moving in an asymmetric single-well potential or shuttling near the centre of H-bond **(1)** and two vibrational modes for the proton moving in an asymmetric double-well potential with centres of vibration close to H₃PO₄ and H₂O. Therefore, in the present work, three characteristic vibrational frequencies were employed in the analyses of the dynamics of proton dissociation.

Examples of the vibrational spectra of proton dissociation in H-bond **(1)** of structure **G2-[1]**, which were obtained from BOMD simulations at 298, 315, and 350 K, are shown in Figure 3.21. Only the results at 298 K are discussed in detail. The three characteristic peaks, labelled **A**, **B**, and **C**, are outstanding at $\nu_A^{\text{OH,MD}} = 1052 \text{ cm}^{-1}$, $\nu_B^{\text{OH,MD}} = 1378 \text{ cm}^{-1}$, and $\nu_C^{\text{OH,MD}} = 1877 \text{ cm}^{-1}$.

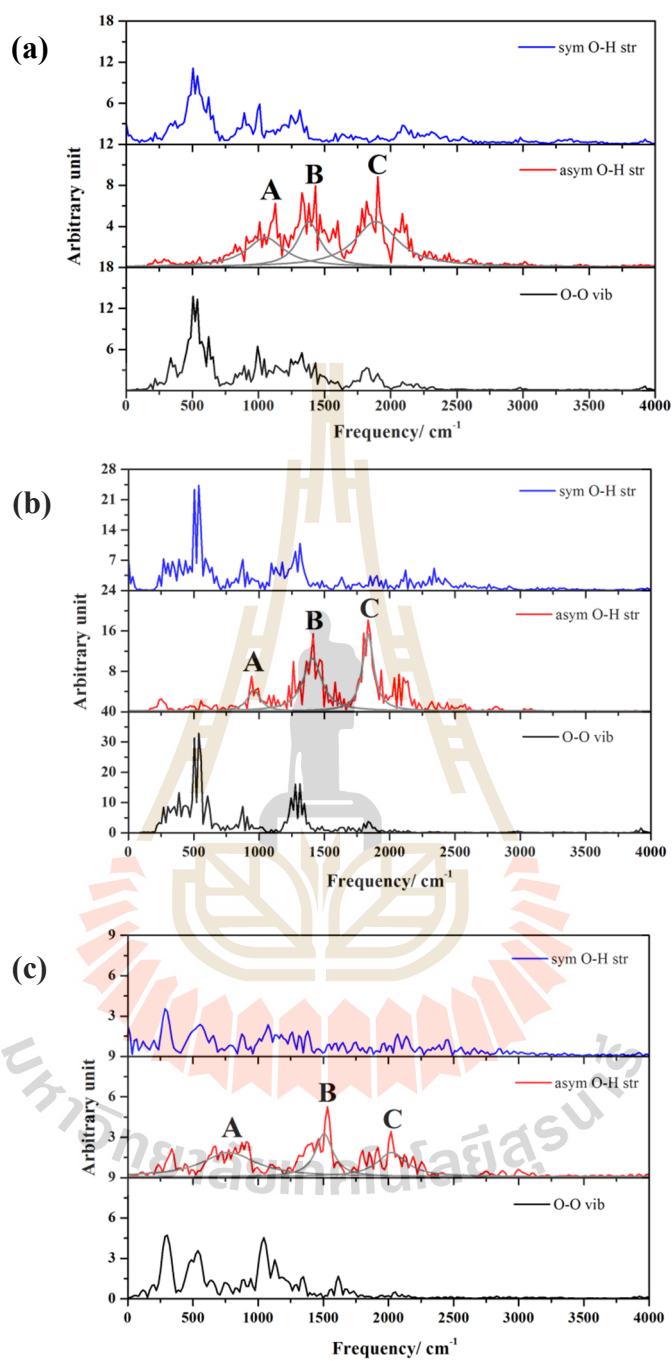
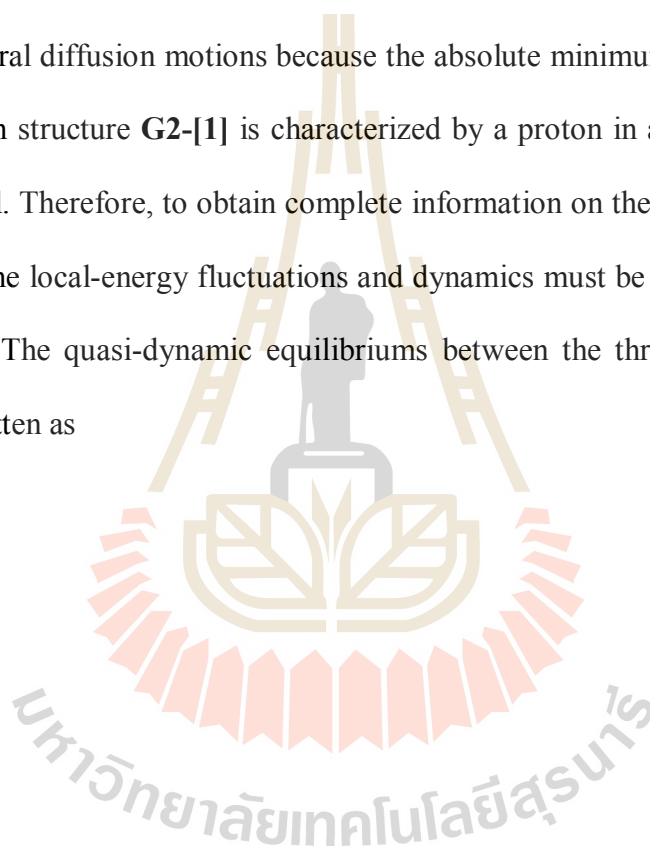
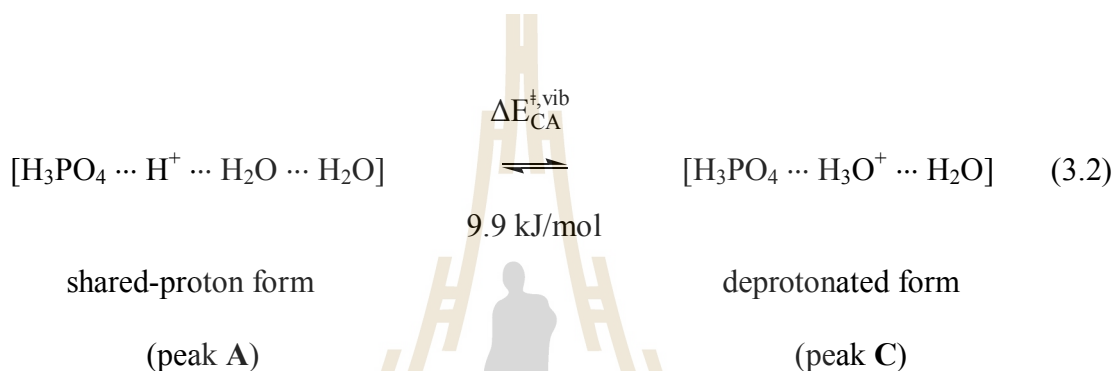
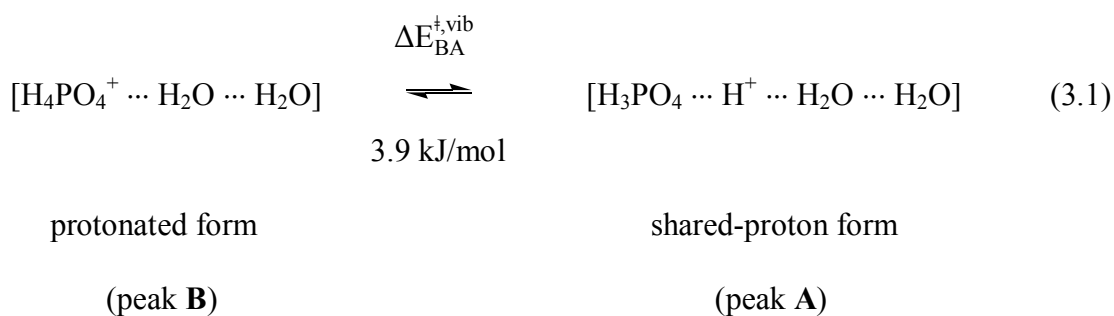


Figure 3.21 Vibrational spectra of a proton in H-bond (1) of structure G2-[1] obtained from BOMD simulations at (a) 298 K, (b) 315 K, and (c) 350 K.

Based on the structures of the cross-sectional plots in Figure 3.13 and the ν^{OH} values shown in Table 3.2, peak **A** can be assigned to the oscillatory shuttling motion, whereas peaks **B** and **C** are the structural diffusion motions in the protonated forms (H_4PO_4^+ and H_3O^+), which correspond to the proton moving on paths **AB** and **AC** in Figure 3.13, respectively. It should be stressed that the RIMP2/TZVP calculations with the harmonic approximation did not yield the vibrational frequencies of the structural diffusion motions because the absolute minimum energy geometry of H-bond (**1**) in structure **G2-[1]** is characterized by a proton in an asymmetric single-well potential. Therefore, to obtain complete information on the motion of a proton in an H-bond, the local-energy fluctuations and dynamics must be included in the model calculations. The quasi-dynamic equilibriums between the three limiting forms are therefore written as





From the characteristic vibrational frequencies, the vibrational energies for the interconversion between the protonated (H_4PO_4^+ , peak **B**) and shared-proton (peak **A**) structures shown in equation (3.1), and the protonated (H_3O^+ , peak **C**) and shared-proton (peak **A**) structures shown in equation (3.2) can be approximated at 298 K as $\Delta v_{BA}^{\text{OH,MD}} = 326$ and $\Delta v_{CA}^{\text{OH,MD}} = 825 \text{ cm}^{-1}$, which correspond to $\Delta E_{BA}^{\ddagger, \text{vib}} = 3.9$ and $\Delta E_{CA}^{\ddagger, \text{vib}} = 9.9 \text{ kJ/mol}$, respectively (Phonyiem, Chaiwongwattana, Lao-ngam, and Sagarik, 2011).

The trends in the characteristic vibrational frequencies ($\nu_A^{\text{OH,MD}}$, $\nu_B^{\text{OH,MD}}$, and $\nu_C^{\text{OH,MD}}$) with respect to temperature are illustrated in Figure 3.22; these show uniform changes in the vibrational frequencies of proton dissociation over the entire temperature range: as the temperature increases from 298 to 430 K, the oscillatory shuttling peak (peak **A**) red shifts, reflecting more polarization in H-bond (**1**), whereas the structural diffusion peaks (peaks **B** and **C**) blue shift, indicating larger proton displacement at elevated temperatures. Due to the vibrational interference effects, the vibrational spectra of a proton in H-bond (**3**) of structure **C4-[1]** are complicated, especially at elevated temperatures. Therefore, only the vibrational spectra at 298 K, which is shown in Figure 3.23, were analyzed. These are characterized by a characteristic oscillatory shuttling peak (peak **A**) at $\nu_A^{\text{OH,MD}} = 893 \text{ cm}^{-1}$ and a structural diffusion peak (peak **B**) at $\nu_B^{\text{OH,MD}} = 1515 \text{ cm}^{-1}$, which results in $\Delta\nu_{\text{BA}}^{\text{OH,MD}} = 622 \text{ cm}^{-1}$ and $\Delta E_{\text{BA}}^{\ddagger,\text{vib}} = 7.4 \text{ kJ/mol}$. The $\Delta E_{\text{BA}}^{\ddagger,\text{vib}}$ is lower than that of the Zundel complex in continuum aqueous solvent at 350 K, which was found to be 8.9 kJ/mol (Lao-ngam, Phonyiem, Chaiwongwattana, Kawazoe, and Sagarik, 2013), confirming the slightly higher efficiency of proton transfer in the presence of the solute.

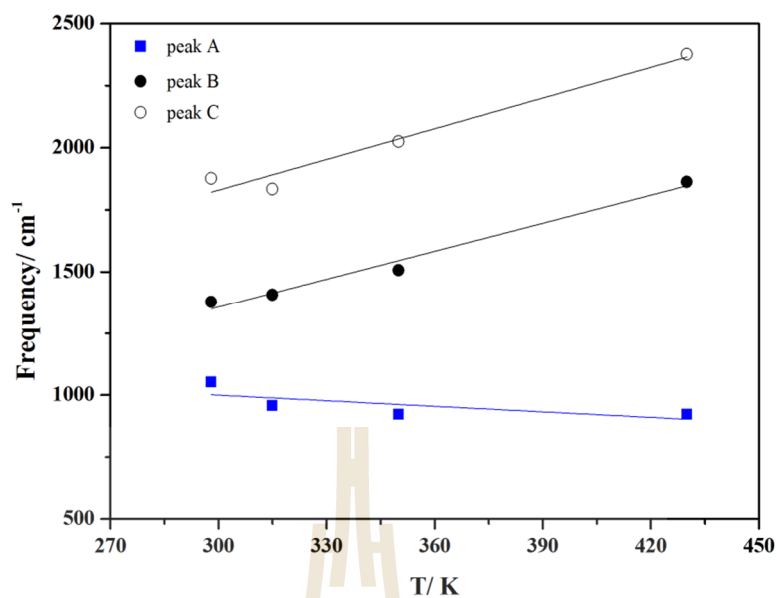


Figure 3.22 Trends in the characteristic oscillatory shuttling (peak A) and structural diffusion (peaks B and C) frequencies of proton dissociation in H-bond (**1**) of structure G2-[1] obtained from BOMD simulations over the temperature range of 298–430 K.

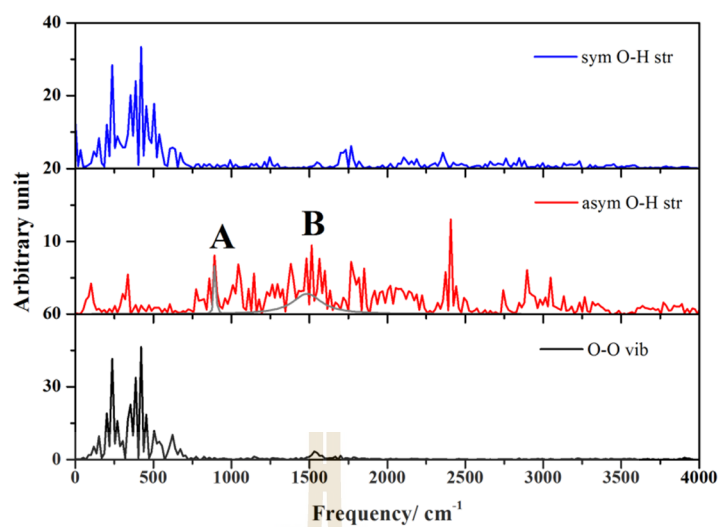
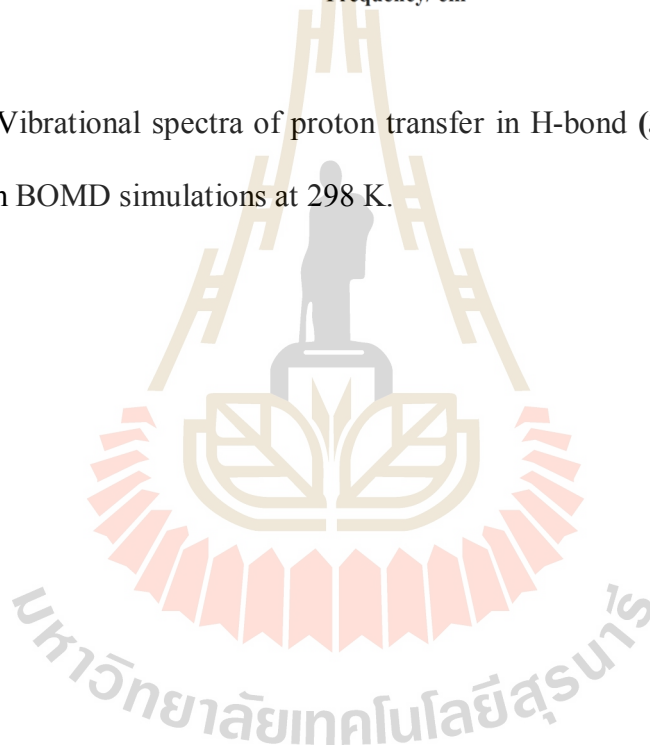
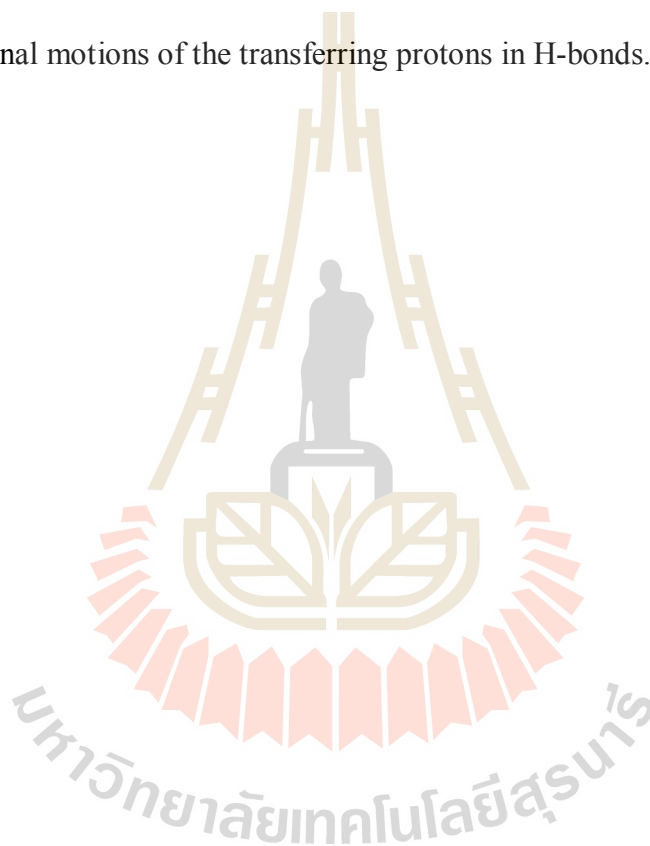


Figure 3.23 Vibrational spectra of proton transfer in H-bond (3) of structure C4-[1] obtained from BOMD simulations at 298 K.



Additional information on the dynamics of proton dissociation can be obtained from the ^1H NMR chemical shift spectra of H-bond **(1)** in structure **G2-[1]**, which were obtained from the BOMD simulations over the temperature range of 350 to 430K. These are shown as examples in Figure 3.24. The ^1H NMR chemical shift spectra at 350 K are characterized by two well-defined peaks at 20.3 and 19.5 ppm and a broad peak at 18.0 ppm (labelled **A**, **C**, and **B** in panel **(I)** of Figure 3.24 (a), respectively). According to the static results, peak **A** is associated with a proton at the centre of H-bond **(1)**, whereas peaks **C** and **B** are the protonated forms, H_3O^+ and H_4PO_4^+ , respectively. Because peaks **A** and **C** overlap, the ^1H NMR line width analyses had to be made using two Lorentzian peak functions, namely peaks **A** and **B** in panel **(II)** of Figure 3.24. The slope of the plot of $\ln T_2^*$ and $1000/T$ in Figure 3.25, which was obtained from the analysis of peak **A**, yielded an activation energy ($\Delta E^{\ddagger, \text{NMR}}$) of deprotonation along path **AC** of 10.8 kJ/mol, which is in excellent agreement with the $\Delta E_{\text{CA}}^{\ddagger, \text{vib}}$ value obtained for the same path (see equation (3.2)) and the ^1H NMR line width measurement over the temperature range of 293 to 353 K of 11 kJ/mol (Chung, Bajue, and Greenbaum, 2000). As the same motional narrowing was observed at elevated temperatures with almost the same activation energies, and the ^1H NMR chemical shifts of protonated H-bonds were shown in the previous work (Lao-ngam, Phonyiem, Chaiwongwattana, Kawazoe, and Sagarik, 2013) to be sensitive only to the H-bond distances, one can conclude that the ^1H NMR line width measurement reflected the characteristic local-vibrational motions of the transferring proton, not the local-rotational motions as anticipated in Chung *et al.* (Chung, Bajue, and Greenbaum, 2000); the previous work of ^1H NMR line width analyses revealed that the chemical shifts of the shared-protons in protonated water clusters are not

sensitive to the rotational motions, for example, for $\text{H}^+(\text{H}_2\text{O})_n$, $n = 4$, the chemical shifts of protons in the *cis* and *trans* H-bond structures are almost the same, 20.93 and 20.99 ppm, respectively (Lao-ngam, Phonyiem, Chaiwongwattana, Kawazoe, and Sagarik, 2013), and those for the planar and perpendicular structures of the protonated imidazole dimers ($\text{H}^+(\text{Im})_2$) are 21.18 and 21.63 ppm, respectively. The microscopic dynamics probed by the ^1H NMR line width analyses are, therefore, the characteristic local-vibrational motions of the transferring protons in H-bonds.



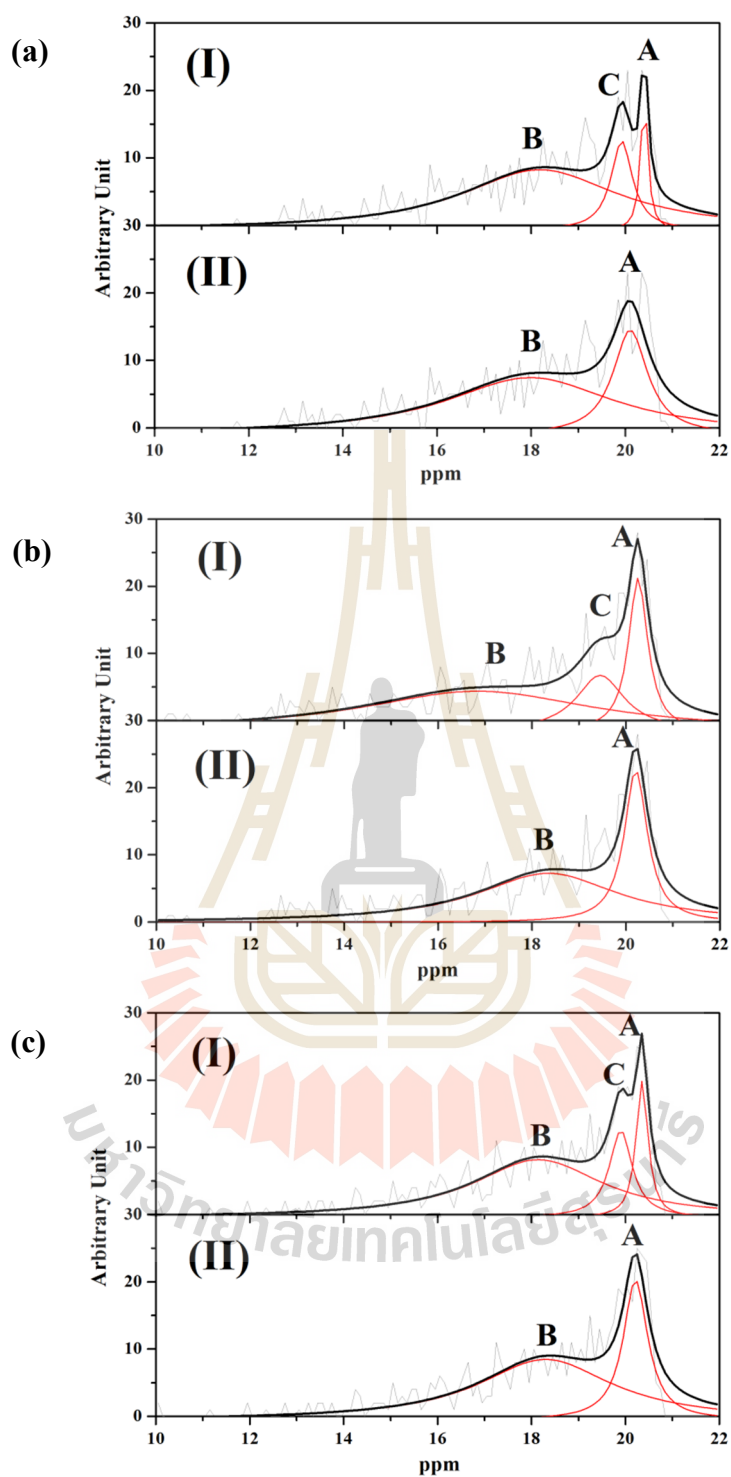
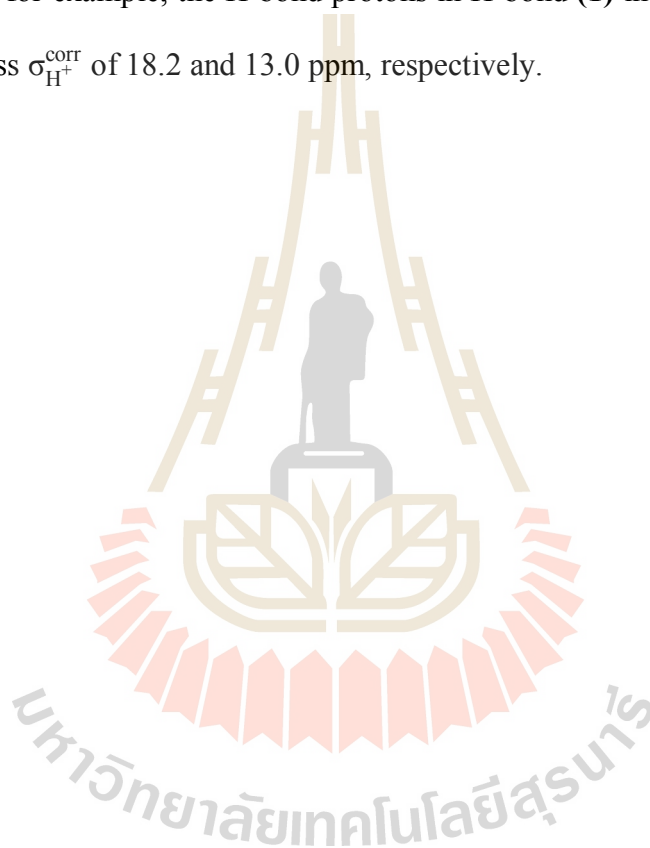


Figure 3.24 Examples of the ^1H NMR chemical shift spectra of proton dissociation in H-bond (1) of structure G2-[1] obtained from BOMD simulations at (a) 350 K, (b) 380 K, and (c) 400 K, respectively.

The analysis of peak **B** yielded an $\Delta E^{\ddagger, \text{NMR}}$ value on path **AB** of 8.9 kJ/mol, which is considerably higher than the corresponding $\Delta E_{\text{BA}}^{\ddagger, \text{vib}}$ of 3.9 kJ/mol. The difference is because the oxygen atom in H_3PO_4 possesses a higher electron density than that of H_2O , resulting in a higher shielding effects at the H-bond proton, which is sensitive to not only its position, but also vibrational interferences and environment, for example, the H-bond protons in H-bond **(1)** in structures **G2-[2]** and **G2-[1]** possess $\sigma_{\text{H}^+}^{\text{corr}}$ of 18.2 and 13.0 ppm, respectively.



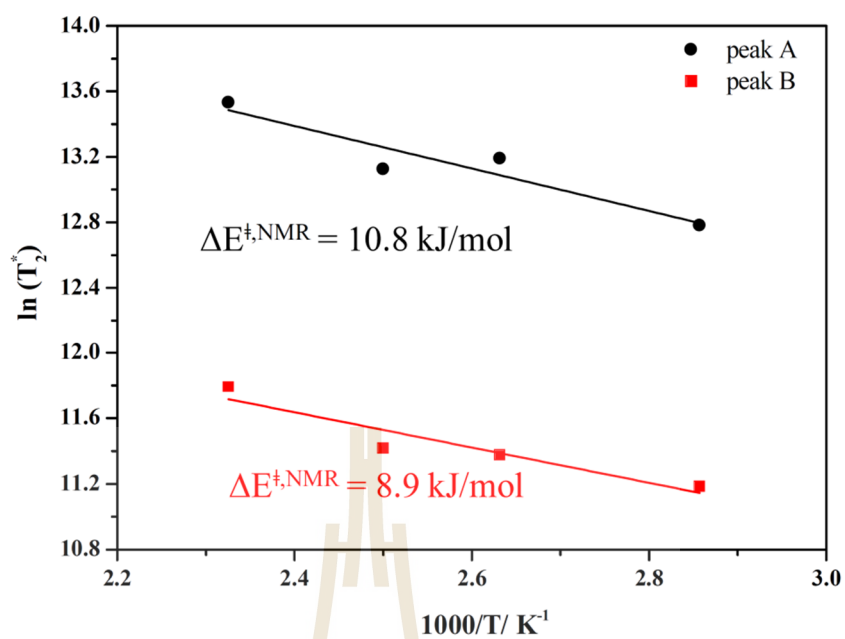


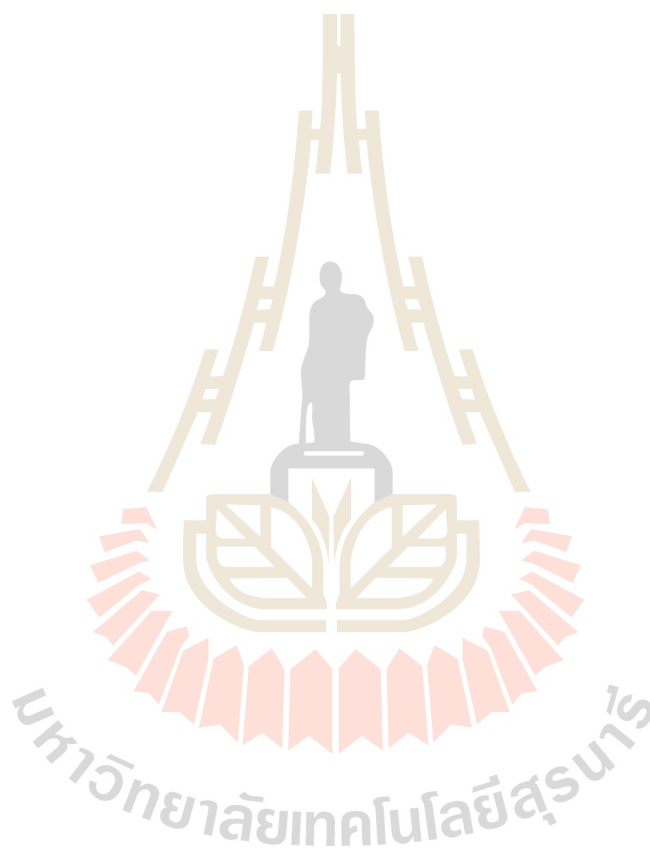
Figure 3.25 Plots of the natural log of the effective transverse relaxation time (T_2^*) as a function of $1000/T$ for peaks **A** and **B**. Peak **A** is associated with protons moving in single-well potential, whereas peaks **B** and **C** are connected to the double-well potentials.

3.3 References

- Chaiwongwattana, S., Phonyiem, M., Vchirawongkwin, V., Prueksaaron, S., and Sagarik, K. (2012). Dynamics and mechanism of structural diffusion in linear hydrogen bond. **Journal of Computational Chemistry**. 33: 175-188.
- Chung, S. H., Bajue, S., and Greenbaum, S. G. (2000). Mass transport of phosphoric acid in water: A ^1H and ^{31}P pulsed gradient spin-echo nuclear magnetic resonance study. **The Journal of Chemical Physics**. 112: 8515-8521.
- Greenwood, N. N., and Thompson, A. (1959). 701. The mechanism of electrical conduction in fused phosphoric and trideuterophosphoric acids. **Journal of the Chemical Society (Resumed)**: 3485-3492.
- He, R., Li, Q., Xiao, G., and Bjerrum, N. J. (2003). Proton conductivity of phosphoric acid doped polybenzimidazole and its composites with inorganic proton conductors. **Journal of Membrane Science**. 226: 169-184.
- Koeppe, B., Guo, J., Tolstoy, P. M., Denisov, G. S., and Limbach, H.-H. (2013). Solvent and H/D Isotope Effects on the Proton Transfer Pathways in Heteroconjugated Hydrogen-Bonded Phenol-Carboxylic Acid Anions Observed by Combined UV-vis and NMR Spectroscopy. **Journal of the American Chemical Society**. 135: 7553-7566.
- Lao-ngam, C., Phonyiem, M., Chaiwongwattana, S., Kawazoe, Y., and Sagarik, K. (2013). Characteristic NMR spectra of proton transfer in protonated water clusters. **Chemical Physics**. 420: 50-61.
- Munson, R. A., and Lazarus, M. E. (1967). Influence of ionic solutes upon the conductivity of molten phosphoric acid. **The Journal of Physical Chemistry**. 71: 3245-3248.

Phonyiem, M., Chaiwongwattana, S., Lao-ngam, C., and Sagarik, K. (2011). Proton transfer reactions and dynamics of sulfonic acid group in Nafion[®]. **Physical Chemistry Chemical Physics**. 13: 10923-10939.

Sagarik, K., Phonyiem, M., Lao-ngam, C., and Chaiwongwattana, S. (2008). Mechanisms of proton transfer in Nafion[®]: elementary reactions at the sulfonic acid groups. **Physical Chemistry Chemical Physics**. 10: 2098-2112.



CHAPTER IV

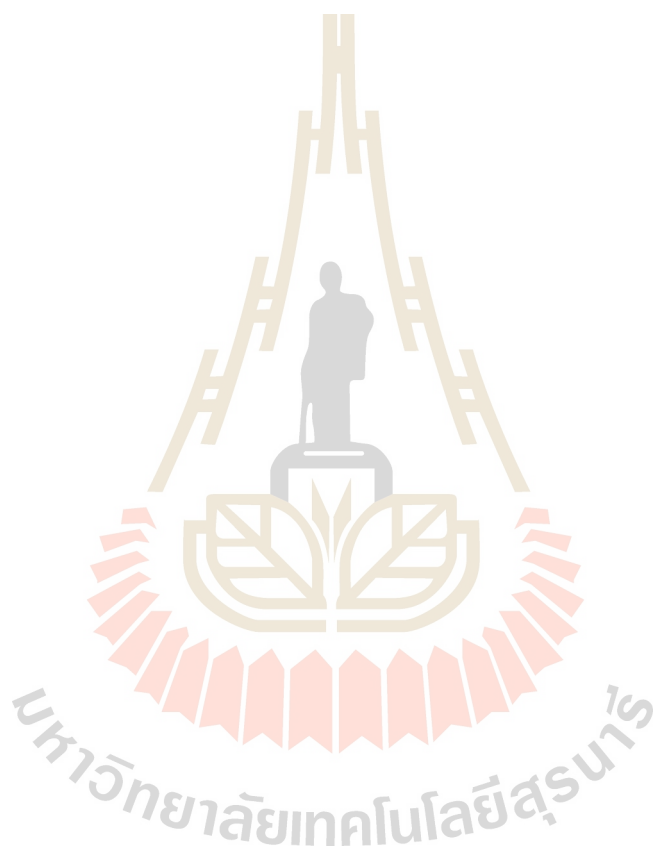
CONCLUSION

The dynamics and mechanisms of proton dissociation and transfer in hydrated H_3PO_4 clusters under excess proton conditions were studied using RIMP2/TZVP calculations and BOMD simulations over the temperature range of 298–430 K in both low ($\epsilon = 1$) and high local-dielectric constant ($\epsilon = 78$) environments. The theoretical study emphasized the dynamics and H-bond arrangements in a short-time scale which could promote intermediate complex formation, and the roles played by the local-dielectric environment. The theoretical investigations were based on the concept of presolvation, and the $\text{H}_3\text{PO}_4\text{-H}_3\text{O}^+ \text{-} n\text{H}_2\text{O}$ complexes ($n = 1\text{-}3$) were demonstrated to be effective presolvation models. The static results obtained from the RIMP2/TZVP calculations revealed that only the linear H-bond chains with asymmetric hydration at H_4PO_4^+ are susceptible to proton dissociation and transfer and that the structure with $n = 1$ in a low local-dielectric constant environment (structures **G2-[1]**) represents the smallest, most stable intermediate complex for proton dissociation. The RIMP2/TZVP calculations revealed that a proton can transfer from the first to the second hydration shell through the linear H-bond chain with $n = 3$ (structure **C4-[1]**), through the Zundel complex which connects the first and the second hydration shells, and a high local-dielectric constant environment is required to induce and stabilize the intermediate complex. These findings are in accordance

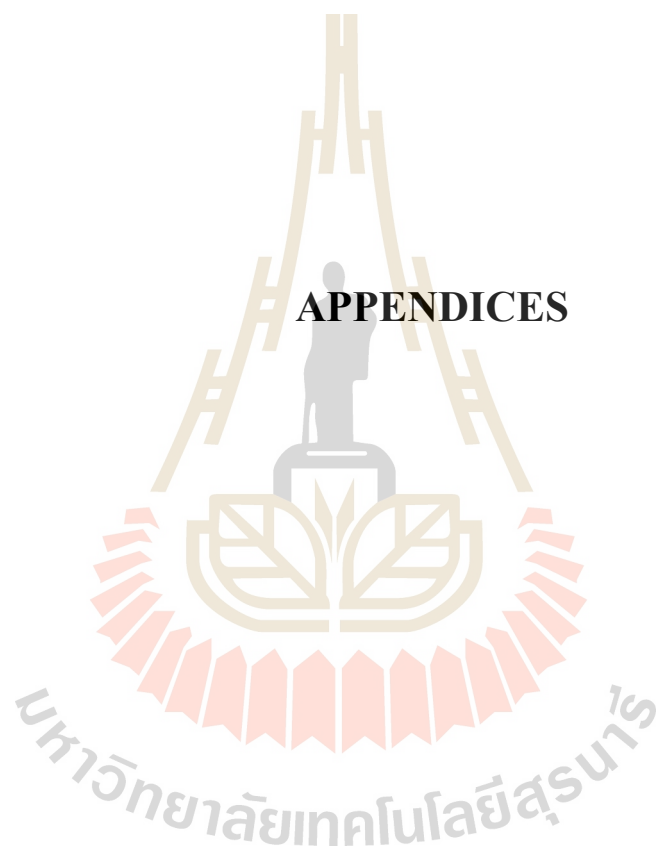
with the LCS concept. Therefore, fluctuations in the number of water molecules and the local-dielectric constant were concluded to play essential roles and were included in the proposed proton dissociation and transfer mechanisms. The two-dimensional potential energy surface (2D-PES) of the transferring proton in the smallest, most stable intermediate complex (structure **G2-[1]**) showed an asymmetric single well potential at the equilibrium R_{O-O} distance, and an asymmetric double-well potential was found at longer R_{O-O} . The cross-sectional plots of the 2D-PES suggested three vibrational modes for proton dissociation from $H_4PO_4^+$: one for the oscillatory shuttling motion and two for the structural diffusion motions. Because *ab initio* calculations with the harmonic approximation yield reliable vibrational frequencies only for the minimum energy geometry (the oscillatory shuttling frequency), the isotropic shielding constants ($\sigma_{H^+}^{corr}$) on the 2D-PES were computed to obtain additional information for the interpretation of the BOMD results. The *ab initio* GIAO method suggested that a proton moving on the structural diffusion path is characterized by a $\sigma_{H^+}^{corr}$ value that varies exponentially with R_{O-H} , whereas a proton on the transition state path (energy crest, $\Delta d_{DA} = 0 \text{ \AA}$) exhibits a $\sigma_{H^+}^{corr}$ value that varies over a narrow range (nearly constant at approximately 12 ppm). The BOMD simulations confirmed that only the linear H-bond chains with asymmetric hydration at $H_4PO_4^+$ are susceptible to proton dissociation and transfer, which is in accordance with the protonic-chain conduction mechanism. The proton transfer profiles obtained from the BOMD simulations indicated that structures **G2-[1]** and **C4-[1]** are indeed the most stable intermediate complexes in the proton dissociation and transfer pathways, respectively. The activation energies ($\Delta E^{\ddagger, Arr}$) of proton dissociation and

transfer, which were obtained from the Arrhenius plots in the temperature range of 298–430 K, are 13.1 and 9.9 kJ/mol, respectively. These values are in good agreement with the experimental activation energies obtained by probing microscopic dynamics, such as the ion-conductivity and conventional ^1H NMR measurements. For proton transfer from the first to the second hydration shell, the vibrational frequencies associated with a proton moving on the oscillatory shuttling and structural diffusion paths, which cannot be obtained through *ab initio* calculations with the harmonic approximation, predicted the vibrational energy for the interconversion between the shared-proton and close contact structures in H_5O_2^+ attached to H_3PO_4 to be slightly lower than that of the Zundel complex. This suggests a slightly higher efficiency of proton transfer in the presence of the H_3PO_4 solute and the roles played by H_3O^+ and H_5O_2^+ . The three characteristic vibrational motions on the proton dissociation pathway, which were suggested by the 2D-PES and vibrational spectra, were also observed in the ^1H NMR chemical shift spectra, and the line-width analyses suggested that the activation energy for proton dissociation is comparable with the ^1H NMR experimental results. Finally, it is not the intention of this work to claim that all the condensed-phase properties of the mixture of H_3PO_4 and H_2O can be studied based on the proposed presolvation models. Instead, the results show specifically how the dynamics of protons in the intermediate complexes can be studied, and related to the rate determining processes in the local proton-transfer mechanisms, which in general consist of the intermediate complex formation and the actual transfer. The present theoretical results, therefore, provide insights into the roles played by a polar solvent and iterate that the dynamics and mechanisms of proton transfer in H-bond clusters

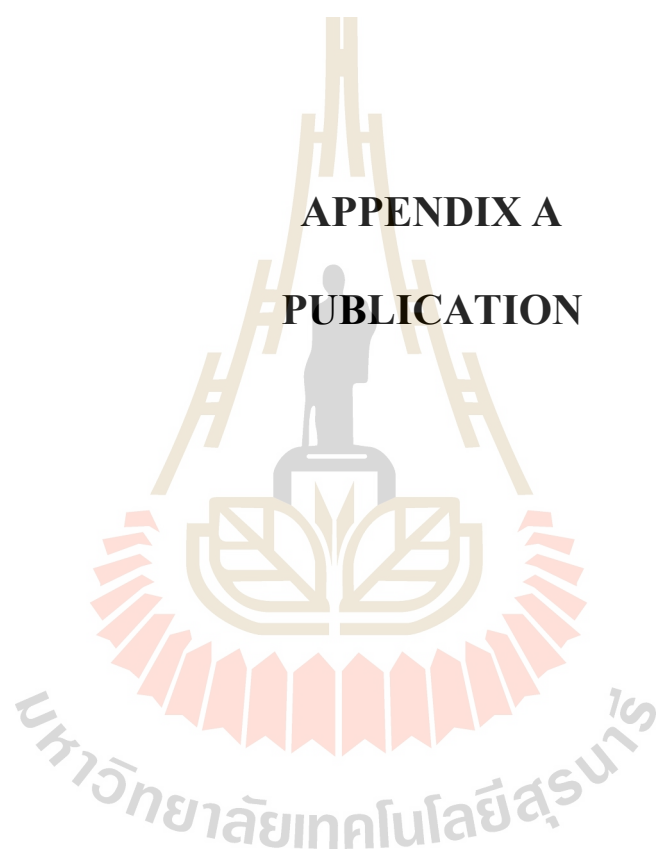
can be obtained from intermediate complexes provided that an appropriate presolvation model is selected and that all of the important rate-determining processes are included in the model calculations.



APPENDICES

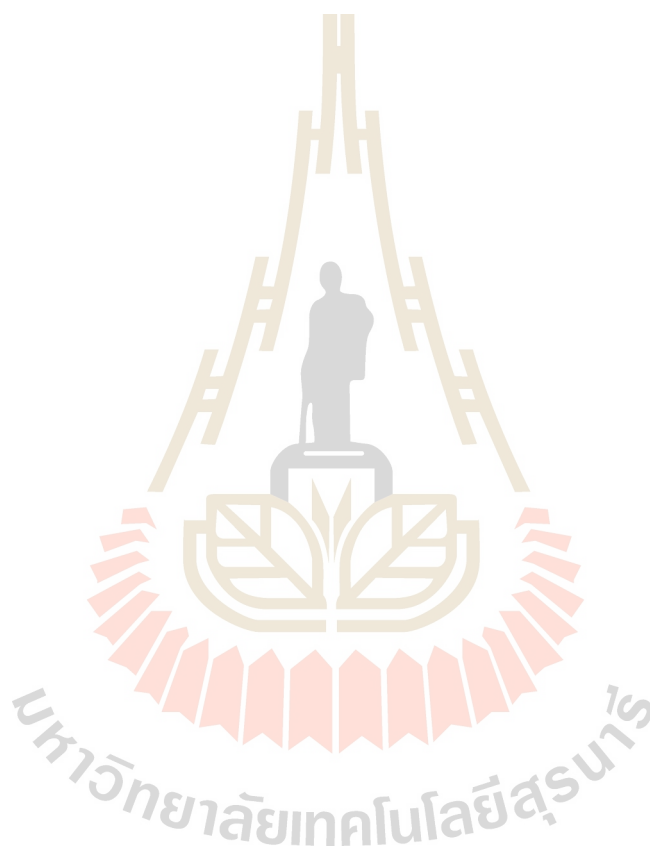


APPENDIX A
PUBLICATION



Publication:

1. Suwannakham, P., Chaiwongwattana, S., and Sagarik, K. (2015). Proton dissociation and transfer in hydrated phosphoric acid clusters. **International Journal of Quantum Chemistry**. 115: 486-501.



Proton Dissociation and Transfer in Hydrated Phosphoric Acid Clusters

Parichart Suwannakham, Sermsiri Chaiwongwattana, and Kritsana Sagarik*

The dynamics and mechanisms of proton dissociation and transfer in hydrated phosphoric acid (H_3PO_4) clusters under excess proton conditions were studied based on the concept of presolvation using the $\text{H}_3\text{PO}_4\text{-H}_3\text{O}^+\text{-}n\text{H}_2\text{O}$ complexes ($n = 1\text{--}3$) as the model systems and *ab initio* calculations and Born–Oppenheimer molecular dynamics (BOMD) simulations at the RIMP2/TZVP level as model calculations. The static results showed that the smallest, most stable intermediate complex for proton dissociation ($n = 1$) is formed in a low local-dielectric constant environment (e.g., $\epsilon = 1$), whereas proton transfer from the first to the second hydration shell is driven by fluctuations in the number of water molecules in a high local-dielectric constant environment (e.g., $\epsilon = 78$) through the Zundel complex in a linear H-bond chain ($n = 3$). The two-dimensional potential energy surfaces (2D-PES) of the intermediate complex ($n = 1$) suggested three characteristic vibrational and ^1H NMR frequencies associated with a proton moving on

the oscillatory shuttling and structural diffusion paths, which can be used to monitor the dynamics of proton dissociation in the H-bond clusters. The BOMD simulations over the temperature range of 298–430 K validated the proposed proton dissociation and transfer mechanisms by showing that good agreement between the theoretical and experimental data can be achieved with the proposed rate-determining processes. The theoretical results suggest the roles played by the polar solvent and iterate that insights into the dynamics and mechanisms of proton transfer in the protonated H-bond clusters can be obtained from intermediate complexes provided that an appropriate presolvation model is selected and that all of the important rate-determining processes are included in the model calculations. © 2015 Wiley Periodicals, Inc.

DOI: 10.1002/qua.24873

Introduction

Proton transfer reactions have been considered important processes in electrochemical devices, such as fuel cells,^[1–3] because the efficiency of fuel cells depends on the transportation of protons (H^+) generated at the anode across the liquid electrolyte or solid proton exchange membrane to the cathode. The majority of commercially available proton exchange membrane fuel cells use Nafion[®], which is a polymer electrolyte membrane that was introduced by DuPont in 1967.^[3] The efficiency of proton transfer in Nafion[®] depends strongly on the hydration of the hydrophilic domains, which are extensively interconnected in the polymer membrane.^[4] This implies that Nafion[®]-based fuel cells are not applicable at temperatures higher than the boiling point of water. This limitation has stimulated the development of alternative proton-conducting materials in the past decades.^[5] As an acid with a high proton-solvating ability and self-ionization property, phosphoric acid (H_3PO_4) has been used effectively in fuel cells (PAFCs).^[5,6] Although theoretical and experimental studies on proton transfer in PAFCs have been reported,^[4,7–9] the local dynamics and mechanisms in hydrated H_3PO_4 clusters are not well understood, especially at the molecular level. Because the basic chemistry of H_3PO_4 has been discussed in detail in review articles,^[5,6,10] only the theoretical and experimental information relevant to this study will be summarized.

Because all hydrogen atoms in H_3PO_4 can form extensive hydrogen-bond (H-bond) networks in the liquid state, the efficiency of proton transfer in PAFCs is high.^[5] The self-ionization

property and high intrinsic-proton concentration allow the proton transfer process in liquid H_3PO_4 to be nearly exclusively through the structural diffusion mechanism, which is regarded as the protonic-chain conduction mechanism.^[11] However, the introduction of an ionizing solute other than water into liquid H_3PO_4 breaks the protonated H-bond chains, resulting in a decrease in its proton conductivity in the liquid state.^[12] To study the dynamics of mobile species in 85 wt.% (14.6 M) H_3PO_4 solution, ^1H and ^{31}P pulsed gradient spin-echo (PGSE) NMR measurements were conducted over the temperature range of 293–353 K.^[13] The self-diffusion coefficients (D) calculated from the attenuation of the echo amplitude suggested that a proton diffuses much faster than a phosphorus-carrying species, with the activation energies of 25 and 36 kJ/mol for the ^1H and ^{31}P species, respectively. Based on the temperature

P. Suwannakham, S. Chaiwongwattana and K. Sagarik
School of Chemistry, Institute of Science, Suranaree University of Technology,
Nakhon Ratchasima 30000, Thailand
E-mail: kritsana@sut.ac.th

Contract grant sponsor: The Royal Golden Jubilee (RGJ) Ph.D. Program of Thailand Research Fund (TRF) and Suranaree University of Technology (SUT); contract grant number: PHD/0085/2552 (K.S. and P.S.).

Contract grant sponsor: The Advanced Research Scholarship of Thailand Research Fund (TRF); contract grant number: BRG-5580011 (K.S.).

Contract grant sponsor: SUT post-doctoral research fellowship from Suranaree University of Technology (S.C.).

Contract grant sponsor: The Higher Education Research Promotion and National Research University (NRU) Project of the Office of the Higher Education Commission (OHEC), Thailand.

© 2015 Wiley Periodicals, Inc.

dependence of $D \times \eta$, water-mediated proton transfer between phosphate groups was proposed. In Ref. 13, two approaches were applied in the calculations of the activation energies namely, from the slope of the linewidth-temperature dependence (the full width at half-maxima or FWHM), and from a simple Arrhenius-type equation. It was reported that the activation energies obtained from the conventional ^1H NMR (FWHM) and ^1H PGSE NMR techniques (Arrhenius-type equation) are not the same due to different time and length scales probed by each technique; the conventional ^1H NMR probes microscopic dynamics, whereas the ^1H NMR PGSE is sensitive to macroscopic motions.^[13] Analyses of the results obtained from these two ^1H NMR techniques yielded the activation energies of 11 and 25 kJ/mol, respectively. Because the conventional ^1H NMR peaks showed motional narrowing at elevated temperatures, the authors anticipated that the smaller activation energy (11 kJ/mol) is associated with the local motions such as rotations.

Microscopic mechanism of proton transfer in neat liquid H_3PO_4 was discussed based on the results of Car–Parrinello molecular dynamics (CPMD) simulations on 54 H_3PO_4 molecules,^[14] in which the fast proton transfer was suggested to involve a structural diffusion which is driven by specific H-bond rearrangements in the surrounding environment. It was concluded that, in neat liquid H_3PO_4 , strong, polarizable H-bonds produce coupled-proton motion, and a pronounced protic dielectric response of the medium, which lead to the formation of extended, polarized H-bond chain, whereas in aqueous media, proton can only be displaced over short distances, and the transportation of excess charge defects is driven by “local H-bond rearrangement.”^[14] The extent of the H-bond network of water affected in the presence of proton was studied,^[15] in which structure dynamics of the proton in liquid water were investigated using terahertz time-domain spectroscopy and polarization-resolved femtosecond midinfrared pump-probe spectroscopy, and the number of affected water molecules around protons were reported. In contrast to the conclusion in Ref. [14], it was found that “addition of protons results in a very strong decrease of the dielectric response of liquid water that corresponds to 19 ± 2 water molecules per dissolved proton. The depolarization results from water molecules (about 4) that are irrotationally bound to the proton and from the motion of water (corresponding to the response of about 15 water molecules) involved in the transfer of the proton charge.” Small and multivalent cations have stronger hydration, and larger depolarization effects, for example, only about 10 water molecules are affected by addition of larger cations such as Mg^{2+} .

In our previous work,^[16] the characteristic vibrational and ^1H NMR spectra of the transferring protons in protonated water clusters were studied through theoretical methods using the $\text{H}^+(\text{H}_2\text{O})_n$ complexes ($n = 2-5$) as model systems and *ab initio* calculations at the RIMP2/TZVP level and Born–Oppenheimer molecular dynamics (BOMD) simulations as the model calculations. The theoretical investigations were based on the concept of presolvation,^[14] and a presolvation model was selected and used in the static and dynamic calculations. The two-dimensional potential energy surface (2D-PES) of the proton in

the smallest, most stable intermediate complex (the Zundel complex, $\text{H}^+(\text{H}_2\text{O})_2$) was constructed as a function of the H-bond distance ($R_{\text{O}-\text{O}}$) and the asymmetric stretching coordinate (Δd_{DA}), and this information was used to identify and characterize the low-interaction energy path (structural diffusion path) and the path with $\Delta d_{\text{DA}} = 0 \text{ \AA}$ (oscillatory shuttling path). For these strong, protonated H-bonds, the *ab initio* gauge including atomic orbital (GIAO) method showed that the ^1H NMR shielding constant ($\sigma_{\text{H}}^{\text{corr}}$) of the proton moving on the oscillatory shuttling path varies over a narrow range and is sensitive only to the H-bond distances ($R_{\text{O}-\text{O}}$ and $R_{\text{O}-\text{H}}$) and not to the water coordination number and the local chemical environment. In contrast, the $\sigma_{\text{H}}^{\text{corr}}$ of a proton moving on the structural diffusion path varies exponentially with $R_{\text{O}-\text{H}}$. The BOMD simulations over the temperature range of 350–430 K revealed that the activation energies for proton exchange in the smallest, most stable intermediate complex, which were obtained from the first-order rate constants (k), vibrational spectra, and a simple ^1H NMR line-shape analysis, are consistent and in good agreement with the experimental results. The theoretical results suggested guidelines and possibilities, as well as a complementary method, for the study of the structural diffusion processes in strong, protonated H-bonds using vibrational and ^1H NMR spectra.

To continue our series of studies on proton transfer reactions,^[17–20] the dynamics and mechanisms of proton dissociation and transfer in hydrated H_3PO_4 clusters under excess proton conditions were studied in this work. The theoretical study emphasized the dynamics and H-bond arrangements in a short-time scale which could promote intermediate complex formation, and showed how H_3O^+ and H_5O_2^+ facilitate and mediate proton dissociation and transfer in the hydrated H_3PO_4 clusters, as well as the roles played by the local-dielectric environment. Insights into the proton dissociation and transfer processes were obtained from analyses of the characteristic vibrational and ^1H NMR spectra of the transferring protons, which were derived from BOMD simulations over the temperature range of 298–430 K. The static and dynamic results were discussed in comparison with available theoretical and experimental data on the same and similar systems.

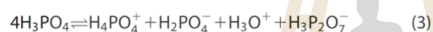
Computational Methods

Presolvation model

Because proton transfers in H-bonds are complicated, care must be exercised in selecting the model systems. In this work, the concept of presolvation^[11] was applied in the study of proton dissociation and transfer in hydrated H_3PO_4 clusters; “the local energy fluctuations and dynamics in aqueous solution lead to the weakening or breaking of some H-bonds in the first and second hydration shells, resulting in a reduction in the water coordination number such that the proton-accepting species possesses a hydration structure corresponding to the species into which it will be transformed to complete the structural diffusion process.”^[21] Because some H-bonds in the first and second hydration shells are

instantaneously disrupted, the presolvation state can be resolved, and the dynamics of the structural diffusion process can be studied using an appropriate presolvation model. The formation of the presolvation state generally requires removal of some solvent environment, and takes place through the protonic-chain conduction mechanism.^[11,16,18,20,22] The concept of presolvation is supported by the observation that, due to the local geometrical requirements, H-bonds in aqueous solution can be considered as "forming" or "breaking"; experiments based on thermochemistry and vibrational spectroscopy have shown that 10–70% of H-bonds in water can be considered as broken within the temperature range of 273–299 K.^[23] Although the proton dissociation and transfer processes in hydrated H_3PO_4 clusters are our main interest, some fundamental information on concentrated H_3PO_4 solutions can be used as guidelines to construct the presolvation model as follows.

According to experiments,^[12] the equilibriums in concentrated H_3PO_4 solution at 16.8 M can be represented by



and the fast proton transfer involves the self-dissociation and dehydration reactions in Eqs. (1) and (2), respectively. Based on the equilibrium constants at 298 K, Chung et al.^[13] suggested that the dominant species in 85 wt.% (14.6 M) H_3PO_4 solution is undissociated H_3PO_4 (97.6%), the presence of condensed phosphates can be neglected, and the mechanism for anion (H_2PO_4^-) transport is vehicular type. These findings are supplemented by the experimental results in Ref. 12, in which H_3PO_4 , H_4PO_4^+ , and H_3O^+ were concluded to play the most important roles in the structural diffusion in the liquid and concentrated solution. Therefore, our presolvation models for proton dissociation and transfer consist of H_3PO_4 , H_2O , H_4PO_4^+ , and H_3O^+ ; the protonated forms must be included to represent the acid conditions.

The size of the presolvation model was determined based on the theoretical study in Ref. 24, in which the extent of the Grotthuss chains in equimolar mixture of H_3PO_4 and H_2O (1:1 molar ratio) was examined using CPMD simulations. It appeared that the properties of the H-bonds in this system are virtually identical to those of pure H_3PO_4 (no resemblance to liquid water), and the weak solvent coupling and sufficient degree of configurational disorder result in fast proton transport. Based on the proton coupling correlation function as a function of H-bond connectivity, the probability of two quasicohesive proton transfer events within two neighboring H-bonds is about 4% when the relaxation of the H-bond network, $\tau_{\text{res}} = 0$ fs, about two times lower than in neat liquid H_3PO_4 . As the relay time parameter increased to $\tau_{\text{res}} = 50$ fs, the probabilities to form chains of three and four consecutive H-bonds are about 18 and 2%, respectively. Because the probability to form four consecutive H-bonds is significantly lower than that in neat liquid H_3PO_4 (about 10%), the authors con-

cluded that the presence of water opposes the formation of extensive Grotthuss chains,^[14,24] and one could anticipate that four consecutive H-bonds are sufficient to take into account the quasicohesive proton transfer events in the hydrated H_3PO_4 systems. Additionally, because the dynamics in short-time and -length scales are of interest, and the cation in the present system is a protonated H_3PO_4 , which is considerably larger than proton and Mg^{2+} ,^[15] it is reasonable to anticipate that the number of affected water molecules are much less than these two cations.

Based on the above discussions, and because the dynamics of protons in the intermediate complexes in a short-time scale are of interest, to implement the concept of presolvation, the H-bond clusters formed from H_3PO_4 , H_3O^+ , and $n\text{H}_2\text{O}$ ($n = 1-3$) were proposed as a candidate presolvation model. The proposed presolvation model was confirmed by our static and dynamic calculations, which revealed that the intermediate complexes of proton dissociation and transfer (with shared-proton structures) are formed only in the H-bond clusters with $n \leq 3$. In this study, H_4PO_4^+ and H_3PO_4 are considered the protonated and deprotonated forms, respectively.

Quantum chemical methods

Three basic steps that were applied successfully in our previous investigations were used in this work^[25-27]: (1) searching for the intermediate complexes in the proton transfer pathway using the Test-particle model (T-model) potentials;^[25-35] (2) refining the T-model-optimized structures using an accurate quantum chemical method; and (3) performing BOMD simulations on the candidate intermediate complexes using the refined structures as the starting configurations. Because the effects of electron correlations may play important roles in the present model systems, the quantum chemical calculations were performed using the second-order Møller–Plesset perturbation theory (MP2) with the resolution of the identity (RI) approximation^[36] and the TZVP basis set (this process is abbreviated RIMP2/TZVP calculations).^[36] Additionally, due to the potential applications of the density functional theory (DFT) methods in the study of proton transfer in larger H-bond systems and the fact that our previous theoretical results were reported based on B3LYP/TZVP calculations,^[17-19] quantum chemical calculations were also conducted at this level of theory. The applicability and performance of RIMP2/TZVP and B3LYP/TZVP calculations were compared and discussed. Additionally, to study the effects of a polar solvent on proton dissociation and transfer, a continuum aqueous solvent was included in the model calculations. Because the conductor-like screening model (COSMO)^[37] was applied successfully in similar H-bond systems,^[17-19] the proton dissociation and transfer were studied both in the gas phase and in COSMO with $\epsilon = 78$. All of the theoretical calculations were performed using TURBOMOLE 6.4.^[38-40]

Static calculations

Structures and energies. The absolute and local minimum energy geometries of the $\text{H}_3\text{PO}_4\text{-H}_3\text{O}^+-n\text{H}_2\text{O}$ complexes

($n = 1-3$), which were obtained from the T-model potentials, were refined using both B3LYP/TZVP and RIMP2/TZVP geometry optimizations. The tendency of proton dissociation and transfer, as well as the structure of the smallest, most stable intermediate complex, in the presolvation model were primarily anticipated from the asymmetric stretching coordinate (Δd_{DA}), which was computed from $\Delta d_{DA} = |d_{A-H} - d_{B \cdots H}|$, where d_{A-H} and $d_{B \cdots H}$ are the A-H and B \cdots H distances in the A-H \cdots B H-bond, respectively. The interaction energies (ΔE) of the H-bond complexes were computed from $\Delta E = E(\text{H}_3\text{PO}_4\text{-H}_3\text{O}^+ - n\text{H}_2\text{O}) - [E(\text{H}_3\text{PO}_4) + E(\text{H}_3\text{O}^+) + nE(\text{H}_2\text{O})]$, where $E(\text{H}_3\text{PO}_4\text{-H}_3\text{O}^+ - n\text{H}_2\text{O})$ is the total energy of the optimized structure of the $\text{H}_3\text{PO}_4\text{-H}_3\text{O}^+ - n\text{H}_2\text{O}$ complex; $E(\text{H}_3\text{PO}_4)$, and $E(\text{H}_3\text{O}^+)$ and $E(\text{H}_2\text{O})$ are the total energies of the optimized structures of the isolated species.^[17,18] The solvation energies (COSMO with $\epsilon = 78$) were approximated by $\Delta E^{\text{sol}} = E(\text{H}_3\text{PO}_4\text{-H}_3\text{O}^+ - n\text{H}_2\text{O})^{\text{COSMO}} - E(\text{H}_3\text{PO}_4\text{-H}_3\text{O}^+ - n\text{H}_2\text{O})$, where $E(\text{H}_3\text{PO}_4\text{-H}_3\text{O}^+ - n\text{H}_2\text{O})^{\text{COSMO}}$ and $E(\text{H}_3\text{PO}_4\text{-H}_3\text{O}^+ - n\text{H}_2\text{O})$ are the total energies of the optimized structures obtained with and without COSMO, respectively.^[17,18]

Because the dynamics of a proton are governed by the potential energy surface on which the transferring proton moves and the O-O and O-H⁺ vibrations in the O-H⁺ \cdots O H-bond are coupled,^[20] to provide energetic information for the discussion of the structural diffusion process, two-dimensional potential energy surfaces (2D-PES) of the transferring proton in the smallest, most stable intermediate complex were constructed both in the gas phase and in COSMO through the calculation of ΔE at various R_{O-O} and R_{O-H} distances.^[16] Two sets of equally spaced grid points were generated from ΔE and 2D-PES and plotted as a function of R_{O-O} and Δd_{DA} using the SURFER program.^[41] The interaction energy path connecting the single- and double-well potentials, as well as the path with the highest energy barriers, were identified and studied in detail.

Vibrational and NMR spectra. To obtain vibrational signatures of the transferring protons which can be used as guidelines for the discussion of the dynamic results, the harmonic vibrational frequencies of molecules in the presolvation model were computed from the numerical second derivatives of the B3LYP/TZVP and RIMP2/TZVP total energies, from which analyses of the normal modes in terms of the internal coordinates were made using the NUMFORCE and AOFORCE programs, respectively.^[38] The programs are included in TURBOMOLE 6.4.^[38-40] Only the asymmetric O-H stretching frequencies of the H-bond protons (ν^{OH}) were analyzed and discussed in detail.^[17-20] The threshold asymmetric O-H stretching frequencies of proton dissociation from H_4PO_4^+ ($\nu^{\text{OH}*}$) were estimated from the plots of ν^{OH} and Δd_{DA} .^[17,18] The relationships between ν^{OH} and Δd_{DA} were represented by the reflected normal distribution functions, the second derivatives of which are equal to zero at $\nu^{\text{OH}} = \nu^{\text{OH}*}$.^[17,18] For the B3LYP/TZVP and RIMP2/TZVP calculations, the scaling factors of 0.9614^[42] and 0.9434^[38] were used in the calculations of the vibrational frequencies, respectively.

As an effective probe for H-bond formation,^[43] isotropic shielding constants were computed at both the RIMP2/TZVP

and the B3LYP/TZVP levels^[44] using the GIAO method.^[45,46] The ¹H NMR shielding constants at the RIMP2/TZVP level ($\sigma_{\text{H}^+}^{\text{corr}}$) were derived from^[47]

$$\sigma_{\text{H}^+}^{\text{corr}} = \sigma_{\text{H}^+}^{\text{HF}} + 2/3(\sigma_{\text{H}^+}^{\text{RIMP2}} - \sigma_{\text{H}^+}^{\text{HF}}) \quad (4)$$

where $\sigma_{\text{H}^+}^{\text{HF}}$ and $\sigma_{\text{H}^+}^{\text{RIMP2}}$ are the isotropic shielding constants obtained at the Hartree-Fock and RIMP2 levels, respectively. The ¹H NMR chemical shifts of the H-bond protons ($\delta_{\text{H}^+}^{\text{corr}}$) were derived from $\sigma_{\text{H}^+}^{\text{corr}}$ with respect to tetramethylsilane,^[48] which was computed at the MP2/TZVP level to be 31.97 ppm.^[44] Based on the observation that the isotropic shielding constants of protons in strong, protonated H-bonds depend only on the H-bond distance (R_{O-O}) and not the neighboring water molecules^[49] and the conclusion that the effects of a continuum solvent (reaction field) on the H-bond structures are small,^[44,50,51] it is reasonable to discuss only the ¹H NMR shielding constants of the smallest, most stable intermediate complex in the gas phase.^[16] To correlate the ¹H NMR shielding constants with the structures of 2D-PES, the $\sigma_{\text{H}^+}^{\text{corr}}$ of the proton on the structural diffusion (the low-interaction energy path connecting the single- and double-well potentials) and oscillatory shuttling paths (the path with $\Delta d_{DA} \approx 0$ Å) were computed and plotted as a function R_{O-H} .^[16]

Dynamic calculations

BOMD simulations. The equilibrium structures of the model systems obtained from the RIMP2/TZVP calculations were used as the starting configurations in BOMD simulations. In our previous work,^[18,52,53] the applicability and performance of the NVT ensemble for the study of the dynamics of proton transfer were examined in detail. Because the energy released and absorbed during the proton transfer process can be managed by a thermostat bath, the local temperature can be maintained throughout the course of the NVT-BOMD simulations provided that an appropriate thermostat relaxation time is chosen. In the previous and present work, a Nosé-Hoover chain thermostat^[54-57] was applied to each degree of freedom in the model systems, and a thermostat relaxation that was 20-fold larger than the time step was proven to be appropriate for the generation of reasonable local-energy fluctuations.^[16,18,19,52,53] As an example,^[58] the NVT-BOMD simulations of the Zundel complex at 350 K yielded local-energy fluctuation of only approximately 0.4 kJ/mol/degree of freedom compared with the activation energy obtained from the ¹H NMR measurements of approximately 10 kJ/mol.^[59] Additionally, to confirm that the energetics and dynamics are well represented, energy conservation and MSD plots were constructed.^[53] Because the trend of the energy conservation plot showed no systematic drift and the correct linear relationship was obtained for the MSD plot, one can conclude that the dynamics of the transferring proton, which were obtained under the present NVT-BOMD simulations conditions, including the Nosé-Hoover thermostat, are reasonable and very well represented, especially in the case in which the structures of the model systems are at equilibrium and not substantially

changed in the BOMD simulations. In this work, 2000 and 20000 BOMD steps of 1 fs were devoted to the equilibration and the property calculations, corresponding to 2 and 20 ps, respectively.

The activation energies ($\Delta E^{\ddagger,Arr}$) of proton dissociation and transfer from the first hydration shell were determined from the Arrhenius equation by performing BOMD simulations over the temperature range of 298–430 K. The first-order rate constants (k) for the exchange between the shared-proton ($O \cdots H^+ \cdots O$) and close-contact ($O-H^+ \cdots O$) structures were approximated from the exponential relaxation behavior of the envelopes of the velocity autocorrelation functions (VACF) of the O—O vibrations^[16,18,52,53] and the $\Delta E^{\ddagger,Arr}$ from the linear relationship between $\ln(k)$ and $1000/T$.

Vibrational and NMR spectra. Because the harmonic approximation yields reliable vibrational frequencies only at stationary points on the total energy surface, to completely understand the vibrational behaviors of the transferring protons, especially in distorted H-bond structures, BOMD simulations must be performed, from which the vibrational spectra were determined by Fourier transformation of the VACF. Because conventional vibrational analysis of the VACF of atoms cannot yield the information on the types of motions associated with the frequencies of interest, attempt was made in Ref. 60 to describe vibrational modes using an appropriate correlation function technique. In this approach, the velocity vectors associated with the vibrational modes were defined and used in the calculations of the VACF, from which the vibrational spectra and the lifetimes of the motions were computed. In our previous work,^[18,53,58,61] the symmetric and asymmetric O—H stretching frequencies, as well as the O—O vibrational frequencies, were computed using the predefined-velocity vectors in Figure 1a.^[60] As the definitions of the velocity vectors were different, the symmetric and asymmetric O—H stretching peaks were quite well separated (Fig. 8). It should be noted that, due to similar definitions of the velocity vectors of the symmetric O—H stretching and the O—O vibration, some interferences (mixings) between these two modes can be observed. Because we have shown in our previous studies^[18,53,58,61] that the characteristic vibrational motions of the transferring protons discussed based on the asymmetric O—H stretching frequencies were very reasonable, the same approach was used in this work.

Remarks should be made on the computational aspects of the vibrational spectra reported in this work, and the absorption IR spectra obtained from ultrafast vibrational spectroscopy, for example, transient-hole burning, and vibrational-echo techniques.^[62] Our vibrational spectra were computed from the Fourier transformation of the VACF, whereas the ultrafast absorption vibrational spectra can be obtained theoretically based on the Fourier transformation of the quantum dipole time-correlation function and response functions. Therefore, these two approaches do not yield exactly the same vibrational properties; the former are associated with the local vibrational modes, whereas the latter are connected to the vibrational transition frequencies of local oscillators.

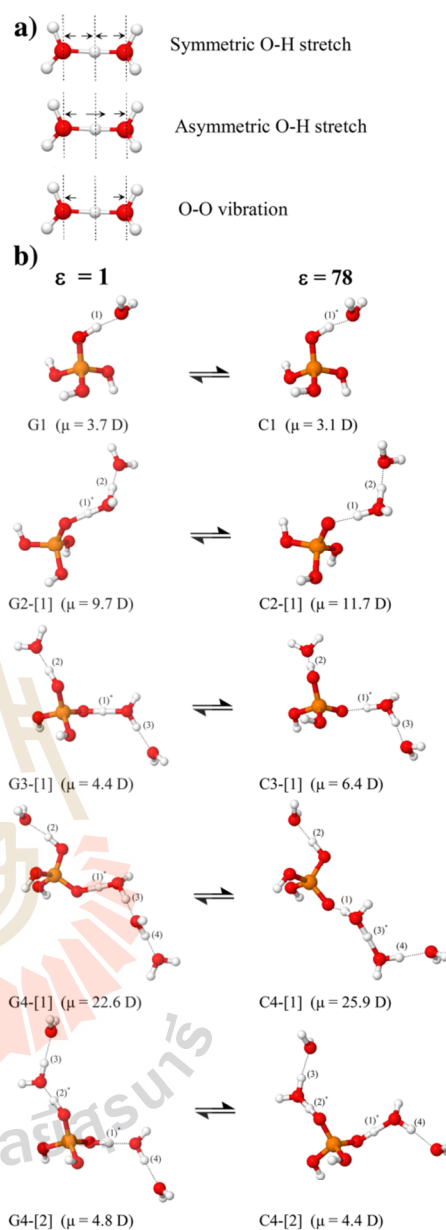


Figure 1. (a) Definitions of the velocity vectors used in the calculations of the symmetric and asymmetric O—H stretching frequencies, as well as the O—O vibrational frequencies. (b) Linear H-bond structures of the $H_3PO_4 \cdots H_3O^+ \cdots nH_2O$ complexes ($n = 1-3$) potentially involved in proton dissociation and transfer. These were obtained from the RIMP2/TZVP calculations in the gas phase and continuum aqueous solvent. * = H-bond susceptible to proton transfer; μ = dipole moment.

Because, in this study, the vibrational frequencies were used in the discussion of the characteristic vibrational motions of the transferring protons, and it was not our intention to calculate the absorption IR spectra *per se*, the Fourier transformation of the VACF was used. It should be added that, for strong H-bond systems such as liquid water, the ultrafast absorption IR spectra are complicated due to the pronounced non-Condon effects, defined as “the dependence of the vibrational transition dipole moment of a particular molecule on the rotational and translational coordinates of all the molecules in the liquid,” and conventional theoretical methods to calculate absorption IR spectra do not take into account these effects.^[62] It was demonstrated that inclusion of the non-Condon effects in the model calculations is important for an accurate calculation of the homodyned and heterodyned three-pulse echoes, which are not the objectives of this study.

The vibrational energies for the interconversion between the oscillatory shuttling and structural diffusion motions ($\Delta v_{\text{BA}}^{\text{OH,MD}}$) were approximated from the difference between the structural diffusion ($v_{\text{B}}^{\text{OH,MD}}$) and oscillatory shuttling ($v_{\text{A}}^{\text{OH,MD}}$) frequencies.^[18] In this study, the dynamics of the protons were also discussed using the ^1H NMR chemical shift spectra ($\delta_{\text{H}^+}^{\text{corr, MD}}$) obtained from the BOMD simulations over the temperature range of 298–430 K.^[63,64] In the calculations of the ^1H NMR chemical shift spectra, a statistical sampling of the structures of the smallest, most stable intermediate complex was performed every five BOMD steps,^[16] and two thousand five hundred H-bond structures were used in the calculations of the instantaneous ^1H NMR shielding constants ($\sigma_{\text{H}^+}^{\text{corr, MD}}$) using the *ab initio* GIAO method at the RIMP2/TZVP level. The ^1H NMR chemical shift spectra were represented by Lorentzian peak functions,^[65] from which the activation energies ($\Delta E^{\text{t,NMR}}$) for the exchange between the shared-proton and close-contact structures were obtained through a simple line shape analysis. Based on the assumption that the change in the ^1H NMR line width ($\Delta\delta_{\text{H}^+}^{\text{corr, MD}}$) as a function of temperature is correlated with the exchange rate, which can be used to determine $\Delta E^{\text{t,NMR}}$ through the Arrhenius equation,^[64] $\Delta\delta_{\text{H}^+}^{\text{corr, MD}}$ was approximated as the FWHM of the ^1H NMR chemical shift spectra.^[66] In this study, the effective transverse relaxation times (T_2) were calculated from $\Delta\delta_{\text{H}^+}^{\text{corr, MD}}$ using $T_2 = 1/(\pi\Delta\delta_{\text{H}^+}^{\text{corr, MD}})$ and the $\Delta E^{\text{t,NMR}}$ from the plots of $\ln(T_2)$ and $1000/T$.^[64]

Results and Discussions

Static results

All of the static results obtained from the RIMP2/TZVP and B3LYP/TZVP calculations are given in Tables S1 and S2, respectively. The equilibrium structures that may be involved in proton dissociation and transfer, which were obtained from the RIMP2/TZVP calculations in the gas phase and continuum aqueous solution, are shown in Figure 1b, with the dipole moment (μ). To simplify the discussion, the H-bond structures were labelled with a three-character code, the **Gn-[m]** or **Cn-[m]**: **G** = H-bond structure in the gas phase, and

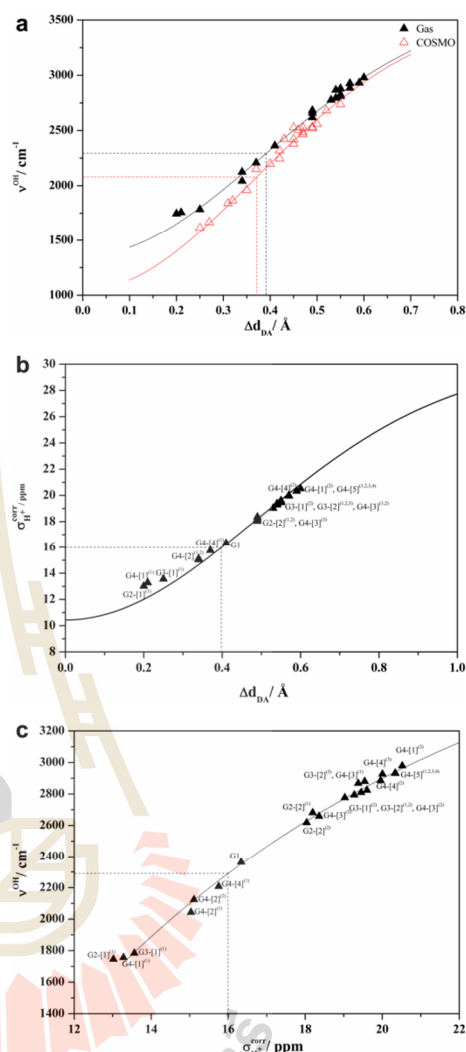
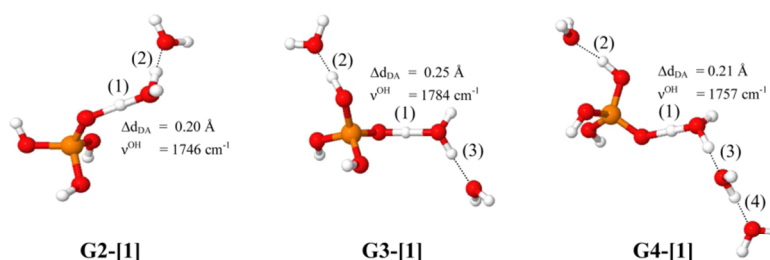


Figure 2. Analyses of the static results of the $\text{H}_3\text{PO}_4 \cdot \text{H}_3\text{O}^+ \cdot n\text{H}_2\text{O}$ complexes ($n = 1-3$) obtained from the RIMP2/TZVP calculations. The dashed lines separate the protons that are susceptible from those that are not susceptible to dissociation. (a) Plots of the asymmetric O–H stretching frequency (ν^{OH}) as a function of the asymmetric stretching coordinate (Δd_{DA}) in the gas phase and continuum aqueous solvent. (b) Plot of ^1H NMR shielding constant ($\sigma_{\text{H}^+}^{\text{corr}}$) and asymmetric stretching coordinate (Δd_{DA}) in the gas phase. (c) Correlation between the asymmetric O–H stretching frequency (ν^{OH}) and the ^1H NMR shielding constant ($\sigma_{\text{H}^+}^{\text{corr}}$) in the gas phase.

the **C** = H-bond structure in continuum aqueous solution, where **n** is the number of water molecules. Different H-bond structures with the same number of water molecules are distinguished by **[m]**. For example, according to the three-



Scheme 1. Effects of extension of the linear H-bond chains in the gas phase.

character code, **G3-[1]** and **G3-[2]** are different H-bond structures (**[1]** and **[2]**, respectively) with the same number of water molecules ($n = 3$) in the gas phase (**G**). In contrast, **G2-[1]** and **C2-[1]** are the same H-bond structure ($n = 2$, $m = 1$) in the gas phase (**G**) and continuum aqueous solution (**C**), respectively.

DFT and RIMP2 calculations. The correlations between the RIMP2/TZVP and B3LYP/TZVP results are shown in Figure S1 in the Supporting Information. These are represented by linear functions with R^2 values in the range of 0.986–0.999, reflecting excellent agreement between the two methods, for example, $R^2 = 0.999$ for the interaction (ΔE) and solvation energies (ΔE^{sol}). The investigation of the protonated H-bond structures in Supporting Information Tables S1 and S2 showed that the equilibrium structures obtained from both methods are generally the same and that the ΔE obtained from the RIMP2/TZVP calculations are slightly lower (more negative) than those obtained from the B3LYP/TZVP calculations, indicating a better representation of the effects of electron correlation through the RIMP2/TZVP method.

The trends of the vibrational and NMR results are quite similar at both levels of theory. For the RIMP2/TZVP calculations, the plots of ν^{OH} and Δd_{DA} shown in Figure 2 yielded threshold asymmetric O-H stretching frequencies ($\nu^{\text{OH}*}$) for deprotonation in H-bond (**1**) at 2295 cm^{-1} in the gas phase and at 2078 cm^{-1} in continuum aqueous solution. These values are slightly lower than those obtained from the B3LYP/TZVP calculations: $\nu^{\text{OH}*} = 2306$ and 2136 cm^{-1} , respectively. The ^1H NMR shielding constants obtained from the RIMP2/TZVP calculations ($\sigma_{\text{H}}^{\text{corr}}$) are slightly smaller than those obtained from the B3LYP/TZVP calculations (σ_{H}^+), confirming that more associated H-bond complexes are obtained with the RIMP2/TZVP method. The plots of ν^{OH} and $\sigma_{\text{H}}^{\text{corr}}$ and of $\sigma_{\text{H}}^{\text{corr}}$ and Δd_{DA} shown in Figure 2 yielded threshold ^1H NMR shielding constant ($\sigma_{\text{H}}^{\text{corr}*}$) for deprotonation in H-bond (**1**) of 16 ppm in the gas phase, whereas the protonated forms (H_4PO_4^+ and H_3O^+) in the linear H-bond chains possess $\sigma_{\text{H}}^{\text{corr}}$ values in the ranges of 15–17 ppm and of 13–14 ppm, respectively, corresponding to ^1H NMR chemical shifts ($\delta_{\text{H}}^{\text{corr}}$) of 17–15 ppm and of 19–18 ppm, respectively.

Because the RIMP2/TZVP and B3LYP/TZVP calculations yielded the same trends in the structural, energetic, and

spectroscopic properties, this study concluded that, in the case of restricted computational resources, the B3LYP/TZVP method can be applied in the study of hydrated H_3PO_4 under excess proton conditions. However, because the sizes of the model systems considered here are moderate, BOMD simulations can be performed based on the RIMP2/TZVP calculations.

Structures and solvent effects. The equilibrium structures of the $\text{H}_3\text{PO}_4\text{-H}_3\text{O}^+\text{-}n\text{H}_2\text{O}$ complexes ($n = 1\text{--}3$) shown in Supporting Information, Tables S1 and S2 can be divided into two groups, namely linear H-bond chains, for example, structures **G1**, **C1**, **G2-[1]**, **C2-[1]**, **G4-[1]**, and **C4-[1]**, and embedded H_4PO_4^+ clusters, for example, structures **G3[2]**, **C3-[2]**, **G4-[4]**, and **C4-[4]**. According to the asymmetric O—H stretching frequencies (ν^{OH}), linear H-bond chains with asymmetric hydration at H_4PO_4^+ , as shown in Figure 1b, are potentially involved in proton dissociation and transfer ($\nu^{\text{OH}} < \nu^{\text{OH}*}$), and this finding supports the protonic-chain conduction mechanism, as in the case of liquid phosphoric acid^[11,12] and methanol.^[53] The values of ν^{OH} in Supporting Information Table S1 and the H-bond structures in Figure 1b also suggest that the shared-proton structures, in which protons stay almost at the center of the H-bond (**1**), are favorable in the gas phase, for example, structures **G2-[1]**, **G4-[1]**, and **G3-[1]**, and that structure **G2-[1]** may represent the smallest, most stable intermediate complex in the proton dissociation pathway ($\Delta d_{\text{DA}} = 0.20 \text{ \AA}$). Most importantly, in the gas phase, the extension of the linear H-bond chains does not increase the tendency of proton transfer from the first to the second hydration shell, for example, protons in the H-bond (**2**) of structure **G2-[1]** and the H-bond (**3**) of structures **G3-[1]** and **G4-[1]** exhibit $\nu^{\text{OH}} > \nu^{\text{OH}*}$ Scheme 1.

The RIMP2/TZVP results shown in Supporting Information Table S1 demonstrate that the ν^{OH} of protons in H-bond (**1**) of the protonated forms (H_4PO_4^+ and H_3O^+) are in the range of 2040 (linear H-bond structure, structure **G4-[2]**) to 2940 cm^{-1} (fully hydrated H_4PO_4^+ , structure **G4-[5]**) and of 1740 (structure **G2-[1]**) to 1790 cm^{-1} (structure **G3-[1]**), respectively. These characteristic vibrational frequencies could be used to differentiate between the protonated and deprotonated forms in BOMD simulations.

The comparison of the structures of the linear H-bond chains and the dipole moments in the gas phase and continuum aqueous solvent shown in Figure 1b, for example,

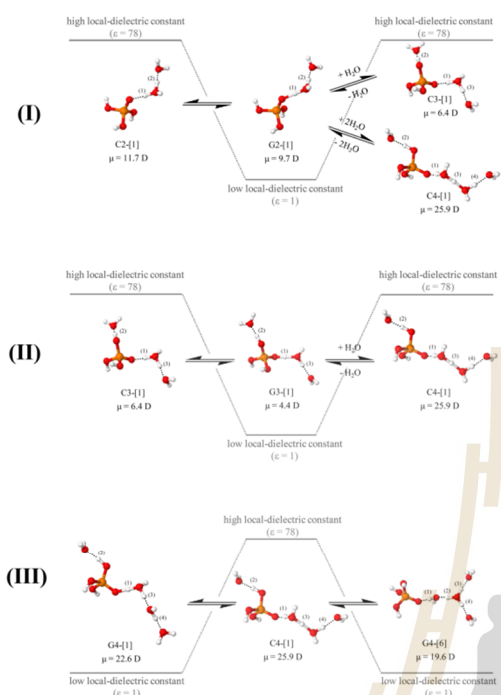


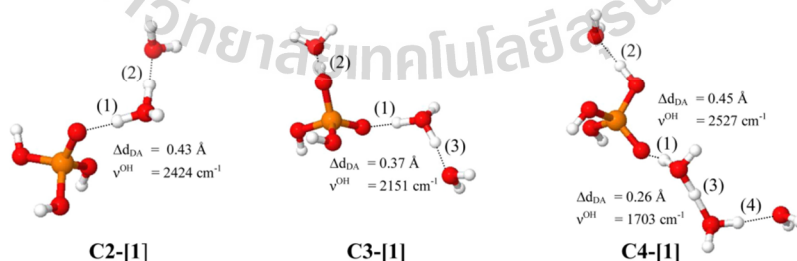
Figure 3. Examples of the elementary steps of proton dissociation (I and II) and transfer (III) in $\text{H}_3\text{PO}_4\text{-H}_3\text{O}^+\text{-}n\text{H}_2\text{O}$ complexes ($n = 1\text{--}3$). These steps involve fluctuations in the number of water molecules and in the local-dielectric constant.

structures **G2-[1]** ($\mu = 9.2$ D) and **C2-[1]** ($\mu = 11.8$ D), revealed prominent effects of solvent polarity on proton dissociation. In the present case, an increase in solvent polarity from $\epsilon = 1$ to $\epsilon = 78$ leads to strong charge redistributions (observed from an increase in the dipole moment), more effective interaction with the electrostatic field of the solvent, and the shift in the proton in the H-bond (1) toward H_2O . The influence of solvent polarity on proton dissociation is in accordance with the

localized-charge solvation (LCS) concept, in which "a polar solvent solvates species with localized charges more efficiently than species with more delocalized charges."^[67] Therefore, in this case, the protonated forms (H_3O^+), for example, structures **C2-[1]** and **C3-[1]**, are more favorable than the shared-proton forms (e.g., structures **G2-[1]** and **G3-[1]**) in continuum aqueous solvent. Based on the LCS concept, the possibility of proton transfer from the first hydration shell could be envisaged from structures **G4-[1]** ($\mu = 22.7$ D) and **C4-[1]** ($\mu = 25.9$ D); when COSMO is switched on, the dipole moment of the linear H-bond chain increases, and the shared-proton structure is moved from from H-bond (1) to H-bond (3), generating a Zundel complex attached to H_3PO_4 with a ν_{OH}^* of the protonated water clusters (1703 and 1987 cm^{-1} , respectively).^[16] Therefore, structure **C4-[1]** may be an intermediate complex for proton transfer from the first to the second hydration shell and should be further studied in BOMD simulations.

Because the linear H-bond chains in a low local-dielectric constant environment ($\epsilon = 1$) represent effective intermediate complexes in the proton dissociation process, for example, structures **G2-[1]** and **G4-[1]**, because structure **C4-[1]** in a high local-dielectric constant environment ($\epsilon = 78$) is the intermediate complex for proton transfer from the first to the second hydration shell, and because H_3O^+ and H_5O_2^+ are stabilized in COSMO, one could anticipate that fluctuations in the number of water molecules and the local-dielectric constant play essential roles in the proton dissociation and transfer processes, and the elementary steps could be formulated from the H-bond structures shown in Figure 1b. Examples of the proposed elementary steps are shown schematically in Figure 3. In this scheme, structures **G2-[1]** and **G3-[1]** in a low local-dielectric constant environment ($\epsilon = 1$) are the intermediate complexes of proton dissociation and are produced through elementary steps (I) and (II), respectively. In addition, for proton transfer from the first to the second hydration shell, structure **C4-[1]** in a high local-dielectric constant environment ($\epsilon = 78$, in Scheme 2) is the most active intermediate complex and is produced through elementary step (III). All of the proposed elementary steps were verified and studied in detail through BOMD simulations.

Two-dimensional potential energy surfaces. The two-dimensional potential energy surfaces (2D-PES) for proton



Scheme 2. Effects of extension of the linear H-bond chains in continuum aqueous solvent.

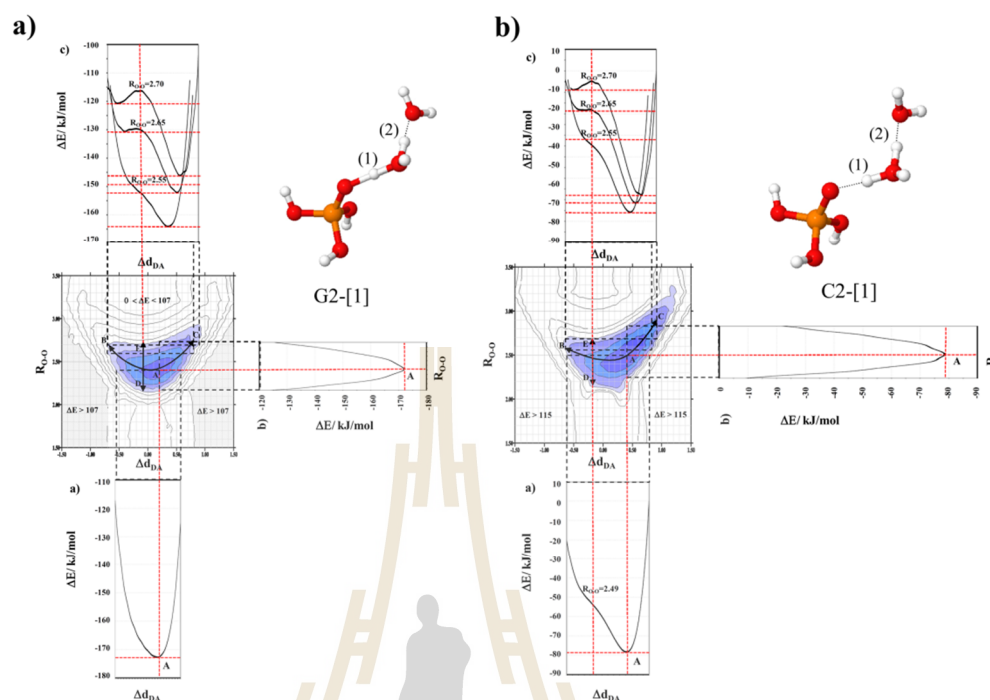


Figure 4. (a) Two-dimensional potential energy surface (2D-PES) of a proton in H-bond (1) of structure **G2-[1]** as a function of R_{O-H} and Δd_{DA} . (b) Two-dimensional potential energy surface (2D-PES) of a proton in H-bond (1) of structure **C2-[1]** as a function of R_{O-H} and Δd_{DA} .

exchange in the smallest, most stable intermediate complexes in the gas phase and continuum aqueous solvent are included in Figure 4, the protons in H-bond (1) of structures **G2-[1]** and **C2-[1]**, respectively. Figure 4a shows that the absolute minimum on the 2D-PES of structure **G2-[1]** is represented by an asymmetric single-well potential at $R_{O-H} \approx 2.4$ Å and $\Delta d_{DA} \approx 0.1$ Å. At a longer R_{O-H} distance, a double-well potential appears with an increase in the energy barrier ($\Delta E^{\text{RIMP2/TZVP}}$) as R_{O-H} increases. Two low-interaction energy paths (energy valleys) connecting the single- and double-well potentials span from **A** to **C** and from **A** to **B**, whereas the path with the highest $\Delta E^{\text{RIMP2/TZVP}}$ ("energy crest" at $\Delta d_{DA} \approx 0$ Å) is from **D** to **E**. The low-interaction energy paths are regarded hereafter as the structural diffusion paths (also denoted paths **AC** and **AB**), and the path with the highest $\Delta E^{\text{RIMP2/TZVP}}$ is regarded as the transition state path (also denoted path **DE**). The cross-sectional plots of the 2D-PES in Figure 4a suggest that the structural diffusion path **AC** is preferred compared with **AB**. Due to the presence of continuum aqueous solvent, the detailed 2D-PES of structure **C2-[1]** is different from that of structure **G2-[1]**. In a high-local dielectric constant environment, such as COSMO with $\epsilon = 78$, the single-well potential becomes more asymmetrical and shifts even closer to H_2O , confirming the previously discussed effects of continuum

aqueous solvent, namely increases in the solvent polarity and in the length of the H-bond chain that induce proton displacement from the solute. The shapes of the single-well potentials of structures **G2-[1]** and **C2-[1]** are consistent with the asymmetric O—H stretching frequencies (ν^{OH}) and the ^1H NMR shielding constants ($\sigma_{\text{H}^+}^{\text{corr}}$) listed in Supporting Information, Table S1; ν^{OH} of H-bond (1) in the gas phase is 1746 cm^{-1} , whereas in continuum aqueous solution, ν^{OH} blue shifts to 2424 cm^{-1} , and $\sigma_{\text{H}^+}^{\text{corr}}$ is 13.0 ppm in the gas phase and increases to 16.6 ppm in continuum aqueous solvent. These values reflect the slightly higher covalent bond character and shielding of a proton in continuum aqueous solvent, which results in the proton staying closer to H_2O .

Characteristic NMR spectra on 2D-PES. To study the dynamics of proton dissociation through BOMD simulations, the ^1H NMR shielding constants ($\sigma_{\text{H}^+}^{\text{corr}}$) of a proton on the preferential structural diffusion path (path **AC**) and the transition state path (path **DE**) in the gas phase and continuum aqueous solvent were computed and plotted as a function of R_{O-H} in Figure 5. The $\sigma_{\text{H}^+}^{\text{corr}}$ of the H-bond protons in the $\text{H}_3\text{PO}_4\text{-H}_2\text{O}^+-n\text{H}_2\text{O}$ complexes ($n = 1-3$) were also included in Figure 5 for comparison. It appears that the trends of $\sigma_{\text{H}^+}^{\text{corr}}$ in the gas phase and continuum aqueous solvent are similar; on the energy crest, $\sigma_{\text{H}^+}^{\text{corr}}$ varies over

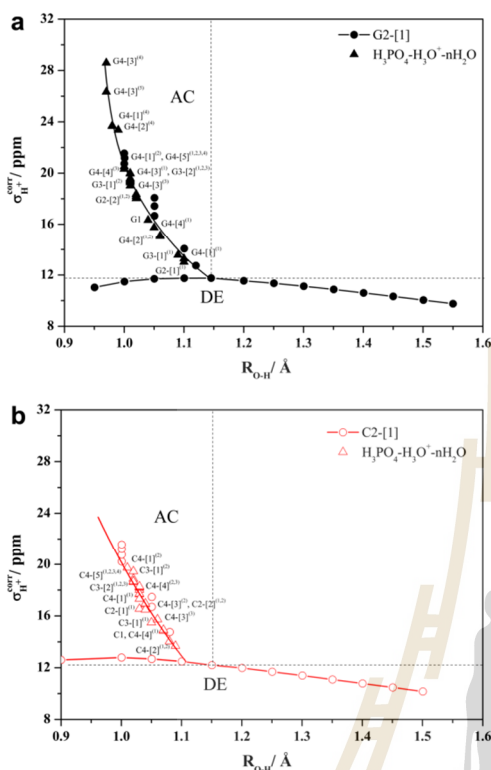


Figure 5. Plots of the ^1H NMR shielding constant ($\sigma_{\text{H}}^{\text{corr}}$) and $R_{\text{O-H}}$ of a proton on the low-interaction energy path (structural diffusion path, AC) and on the path with the highest $\Delta E^{\ddagger, \text{RIMP2/TZVP}}$ (transition state path, DE). These were obtained from the RIMP2/TZVP calculations. (a) Gas phase. (b) Continuum aqueous solvent.

a narrow range (almost constant at approximately 12 ppm), whereas in the energy valley, $\sigma_{\text{H}}^{\text{corr}}$ changes exponentially with $R_{\text{O-H}}$ (from 14 to 12 ppm as $R_{\text{O-H}}$ is increased from 1.10 to 1.15 Å). The latter correspond to ^1H NMR chemical shifts ($\delta_{\text{H}}^{\text{corr}}$) of 18 and 20 ppm, respectively.

Dynamic results

Structures and energy. The BOMD simulations confirmed that only the linear H-bond chains with asymmetric hydration at H_3PO_4^+ are susceptible to proton dissociation and transfer and that the structures **G2-[1]** and **C4-[1]** are the most stable intermediate complexes in these processes, respectively. To further study the effects of a polar solvent and verify the proposed elementary steps shown in Figure 3, the proton transfer profiles^[20] of H-bonds (1) and (2) in structures **G2-[1]** and **C2-[1]** and H-bonds (1) and (3) in structures **G4-[1]** and **C4-[1]** at 298 K were constructed and are shown in Figure 6. For proton dissociation in H-bond (1), the oscillatory shuttling motion, which is a characteristic of the intermediate complex and

determines the rate of proton dissociation, was observed only in structures **G2-[1]** and **G4-[1]** (see panel (II) of Figures 6a and 6c, respectively). Because the oscillatory shuttling vibrational frequencies of a proton in H-bond (1) of structure **G2-[1]**, which were obtained from both static and dynamic calculations, are lower than those obtained for structure **G4-[1]**, structure **G2-[1]** was confirmed to be the smallest, most stable intermediate complex. In continuum aqueous solvent, the proton transfer profiles of H-bond (1) in structures **C2-[1]** and **C4-[1]** [see panel (II) of Figures 6b and 6d] indicated that a proton prefers to stay close to H_2O , which rules out the possibility that both structures are intermediate complexes in the proton dissociation process. The proton transfer profile in panel (VI) of Figure 6d confirmed that structure **C4-[1]** is the intermediate complex for proton transfer from the first to the second hydration shell, which implies that continuum aqueous solvent is required to induce and stabilize the shared-proton structure in H-bond (3).

Activation energies of proton dissociation and transfer. The activation energies ($\Delta E^{\ddagger, \text{Arr}}$) of the rate-determining processes in proton dissociation and transfer in the $\text{H}_3\text{PO}_4\text{-H}_3\text{O}^+\text{-nH}_2\text{O}$ complexes ($n = 1-3$) were obtained from BOMD simulations of the most stable intermediate complexes over the temperature range of 298–430 K. The Arrhenius plot in Figure 7a yielded an $\Delta E^{\ddagger, \text{Arr}}$ of proton dissociation for H-bond (1) of structure **G2-[1]** of 13.1 kJ/mol, whereas the Arrhenius plot of H-bond (3) in structure **C4-[1]**, which is shown in Figure 7b, suggests an $\Delta E^{\ddagger, \text{Arr}}$ of proton transfer from the first to the second hydration shell of 9.9 kJ/mol. The latter is slightly lower than the $\Delta E^{\ddagger, \text{Arr}}$ of proton exchange in the Zundel complex of 10.2 kJ/mol^[16] and is compatible with the activation energies obtained from ion conductivity measurements of 85–100 wt.% H_3PO_4 solutions at 293 K, which were reported to be in the range of 7.8–14 kJ/mol,^[68] and ^1H NMR line width analyses over the temperature range of 293–353 K of 11 kJ/mol.^[13] Therefore, the activation energies obtained from the BOMD simulations confirmed elementary step (III) in Figure 3, in which structure **C4-[1]** is proposed to be the most stable intermediate complex for proton transfer from the first to the second hydration shell.

Vibrational and NMR spectra. Before the vibrational spectra of proton dissociation and transfer are discussed, remarks should be made on the characteristic vibrational motions in protonated H-bonds. For a symmetric donor-acceptor pair, such as in the Zundel complex, the dynamics of the transferring proton are characterized by two vibrational modes, namely the oscillatory shuttling motion, in which the proton shuttles at the center of the H-bond (proton moves in a symmetric single-well potential), and the structural diffusion motion, in which the center of the vibration is slightly shifted toward an oxygen atom (proton moves on the structural diffusion path).^[16] However, for an asymmetric donor-acceptor pair, such as in H-bond (1) of structure **G2-[1]**, the cross-sectional plots in Figure 4 suggested three different modes of vibration, namely a vibrational mode associated with the proton moving in an asymmetric single-well potential or

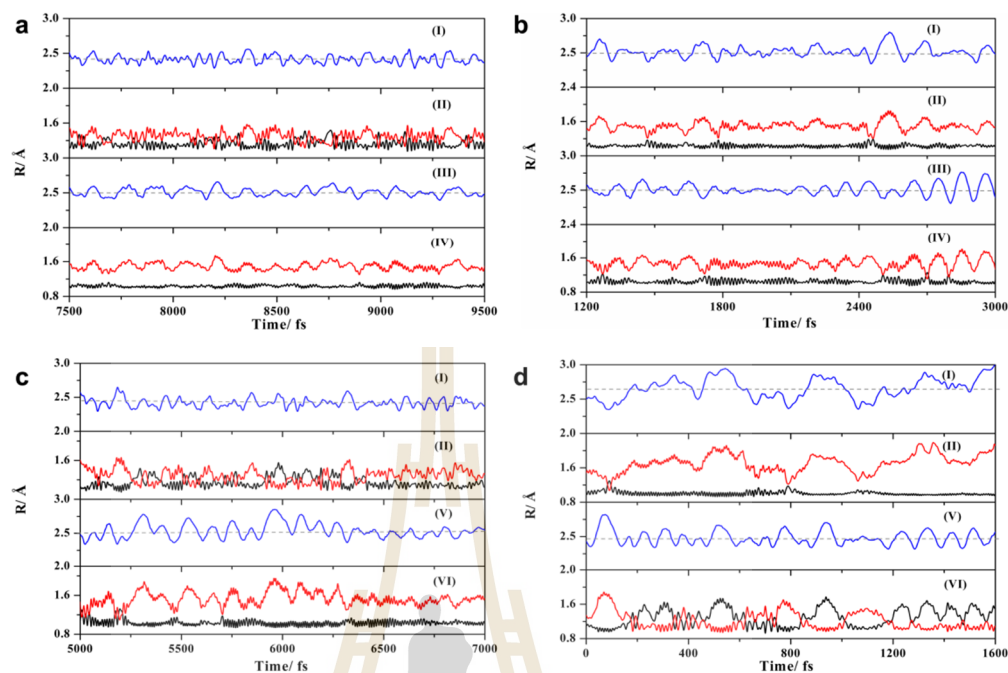
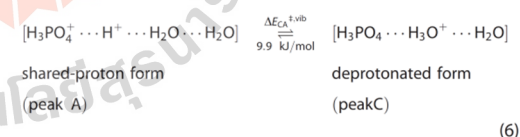
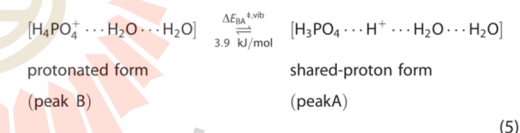


Figure 6. Variations in the R_{O-O} and R_{O-H} distances in H-bonds determined through BOMD simulations at 298 K. (a) and (b) Structures **G2-[1]** and **C2-[1]**, respectively. (c) and (d) Structures **G4-[1]** and **C4-[1]**, respectively. Panels (I) and (II) are the R_{O-O} and R_{O-H} of H-bond (1). Panels (III) and (IV) are the R_{O-O} and R_{O-H} of H-bond (2). Panels (V) and (VI) are the R_{O-O} and R_{O-H} of H-bond (3).

shuttling near the center of H-bond (1) and two vibrational modes for the proton moving in an asymmetric double-well potential with centers of vibration close to H_3PO_4 and H_2O . Therefore, in this work, three characteristic vibrational frequencies were used in the analyses of the dynamics of proton dissociation.

Examples of the vibrational spectra of proton dissociation in H-bond (1) of structure **G2-[1]**, which were obtained from BOMD simulations at 298, 315, and 350 K, are shown in Figure 8. Only the results at 298 K are discussed in detail. The three characteristic peaks, labelled **A**, **B**, and **C**, are outstanding at $\nu_A^{OH,MD} = 1052 \text{ cm}^{-1}$, $\nu_B^{OH,MD} = 1378 \text{ cm}^{-1}$, and $\nu_C^{OH,MD} = 1877 \text{ cm}^{-1}$. Based on the structures of the cross-sectional plots in Figure 4 and the ν^{OH} values shown in Supporting Information, Table S1, peak **A** can be assigned to the oscillatory shuttling motion, whereas peaks **B** and **C** are the structural diffusion motions in the protonated forms ($H_4PO_4^+$ and H_3O^+), which correspond to the proton moving on paths **AB** and **AC** in Figure 4, respectively. It should be stressed that the RIMP2/TZVP calculations with the harmonic approximation did not yield the vibrational frequencies of the structural diffusion motions because the absolute minimum energy geometry of H-bond (1) in structure **G2-[1]** is characterized by a proton in an asymmetric single-well potential. Therefore, to obtain complete information on the motion of a proton in an H-bond, the

local-energy fluctuations and dynamics must be included in the model calculations. The quasidynamic equilibria between the three limiting forms are, therefore, written as



From the characteristic vibrational frequencies, the vibrational energies for the interconversion between the protonated ($H_4PO_4^+$, peak **B**) and shared-proton (peak **A**) structures shown in Eq. (5), and the protonated (H_3O^+ , peak **C**) and shared-proton (peak **A**) structures shown in Eq. (6) can be approximated at 298 K as $\Delta \nu_{BA}^{OH,MD} = 326$ and $\Delta \nu_{CA}^{OH,MD} = 825 \text{ cm}^{-1}$, which correspond to $\Delta E_{BA}^{+vib} = 3.9$ and $\Delta E_{CA}^{+vib} = 9.9 \text{ kJ/mol}$, respectively.^[18]

The trends in the characteristic vibrational frequencies ($\nu_A^{OH,MD}$, $\nu_B^{OH,MD}$, and $\nu_C^{OH,MD}$) with respect to temperature are

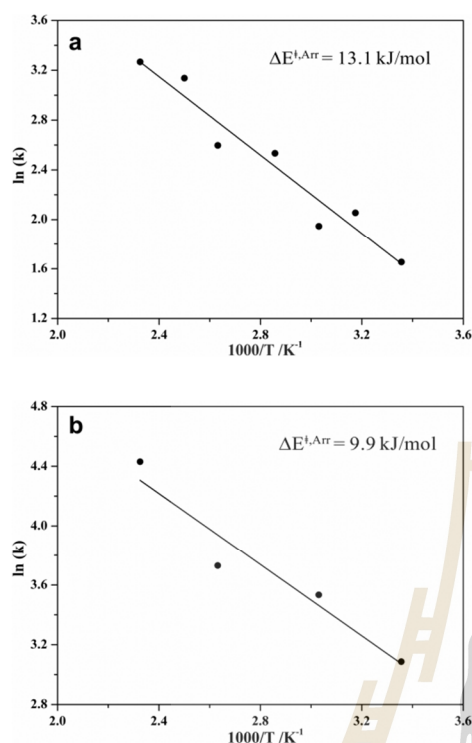


Figure 7. Arrhenius plots obtained from the BOMD simulations over the temperature range of 298–430 K. (a) Proton dissociation in H-bond (1) of structure G2-[1]. (b) Proton transfer in H-bond (3) of structure C4-[1].

illustrated in Figure 8d; these show uniform changes in the vibrational frequencies of proton dissociation over the entire temperature range: as the temperature increases from 298 to 430 K, the oscillatory shuttling peak (peak A) red shifts, reflecting more polarization in H-bond (1), whereas the structural diffusion peaks (peaks B and C) blue shift, indicating larger proton displacement at elevated temperatures. Due to the vibrational interference effects, the vibrational spectra of a proton in H-bond (3) of structure C4-[1] are complicated, especially at elevated temperatures. Therefore, only the vibrational spectra at 298 K, which is shown in Figure 8e, were analyzed. These are characterized by a characteristic oscillatory shuttling peak (peak A) at $\nu_A^{\text{OH,MD}} = 893 \text{ cm}^{-1}$ and a structural diffusion peak (peak B) at $\nu_B^{\text{OH,MD}} = 1515 \text{ cm}^{-1}$, which results in $\Delta\nu_{\text{BA}}^{\text{OH,MD}} = 622 \text{ cm}^{-1}$ and $\Delta E_{\text{BA}}^{\pm,\text{vib}} = 7.4 \text{ kJ/mol}$. The $\Delta E_{\text{BA}}^{\pm,\text{vib}}$ is lower than that of the Zundel complex in continuum aqueous solvent at 350 K, which was found to be 8.9 kJ/mol,^[58] confirming the slightly higher efficiency of proton transfer in the presence of the solute.

Additional information on the dynamics of proton dissociation can be obtained from the ^1H NMR chemical shift spectra of H-bond (1) in structure G2-[1], which were obtained from the BOMD simulations over the temperature range of 350–

430 K. These are shown as examples in Figure 9. The ^1H NMR chemical shift spectra at 350 K are characterized by two well-defined peaks at 20.3 and 19.5 ppm and a broad peak at 18.0 ppm (labelled A, C, and B in panel (I) of Fig. 9a, respectively). According to the static results, peak A is associated with a proton at the center of H-bond (1), whereas peaks C and B are the protonated forms, H_3O^+ and H_4PO_4^+ , respectively. Because peaks A and C overlap, the ^1H NMR line width analyses had to be made using two Lorentzian peak functions, namely peaks A and B in panel (II) of Figure 9. The slope of the plot of $\ln T_2^2$ and $1000/T$ in Figure 9d, which was obtained from the analysis of peak A, yielded an activation energy ($\Delta E^{\pm,\text{NMR}}$) of deprotonation along path AC of 10.8 kJ/mol, which is in excellent agreement with the $\Delta E_{\text{BA}}^{\pm,\text{vib}}$ value obtained for the same path (Eq. (5)) and the ^1H NMR line width measurement over the temperature range of 293–353 K of 11 kJ/mol.^[13] As the same motional narrowing was observed at elevated temperatures with almost the same activation energies, and the ^1H NMR chemical shifts of protonated H-bonds were shown in our previous work^[16] to be sensitive only to the H-bond distances, one can conclude that the ^1H NMR line width measurement reflected the characteristic local-vibrational motions of the transferring proton, not the local-rotational motions as anticipated in Ref. 13; our ^1H NMR line width analyses revealed that the chemical shifts of the shared-protons in protonated water clusters are not sensitive to the rotational motions, for example, for $\text{H}^+(\text{H}_2\text{O})_n$, $n = 4$, the chemical shifts of protons in the *cis* and *trans* H-bond structures are almost the same, 20.93 and 20.99 ppm,^[16] respectively, and those for the planar and perpendicular structures of the protonated imidazole dimers ($\text{H}^+(\text{Im})_2$) are 21.18 and 21.63 ppm, respectively. The microscopic dynamics probed by the ^1H NMR line width analyses are, therefore, the characteristic local-vibrational motions of the transferring protons in H-bonds.

The analysis of peak B yielded an $\Delta E^{\pm,\text{NMR}}$ value on path AB of 8.9 kJ/mol, which is considerably higher than the corresponding $\Delta E_{\text{BA}}^{\pm,\text{vib}}$ of 3.9 kJ/mol. The difference is because the oxygen atom in H_3PO_4 possesses a higher electron density than that of H_2O , resulting in a higher shielding effects at the H-bond proton, which is sensitive to not only its position, but also vibrational interferences and environment, for example, the H-bond protons in H-bond (1) in structures G2-[2] and G2-[1] possess $\sigma_{\text{H}}^{\text{OH}}$ of 18.2 and 13.0 ppm, respectively.

Finally, to assess the proposed presolvation models and the proton dissociation and transfer mechanisms, extensive quantum mechanical force field (QMCF) calculations, consisting of one H_4PO_4^+ and 2000 water molecules, were performed at 298 K, in which the theoretical results reported in this work played important roles in the analyses of the dynamic data. Although some of the reported dynamic properties (e.g., the vibrational frequencies of the transferring protons) cannot be directly calculated due to the complexity in the aqueous solution, the QMCF results confirmed the applicability of the presolvation models, especially in the calculations of local-dynamic properties in short-time scale, for example, the vibrational patterns of the oscillatory shuttling and structural

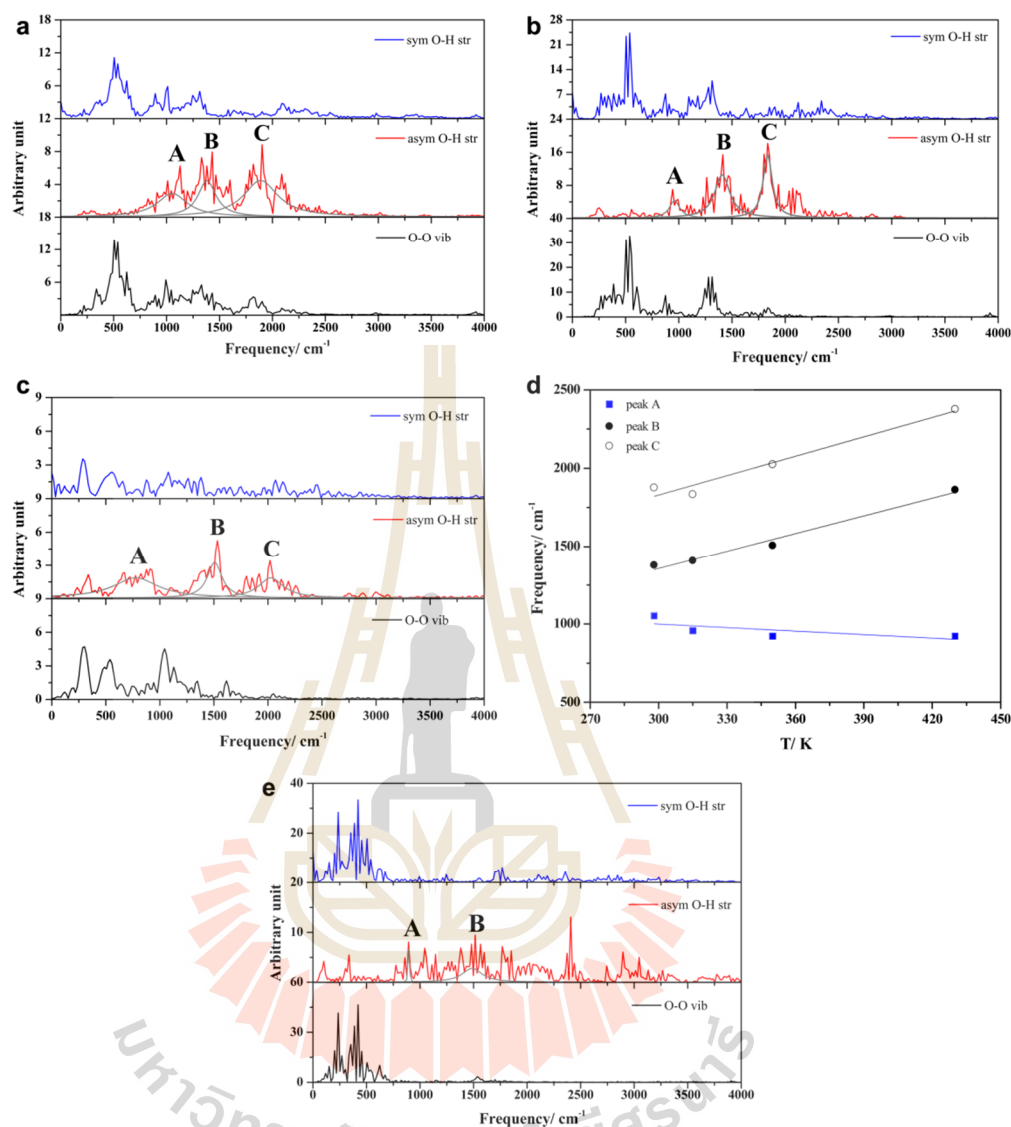


Figure 8. (a)–(c) vibrational spectra of a proton in H-bond (1) of structure G2-[1] obtained from BOMD simulations at 298, 315, and 350 K, respectively. (d) Trends in the characteristic oscillatory shuttling (peak A) and structural diffusion (peaks B and C) frequencies of proton dissociation in H-bond (1) of structure G2-[1] obtained from BOMD simulations over the temperature range of 298–430 K. (e) Vibrational spectra of proton transfer in H-bond (3) of structure C4-[1] obtained from BOMD simulations at 298 K.

diffusion motions, the ¹H NMR spectra, and the lifetimes of the shared-proton intermediate complexes.

Conclusion

The dynamics and mechanisms of proton dissociation and transfer in hydrated H₃PO₄ clusters under excess proton condi-

tions were studied using RIMP2/TZVP calculations and BOMD simulations over the temperature range of 298–430 K in both low ($\epsilon = 1$) and high local-dielectric constant ($\epsilon = 78$) environments. The theoretical study emphasized the dynamics and H-bond arrangements in a short-time scale which could promote intermediate complex formation, and the roles played by the local-dielectric environment. The theoretical investigations

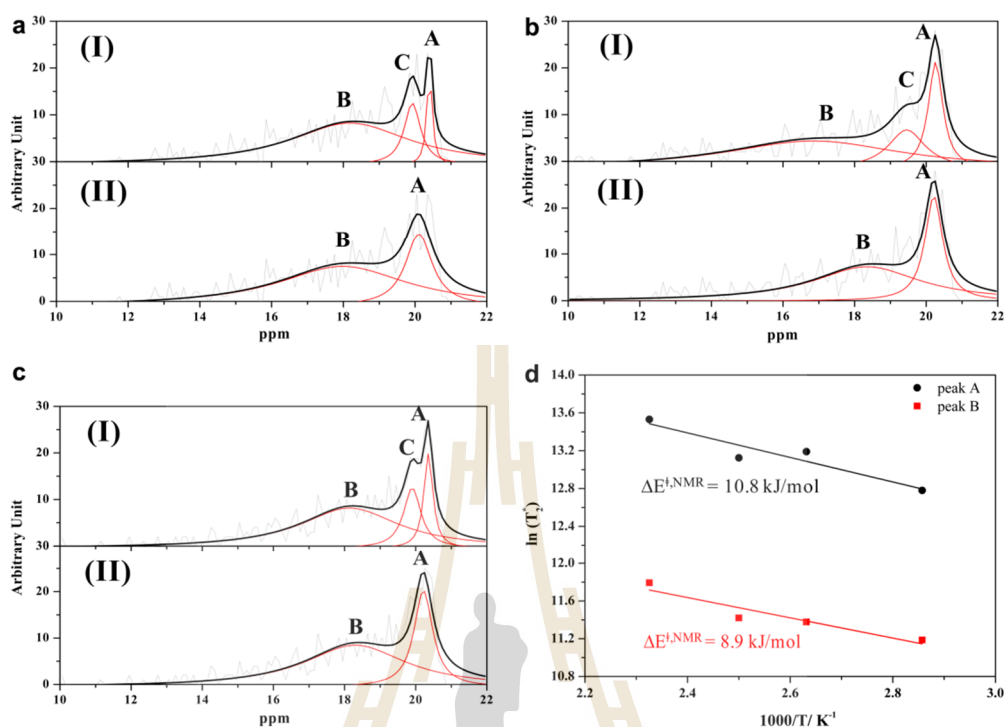


Figure 9. (a)–(c) Examples of the ^1H NMR chemical shift spectra of proton dissociation in H-bond (1) of structure **G2-[1]** obtained from BOMD simulations at 350, 380, and 400 K, respectively. (d) Plots of the natural log of the effective transverse relaxation time (T_2) as a function of $1000/T$ for peaks **A** and **B**. Peaks **A** and **B/C** are associated with protons moving in single- and double-well potentials, respectively.

were based on the concept of presolvation, and the $\text{H}_3\text{PO}_4\text{-H}_3\text{O}^+\text{-nH}_2\text{O}$ complexes ($n = 1\text{--}3$) were demonstrated to be effective presolvation models. The static results obtained from the RIMP2/TZVP calculations revealed that only the linear H-bond chains with asymmetric hydration at H_4PO_4^+ are susceptible to proton dissociation and transfer and that the structure with $n = 1$ in a low local-dielectric constant environment (structures **G2-[1]**) represents the smallest, most stable intermediate complex for proton dissociation. The RIMP2/TZVP calculations revealed that a proton can transfer from the first to the second hydration shell through the linear H-bond chain with $n = 3$ (structure **C4-[1]**), through the Zundel complex which connects the first and the second hydration shells, and a high local-dielectric constant environment is required to induce and stabilize the intermediate complex. These findings are in accordance with the LCS concept. Therefore, fluctuations in the number of water molecules and the local-dielectric constant were concluded to play essential roles and were included in the proposed proton dissociation and transfer mechanisms.

The two-dimensional potential energy surface (2D-PES) of the transferring proton in the smallest, most stable intermedi-

ate complex (structure **G2-[1]**) showed an asymmetric single-well potential at the equilibrium $R_{\text{O-O}}$ distance, and an asymmetric double-well potential was found at longer $R_{\text{O-O}}$. The cross-sectional plots of the 2D-PES suggested three vibrational modes for proton dissociation from H_4PO_4^+ : one for the oscillatory shuttling motion and two for the structural diffusion motions. Because *ab initio* calculations with the harmonic approximation yield reliable vibrational frequencies only for the minimum energy geometry (the oscillatory shuttling frequency), the isotropic shielding constants ($\sigma_{\text{H}}^{\text{corr}}$) on the 2D-PES were computed to obtain additional information for the interpretation of the BOMD results. The *ab initio* GIAO method suggested that a proton moving on the structural diffusion path is characterized by a $\sigma_{\text{H}}^{\text{corr}}$ value that varies exponentially with $R_{\text{O-H}}$, whereas a proton on the transition state path (energy crest, $\Delta d_{\text{DA}} \approx 0$ Å) exhibits a $\sigma_{\text{H}}^{\text{corr}}$ value that varies over a narrow range (nearly constant at approximately 12 ppm).

The BOMD simulations confirmed that only the linear H-bond chains with asymmetric hydration at H_4PO_4^+ are susceptible to proton dissociation and transfer, which is in accordance with the protonic-chain conduction mechanism. The proton transfer profiles obtained from the BOMD simulations

indicated that structures **G2**-[1] and **C4**-[1] are indeed the most stable intermediate complexes in the proton dissociation and transfer pathways, respectively. The activation energies ($\Delta E^{\ddagger, \text{Act}}$) of proton dissociation and transfer, which were obtained from the Arrhenius plots in the temperature range of 298–430 K, are 13.1 and 9.9 kJ/mol, respectively. These values are in good agreement with the experimental activation energies obtained by probing microscopic dynamics, such as the ion-conductivity and conventional ^1H NMR measurements. For proton transfer from the first to the second hydration shell, the vibrational frequencies associated with a proton moving on the oscillatory shuttling and structural diffusion paths, which cannot be obtained through *ab initio* calculations with the harmonic approximation, predicted the vibrational energy for the interconversion between the shared-proton and close-contact structures in H_3O_2^+ attached to H_3PO_4 to be slightly lower than that of the Zundel complex. This suggests a slightly higher efficiency of proton transfer in the presence of the H_3PO_4 solute and the roles played by H_3O^+ and H_5O_2^+ . The three characteristic vibrational motions on the proton dissociation pathway, which were suggested by the 2D-PES and vibrational spectra, were also observed in the ^1H NMR chemical shift spectra, and the line-width analyses suggested that the activation energy for proton dissociation is comparable with the ^1H NMR experimental results.

Finally, we would like to stress that it is not our intention to claim that all the condensed-phase properties of the mixture of H_3PO_4 and H_2O can be studied based on the proposed presolvation models. Instead, we would only like to show specifically how the dynamics of protons in the intermediate complexes can be studied, and related to the rate-determining processes in the local proton-transfer mechanisms, which in general consist of the intermediate complex formation and the actual transfer. The present theoretical results, therefore, provide insights into the roles played by a polar solvent and iterate that the dynamics and mechanisms of proton transfer in H-bond clusters can be obtained from intermediate complexes provided that an appropriate presolvation model is selected and that all of the important rate-determining processes are included in the model calculations.

Acknowledgments

The super- and high-performance computer facilities provided by the following organizations are gratefully acknowledged: the Institute for Materials Research (IMR) of Tohoku University, Schools of Mathematics and Chemistry, SUT; the National Electronics and Computer Technology Centre (NECTEC) of the National Science and Technology Development Agency (NSTDA), and the Thai National Grid Centre (THAIGRID) of the Ministry of Information and Communication Technology (MICT).

Keywords: phosphoric acid · BOMD simulations · proton dissociation · proton transfer · vibrational and NMR spectra · hydrogen bond

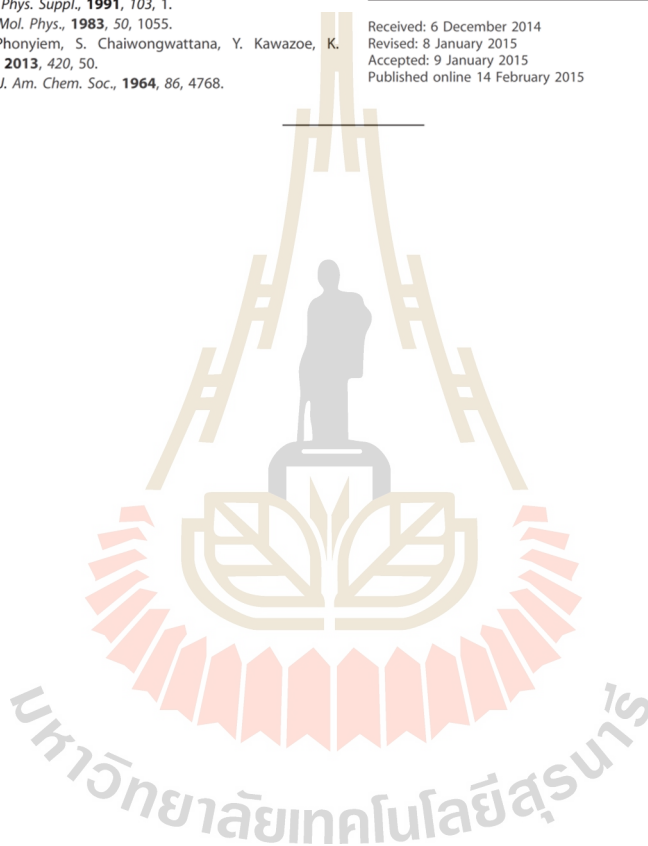
How to cite this article: P, Suwannakham, S, Chaiwongwattana, K, Sagarik. *Int. J. Quantum Chem.* **2015**, *115*, 486–501. DOI: 10.1002/qua.24873

 Additional Supporting Information may be found in the online version of this article.

- [1] T. Koppel, *Powering the Future: The Ballard fuel cell and the race to change the world*, Wiley: New York, **1999**.
- [2] J. Larminie, A. Dicks, *Fuel Cell Systems*, Wiley: Chichester, **2001**.
- [3] C. A. Vincent, B. Scrosati, *Modern Batteries: An Introduction to Electrochemical Power Sources*, Wiley: New York, **1997**.
- [4] K. A. Mauritz, R. B. Moore, *Chem. Rev.*, **2004**, *104*, 4535.
- [5] K. Sundmacher, *Ind. Eng. Chem. Res.*, **2010**, *49*, 10159.
- [6] M. F. H. Schuster, W. Meyer, *Annu. Rev. Mater. Res.*, **2003**, *33*, 233.
- [7] K. D. Kreuer, *Chem. Mater.*, **1996**, *8*, 610.
- [8] K. D. Kreuer, S. J. Paddison, E. Spohr, M. Schuster, *Chem. Rev.*, **2004**, *104*, 4637.
- [9] S. J. Paddison, *Annu. Rev. Mater. Res.*, **2003**, *33*, 289.
- [10] H. Pu, W. H. Meyer, G. Wegner, *J. Polym. Sci. Polym. Phys.*, **2002**, *40*, 663.
- [11] N. N. Greenwood, A. Thompson, *J. Chem. Soc.*, **1959**, 3485.
- [12] R. A. Munson, M. E. Lazarus, *J. Phys. Chem.*, **1967**, *71*, 3245.
- [13] S. H. Chung, S. Bajue, S. G. Greenbaum, *J. Chem. Phys.*, **2000**, *112*, 8515.
- [14] L. Vilčiauskas, M. E. Tuckerman, G. Bester, S. J. Paddison, K. D. Kreuer, *Nat. Chem.*, **2012**, *4*, 461.
- [15] K. J. Tielrooij, R. L. A. Timmer, H. J. Bakker, M. Bonn, *Phys. Rev. Lett.*, **2009**, *102*, 198303.
- [16] C. Lao-ngam, M. Phonyiem, S. Chaiwongwattana, Y. Kawazoe, K. Sagarik, *Chem. Phys.*, **2013**, *420*, 50.
- [17] C. Lao-ngam, P. Asawakun, S. Wannarat, K. Sagarik, *Phys. Chem. Chem. Phys.*, **2011**, *13*, 4562.
- [18] M. Phonyiem, S. Chaiwongwattana, C. Lao-ngam, K. Sagarik, *Phys. Chem. Chem. Phys.*, **2011**, *13*, 10923.
- [19] K. Sagarik, S. Chaiwongwattana, V. Vchirawongkwin, S. Prueksaaron, *Phys. Chem. Chem. Phys.*, **2010**, *12*, 918.
- [20] K. Sagarik, M. Phonyiem, C. Lao-ngam, S. Chaiwongwattana, *Phys. Chem. Chem. Phys.*, **2008**, *10*, 2098.
- [21] S. Chaiwongwattana, C. Lao-ngam, M. Phonyiem, V. Vchirawongkwin, K. Sagarik (submitted).
- [22] V. A. Glezakou, M. Dupuis, C. J. Mundy, *Phys. Chem. Chem. Phys.*, **2007**, *9*, 5752.
- [23] R. O. Watts, I. J. McGee, *Liquid State Chemical Physics*, Wiley: New York, **1976**.
- [24] L. Vilčiauskas, Ph.D. thesis, Universitaet Stuttgart, **2012**.
- [25] H. J. Boehm, R. Ahlrichs, *Mol. Phys.*, **1985**, *55*, 1159.
- [26] K. P. Sagarik, *J. Mol. Struct. (Theochem)*, **1999**, *465*, 141.
- [27] K. P. Sagarik, S. Dokmaisirjan, *J. Mol. Struct. (Theochem)*, **2005**, *718*, 31.
- [28] H. J. Boehm, R. Ahlrichs, *J. Chem. Phys.*, **1982**, *77*, 2028.
- [29] K. Sagarik, S. Chaiyapongs, *Biophys. Chem.*, **2005**, *117*, 18.
- [30] K. P. Sagarik, R. Ahlrichs, *J. Chem. Phys.*, **1987**, *86*, 5117.
- [31] K. P. Sagarik, P. Asawakun, *Chem. Phys.*, **1997**, *219*, 173.
- [32] K. P. Sagarik, S. Chaiwongwattana, P. Sisot, *Chem. Phys.*, **2004**, *1*.
- [33] K. P. Sagarik, V. Pongpituk, S. Chiyapongs, P. Sisot, *Chem. Phys.*, **1991**, *156*, 439.
- [34] K. P. Sagarik, B. M. Rode, *Chem. Phys.*, **2000**, *260*, 159.
- [35] K. P. Sagarik, E. Spohr, *Chem. Phys.*, **1995**, *199*, 73.
- [36] F. Weigend, M. Haeser, *Theor. Chem. Acc.*, **1997**, *97*, 331.
- [37] A. Klamt, G. Schuurmann, *J. Chem. Soc. Perkin Trans. 2*, **1993**, 799.
- [38] TURBOMOLE Tutorial V6.4, a development of University of Karlsruhe and Forschungszentrum Karlsruhe GmbH, 1989–2007, TURBOMOLE GmbH, since 2007; Available at: <http://www.turbomole.com>.
- [39] R. Ahlrichs, M. Baer, M. Haeser, H. Horn, C. Koelmel, *Chem. Phys. Lett.*, **1989**, *162*, 165.
- [40] O. Treutler, R. Ahlrichs, *J. Chem. Phys.*, **1995**, *102*, 346.
- [41] SURFER for Window, Golden Software Inc., 6.04 ed., **1997**.
- [42] A. P. Scott, L. Radom, *J. Phys. Chem.*, **1996**, *100*, 16502.
- [43] R. Konrat, M. Tollinger, G. Kontaxis, B. Kraeutler, *Monat. Chemie*, **1999**, *130*, 961.

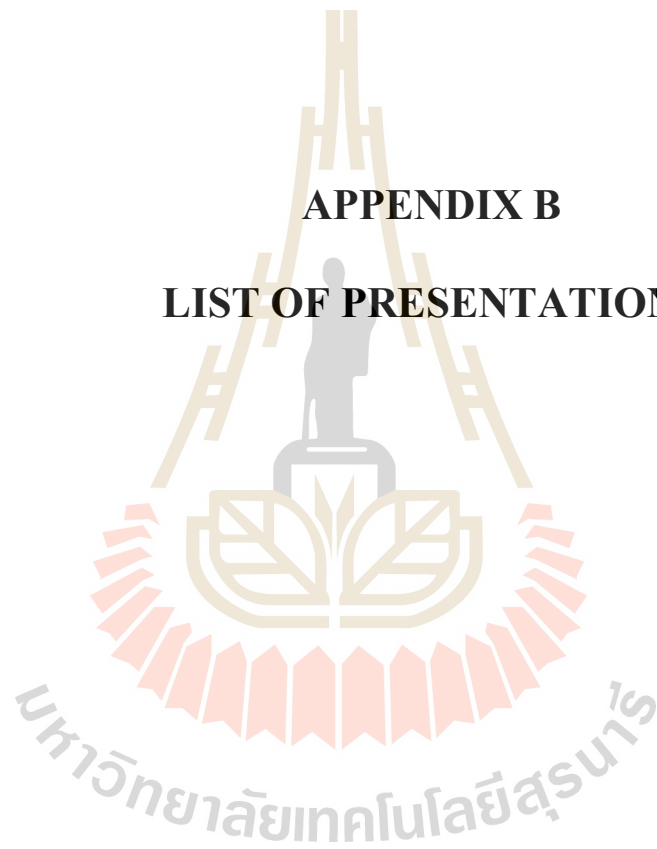
- [44] S. Taubert, H. Konschinn, D. Sundholm, *Phys. Chem. Chem. Phys.*, **2005**, 7, 2561.
- [45] R. Ditchfield, *J. Chem. Phys.*, **1976**, 65, 3123.
- [46] R. Ditchfield, *Mol. Phys.*, **1974**, 27, 789.
- [47] D. B. Chesnut, *Chem. Phys. Letters*, **1995**, 246, 235.
- [48] R.K. Harris, E.D. Becker, S.M. Cabral de Menezes, P.Granger, R.E. Hoffman, K. W. Zilm, *Pure Appl. Chem.*, **2008**, 80, 59.
- [49] D. B. Chesnut, B. E. Rusiloski, *J. Mol. Struct. (THEOCHEM)*, **1994**, 314, 19.
- [50] D. B. Chesnut, *J. Phys. Chem. A*, **2005**, 109, 11962.
- [51] D.B. Chesnut, B. E. Rusiloski, *J. Mol. Struct. (Theochem)*, **1994**, 314 19.
- [52] C. Lao-ngam, P. Asawakun, S. Wannarat, K. Sagarik, *Phys. Chem. Chem. Phys.*, **2011**, 13, 4562.
- [53] S. Chaiwongwattana, M. Phonyiem, V. Vchirawongkwin, S. Prueksaaron, K. Sagarik, *J. Comput. Chem.*, **2012**, 33, 175.
- [54] W. G. Hoover, *Phys. Rev. A*, **1985**, 31, 1695.
- [55] S. Nosé, *J. Chem. Phys.*, **1984**, 81, 511.
- [56] S. Nosé, *Prog. Theor. Phys. Suppl.*, **1991**, 103, 1.
- [57] S. Nosé, M. L. Klein, *Mol. Phys.*, **1983**, 50, 1055.
- [58] C. Lao-ngam, M. Phonyiem, S. Chaiwongwattana, Y. Kawazoe, K. Sagarik, *Chem. Phys.*, **2013**, 420, 50.
- [59] Z. Luz, S. Meiboom, *J. Am. Chem. Soc.*, **1964**, 86, 4768.
- [60] P. Bopp, *Chem. Phys.*, **1986**, 106, 205.
- [61] C. Lao-ngam, P. Asawakun, S. Wannarat, K. Sagarik, *Phys. Chem. Chem. Phys.*, **2011**, 13, 4562.
- [62] J. R. Schmidt, S. A. Corcelli, J. L. Skinner, *J. Chem. Phys.*, **2005**, 123, 044513.
- [63] G. Brunklaus, S. Schauff, D. Markova, M. Klapper, K. Müllen, H.-W. Spiess, *J. Phys. Chem. B*, **2009**, 113, 6583.
- [64] Y. J. Lee, B. Bingöl, T. Murakhtina, D. Sebastiani, W. H. Meyer, G. Wegner, H. W. Spiess, *J. Phys. Chem. B*, **2007**, 111, 9711.
- [65] T. Murakhtina, J. Heuft, E. J. Meijer, D. Sebastiani, *ChemPhysChem*, **2006**, 7, 2578.
- [66] S. R. Narayanan, S. P. Yen, L. Liu, S. G. Greenbaum, *J. Phys. Chem. B*, **2006**, 110, 3942.
- [67] B. Koeppel, J. Guo, P. M. Tolstoy, G. S. Denisov, H.-H. Limbach, *J. Am. Chem. Soc.*, **2013**, 135, 7553.
- [68] R. He, Q. Li, G. Xiao, N. J. Bjerrum, *J. Membr. Sci.*, **2003**, 226, 169.

Received: 6 December 2014
 Revised: 8 January 2015
 Accepted: 9 January 2015
 Published online 14 February 2015



APPENDIX B

LIST OF PRESENTATIONS



List of presentations:

1. Parichart Suwannakham and Kritsana Sagarik. (April 5-7, 2013). Structural Diffusion in Phosphoric Acid Solution (Oral presentation). **RGJ-Ph.D. Congress XIV**, Basic Research for Sustainable Development, Jomtien Palm Beach Hotel and Resort, Pattaya, Chonburi, Thailand.
2. Kritsana Sagarik, Jittima Thisuwan, Parichart Suwannakham, Patama KateSoongern, Pannipa Panajapo, Worapong Bua-ngern and Mayuree Phonyiem. (6-11 July 2014). Proton transfer reaction in Hydrogen bond systems. **IUPAC. MACRO 2014**, Chiang mai, Thailand.
3. Parichart Suwannakham and Kritsana Sagarik. (17-19 June 2015). Solvent effects on proton dissociation and transfer in hydrated phosphoric acid clusters (Poster presentation). **ANSCSE 19**, Ubon Ratchathani University, Ubon Ratchathani, Thailand.
4. Parichart Suwannakham and Kritsana Sagarik. (20-24 September 2015). Dynamics and mechanisms of proton exchange in phosphoric acid-water clusters (Poster presentation). **The 51st Symposium on Theoretical Chemistry “Chemistry in Motion”**, University of Potsdam, Potsdam, Germany.

CURRICULUM VITAE

Name Miss Parichart Suwannakham

Date of Birth January 24, 1988

Education

2004–2008 B.Sc. First Class Honor (Chemistry), Ubon Ratchathani University, Ubon Ratchathani, Thailand.

2009–2015 Ph.D. Candidate (Chemistry), Suranaree University of Technology, Nakhon Ratchasima, Thailand.

Research and Academic Experiences

2014 Visiting scholar, Institute of General, Inorganic and Theoretical Chemistry, University of Innsbruck, Innsbruck, Austria.

2014–2015 Teaching assistant, School of Chemistry, Institute of Science, Suranaree University of Technology, Thailand.

2015–present Research assistant, Computational Chemistry Research Laboratory (CCRL), School of Chemistry, Institute of Science, Suranaree University of Technology, Thailand.

Grant and Fellowship

2009–2014 The Royal Golden Jubilee (RGJ) Ph.D. Program of Thailand Research Fund (TRF) and Suranaree University of Technology (SUT); contract grant number: PHD/0085/2552.

2014–2015 SUT Teaching assistantship.